NMR Spectroscopic Studies on Organocopper Compounds and Silicon Zintl Anions

Dissertation zur Erlangung des Grades

Doktor der Naturwissenschaften (Dr. rer. nat.)

der naturwissenschaftlichen Fakultät IV
Chemie und Pharmazie der Universität Regensburg

vorgelegt von

Tobias Gärtner

aus Neumarkt i. d. Opf.

2009

NMR Spectroscopic Studies on Organocopper Compounds and Silicon Zintl Anions

Dissertation

zur Erlangung des Doktorgrades der Naturwissenschaften

(Dr. rer. nat.)

an der Fakultät für Chemie und Pharmazie

der Universität Regensburg

vorgelegt von

Tobias Gärtner

aus Neumarkt i. d. Opf.

2009

This PhD-thesis was carried out under the supervision of Prof. Dr. Ruth M. Gschwind between October 2006 and December 2009 at the Institute of Organic Chemistry at the University of Regensburg.

The PhD – thesis was submitted on:	19.11.2009	
The colloquium took place on:	18.12.2009	
Board of Examiners:	Prof. Dr. R. Winter	Chairman
	Prof. Dr. R. M. Gschwind	1st Referee
	Prof. Dr. B. König	2nd Referee
	Prof. Dr. A. Pfitzner	Examiner

Für alle,

die das lesen.

Again what learned…wieder was gelernt!

unbekannt

An dieser Stelle ist kurz die Zeit, an alle zu denken, die zum Gelingen dieser Arbeit beigetragen haben. Als erstes sei hier meine Doktormutter Frau Prof. Dr. R. M. Gschwind genannt, bei der ich mich sowohl für die interessante und anspruchsvolle Themenstellung, als auch für die Freiheit bei der Bearbeitung des Themas bedanken möchte. Ausserdem möchte ich mich bei den Professoren Dr. B. König, Dr. A. Pfitzner und Dr. R. Winter für die Ausübung des Amtes als Prüfer bzw. Vorsitzenden recht herzlich bedanken. Desweitern bedanke ich mich bei Prof. Dr. N. Korber für die Ermöglichung der Kooperation.

Gebührender Dank gilt vor allen Dingen auch den Mitarbeitern des Arbeitskreises, aufgrund deren netter und respektvoller Umgangsweise die Arbeit sehr viel Spaß gemacht hat. Dabei denke ich zuerst an Dr. Guido „die Zange“ Federwisch, dessen Kölner Frohnatur die Zeit sehr verkürzt hat, an meinen Laborpartner Roland „die W-Kopplung“ Kleinmaier, der sich seine Arbeit im Lösunsmitteldampf mit Reggae versüßt hat, an Markus „die Stirn“ Schmid, unseren Synthesegott, an Katrin „das *****geweih“ Schober, die leider zu allen aufschauen muss, an Matthias „the Tschöl“ Fleischmann, den Vortragsgott, an Evelyn „die Buschfrau“ Hartmann, an Diana „the studentcalendar“ Drettwan und nicht zuletzt an Maria „die tote Maus“ Neumeier. Auch Hongxia Zhang möchte ich in diesem Zusammenhang meinen Dank aussprechen.

Neben all den Leuten gibt es auch noch die, die es verdient haben separat erwähnt zu werden. Dabei möchte ich mich bei den guten Seelen des Arbeitskreises, Nikola Kastner-Pustet und Ulrike Weck sehr herzlich für die tatkräftige Unterstützung bedanken. Mein Dank gilt zudem der NMR-Abteilung der Universität, Dr. Thomas Burgemeister, Fritz Kastner, Annette Schramm und Georgine Stühler, die stets mit Rat und Tat zur Seite standen, wenn das Röhrchen mal nicht ans Licht wollte. Desweiteren möchte ich mich bei Dr. Christian Gröger und Dr. Werner Kremer für die Festkörper NMR Messungen bedanken.

Nicht vergessen möchte ich auch Prof. Dr. Eiichi Nakamura, an dessen Arbeitskreis ich zwei Monate verbringen durfte, und die Leute, die mir während meines Aufenthaltes in Japan stets zur Seite standen. Hier sind Dr. Laurean Ilies und Sobi Asako herauszuheben.

Ganz besonderer Dank gilt meinen Eltern für die Unterstützung und meinen Brüdern, meinen Schwägerinennen und meinen 6 Nichten und Neffen, die stets für die nötige Ablenkung sorgen. Gedankt sei auch allen Freunden, die leider hier keinen Platz mehr finden.

Ganz besondere Aufmerksamkeit gilt meiner baldigen Ehefrau Steffi, die mich stets mit viel Verständnis unterstützt hat.

Table of Contents

1. Overview

Organocuprates are known to be valuable reagents for C-C-bond formations in 1,4-addition reactions with α,β-unsaturated carbonyl compounds as well as in S_N2-like or S_N2' cross coupling reactions. Since the first report about organocuprate reagents, much effort was spent on the characterisation of the free organocopper reagents and the π- and σ-intermediate structures of the different reactions. Especially, dimethylcuprates are the generally accepted model compounds for mechanistic studies of organocopper reagents. While synthetic and theoretical studies of the mechanisms are known for a long time, it was only a few years ago, when the first spectrocopic evidences about the key-Cu(III)-intermediates were published by our and other research groups. Therefore, this thesis mainly deals with the stabilisation and NMR spectroscopic study of the intermediate structures of addition and substitution reactions of organocuprates. In the second part of this thesis, the question about the behaviour of silicon Zintl anions in ammonia solution is adressed.

Section 2 is a review about the methodology used in NMR spectroscopic investigations on organocopper compounds. It describes the currently known structural and mechanistic details about the catalytical and stoichiometric copper reagents and reactions. This review is published in a contribution to the new edition of the Patai´s series.

Section 3 is an additional note containing different crystal structures of LiI with coordinated solvent derived by X-ray structure analysis. It was possible to prove the NMR spectroscopic results of Gschwind *et al*. from 2005 that addition of THF to Me_2CuLi•LiI in Et_2O-solution results in a separation of the LiI unit from the cuprate to form LiI•$(THF)_3$.

Section 4 describes different chiral and achiral π-intermediate structures of the 1,4-addition reaction and the influence of the salt in Me_2CuLi•LiI and Me_2CuLi•LiCN on the π-intermediates. Additionally, results about supramolecular aggregation in the π-intermediate are discussed.

In Section 5 the NMR spectroscopic detection of the Cu(III) intermediate in S_N2-like substitution reactions of Gilman cuprates with alkyl halides is reported.

Section 6 is about NMR spectroscopic observations of ligand exchange processes in the Cu(III) complexes. DFT calculations are included, which describe the mechanism of ligand exchange.

The second part of this thesis, which is given in Section 7, deals with the NMR spectroscopic investigation of polysilicide Zintl anions in liquid ammonia. Here, high resolution NMR is able to provide important information about the solution behaviour of polysilicides. First promising results are obtained and will soon be published.

2. NMR of Organocopper Compounds*

Tobias Gärtner and Ruth M. Gschwind

* Tobias Gärtner and Ruth M. Gschwind

NMR of Organocopper Compunds in The Chemistry of Organocopper Compunds

Rappoport, Zvi / Marek, Ilan (Eds.)

Wiley-VCH, 1st edition - November 2009;

2.1 Introduction

The importance of Nuclear Magnetic Resonance (NMR) spectroscopy for the structure elucidation of inorganic materials, organometallic complexes, and metal containing biological systems is well documented by numerous recent publications.[1-9] In these studies, the direct NMR observation of metal resonances provides valuable information about the physical and chemical environment of the metal atom and additional information is gained from investigations of the ligand resonances. However, for copper compounds there was little information available about NMR of copper substances in the early volume, "The chemistry of the metal-carbon bond", of the Patai´s series in 1982. Neither direct copper detected nor ligand detected structural information was available, which was interpreted as "possibly indicating a lack of interest in Cu(I) chemistry".[10] Since that time, the relevance of organocopper complexes has grown dramatically. This is documented by a series of recent reviews, which describe the wide applicability of organocopper compounds in catalytic and stoichiometric organic reactions and the actual interest in their reaction mechanisms.[11-23] The high relevance in organic synthesis also necessitates a better understanding of the structure and dynamics of organocopper compounds, in order to enable faster reaction optimisation processes and to some extent a rational control of the reactivity.

However, the NMR properties of the two copper isotopes (Table 1) allow the direct NMR detection of copper resonances mainly in highly symmetric structural arrangements due to their high quadrupole moments. Therefore, for most of the copper complexes, the NMR spectroscopic approach relies on different NMR active nuclei available in the ligands. In Table 1, the NMR properties[24] of selected isotopes, which have been used successfully in structure elucidation of various organocopper compounds, are given.

Nowadays, NMR is the most powerful method for structure analysis in solution, but it is an indirect method and not a direct one, as e.g. X-ray analysis. Therefore, for an accurate structure elucidation via NMR, a sufficient number of structure parameters have to be spectroscopically available. Due to the fact that organocopper compounds and copper complexes often form highly symmetrical supramolecular structures, the available NMR parameters, such as chemical shifts δ, scalar couplings *J*, dipolar interactions, and diffusion coefficients, sometimes do not reveal sufficient information for a complete and independent structure determination by NMR. Therefore, in structure elucidation of copper complexes in solution, very often information from X-ray structures, theoretical calculations, and further

spectroscopic methods are combined with NMR spectroscopic results to reveal structural aspects.

Table 1. Nuclear properties (spin quantum number I, natural abundance N.A., gyromagnetic ratio γ, quadrupole moment Q, and receptivity $R_{N.A.}$ relative to ^{13}C) of isotopes used for NMR investigations on organocopper compounds.

isotope	I	N.A.(%)	γ (10^7 rad $s^{-1}T^{-1}$)	Q (10^{-30} m^2)	$R_{N.A.}$
^{1}H	1/2	99.985	26.7522205	-	$5.87•10^{3}$
^{6}Li	1	7.59	3.937127	-0.0808	$3.79•10^{0}$
^{7}Li	3/2	92.41	10.397704	-4.01	$1.59•10^{3}$
^{13}C	1/2	1.108	6.728286	-	$1.00•10^{0}$
^{15}N	1/2	0.37	-2.7126188	-	$2.23•10^{-2}$
^{31}P	1/2	100	10.8394	-	$3.91•10^{2}$
^{63}Cu	3/2	69.09	7.111791	-22.0	$3.82•10^{2}$
^{65}Cu	3/2	30.91	7.6043	-20.4	$2.08•10^{2}$

2.1.1. General Aspects of NMR of Organocopper Compounds

In solution and solid-state NMR spectroscopy, the direct detection of Cu resonances show some limitations, which are typical for nuclei with large quadrupole moments. Copper possesses two NMR active natural isotopes, ^{63}Cu and ^{65}Cu, with a natural abundance of 69% and 31%, respectively. Both have gyromagnetic ratios similar to that of ^{13}C and their receptivities show very acceptable values, with the slightly better one for ^{63}Cu (Table 1). However, the most restricting parameter for NMR of copper isotopes is the large quadrupole moment (Q) of both copper isotopes. Quadrupole moments arise in every nuclei with a spin quantum number $I \geq 1$ and Table 1 shows, that the NMR spectroscopically favourable isotopes ^{6}Li and ^{7}Li also possess quadrupole moments. This seeming contradiction is caused by the fact that the principal NMR accessibility of an isotope depends on the absolute value of the quadrupole moment and of the electric field gradient (EFG) across the nucleus, with large values being detrimental in case of both parameters. In the following, the influence of quadrupole moment and EFG is shortly explained to understand the limitations in copper NMR.

The quadrupole moment is a measure of the deviations from the spherical symmetric charge distribution of the nucleus, which can be either prolate (lengthened) or oblate (flattened). Consequentially, a quadrupole nucleus owns degenerate energy levels due to different orientations of the quadrupole, in addition to the nuclear spin orientations and further transitions between these energy levels are possible, which are used in Nuclear Quadrupole Resonance (NQR). These energy levels are quantised and split according to an electronic field gradient (EFG), which results from an asymmetric charge distribution around the nucleus due to an anisotropic arrangement of neighbouring electrons and atoms. In solution, the quadrupole coupling cannot be detected due to the isotropic tumbling of the molecules, but acts as an effective relaxation source and can lead to an enormous line broadening of the signals. The effective amount of quadrupolar relaxation is directly correlated with the magnitude of Q^2 and the local EFG.[24-28] As a result, complexes with a high symmetry, i. e. small EFGs and/or small quadrupole moments, show advantageous NMR properties.

In the case of $^{63/65}$Cu NMR spectroscopy it could be shown, that in highly symmetric tetrahedral Cu(I)L_4 or octahedral Cu(I)L_6 complexes the EFGs in these complexes are sufficiently minimized to enable the detection of copper resonances.[26] Contrarily, already an exchange of only one ligand at the copper site to a Cu(I)L_3L'-type structure usually leads to extremely broad line widths or even to an undetectable copper signal. Even for CuL_4 complexes, disturbances of the symmetry induced by solvent, temperature, concentration, or chemical composition are observed as line broadening of the signals.[29-32] Recently, it was also reported that in the case of Cu(I)L_3L'-type complexes the right choice of the ligands reduces significantly the line width by matching exactly the EFG.[31] Nevertheless, despite the large restrictions in NMR spectroscopy of Cu(I) complexes in solution, quite a large amount of $^{63/65}$Cu spectra of highly symmetrical complexes with varying ligands, e.g. phosphites,[27,30,33-37] phosphines,[35,38,39] diphosphines,[38,40-45] nitriles,[29,30,32,36,37,46-55] and carbonyl compounds[26] are reported in literature and some reviews have been published.[25,26,28,56] For copper complexes with reduced symmetry and not detectable copper resonances, only the NMR active nuclei of the ligands can be used for structure elucidation.

In addition, the line widths of all NMR signals are very sensitive to the presence of paramagnetic compounds. Therefore, it is of great importance to avoid paramagnetic nuclei in high resolution NMR. Considering organocopper compounds, the Cu oxidation states +I and +II are by far the most common and only the diamagnetic Cu(I) is observable via NMR. For paramagnetic Cu(II) compounds electron spin resonance (ESR) is the method of choice.

Therefore, for the application of high resolution NMR spectroscopy the absence of Cu(II) ions is very important, because otherwise the line broadening effects are tremendous.[30] In recent studies, the copper oxidation state +III becomes more and more important.[57-59] In this case the ligand field theory predicts for the d^8 electron configuration of Cu(III) a structure dependent situation, where square planar complexes are diamagnetic and tetrahedral ones are paramagnetic. For square planar Cu(III) complexes, this could be experimentally confirmed and consequently tetrahedral and square planar complexes should be distinguishable by different line widths. Hence, NMR spectroscopy of organocopper reagents is rather restricted to Cu(I) and square planar Cu(III) compounds.

2.1.2. NMR Techniques Applied to Organocopper Compounds

High resolution NMR investigations are in general based on the determination of the fundamental NMR parameters chemical shift and scalar coupling. The chemical shifts of $^{63/65}$Cu resonances in different copper complexes can reach the higher positive or negative three-digit area (~ -400 ppm to 800 ppm).[26,60] Originally, CuCl or $K_3[Cu(CN)_4]$ in D_2O were used as standards for $^{63/65}$Cu, but nowadays a solution of the tetrakis(acetonitrile) complex $[Cu(CH_3CN)_4]^+$ is commonly accepted and acts as chemical shift reference of 0 ppm.[26] Because in organocopper chemistry severe line broadening effects very often lead to undetectable $^{63/65}$Cu resonances, the chemical shift values and the coupling patterns of other nuclei, such as ^{1}H, ^{13}C, $^{6/7}$Li, and ^{31}P, are used for structure elucidation.

Besides the chemical shift, the information from scalar coupling constants, i.e. the multiplicity of the signals, is the second important classical parameter in high resolution NMR spectroscopy. Due to the unfavourable nuclear properties of $^{63/65}$Cu, direct couplings to copper are only detected in highly symmetrical complexes. In complexes with reduced symmetry sometimes valuable scalar couplings to the NMR active nuclei across copper are reported. For example, in temperature dependent studies of copper-phosphoramidite complexes,[61] and in organocuprate Cu(I) or Cu(III) π-intermediates,[57-59,62-65] either direct observations of scalar coupling constants across copper or magnetisation transfers via scalar couplings across copper were possible. These studies show that not only the absolute electronegativities and the resulting EFGs are the critical factors for the detection of scalar couplings between ligand nuclei across copper, but also the exchange rate, i.e. the lability of the ligands.

Especially for structural studies of lithium organocopper compounds and intermediates, fully and partially ^{13}C-labelled compounds were synthesized with much effort in order to

observe reliable $J_{H,C}$ and $J_{C,C}$ coupling constants. In achiral Cu(I) π-complexes, INADEQUATE and HMBC experiments were successfully applied for the determination of $J_{C,C}$ and $J_{H,C}$ magnetisation transfers in partially labelled complexes. This spectroscopic approach without any scalar couplings to Li is in contrast to that of other organometallic compounds like e.g. organolithium reagents, where direct scalar couplings to Li are commonly used to determine structures and aggregation levels in solution.[66-74] When Li ions are part of organocopper reagents, the applicability of $J_{Li,X}$ scalar couplings depends on the individual binding properties. For lithium amidocuprates, the existence of $J_{Li,N}$ couplings facilitates the data interpretation, whereas in the case of lithium dialkylcuprates the covalent character of the organocopper-lithium bonds is not sufficient for a detection of scalar couplings.

In addition to chemical shifts and scalar couplings, qualitative dipolar $^{1}H,^{1}H$ homonuclear and $^{1}H,X$ heteronuclear (X = $^{6/7}Li$, ^{13}C, ^{15}N) interactions can provide further structural details[75-86] and the next step of structural refinements is the quantitative determination of NOEs or HOEs, which provide distances between different nuclei. In most of the organic molecules and organometallic complexes with several dipolar interactions, it is possible to assign one NOE/HOE to a known distance, which then serves as a distance reference for the other NOEs and HOEs. In the case of organocuprates, which form highly symmetric species by supramolecular assembling (Section 2.2.3), quantitative NOEs or HOEs for distance measurements are difficult to access, because sometimes only one resonance signal exists. Even for these systems a quantitative NOE/HOE determination is possible, but for that the reintroduction and determination of correlation times τ_C and the measurement of build up curves is necessary.[87] For example, the estimation of τ_C of organocuprates was made via the maximum HOE enhancement η_{max} of the ^{1}H-^{6}Li HOE and with the help of the Solomon equations.[87,88] The initial build up rate $\sigma_{^{1}H,^{6}Li}$ of the HOE (Figure 1) then provides the H-Li distance. Because in the cross relaxation rate of the ^{1}H-^{6}Li HOE the distance r_{H-Li} is the only unknown parameter, in case the correlation time, the isotope specific constants, the gyromagnetic ratio γ and the resonance frequency ω are known (equation 1).

$$\sigma_{^{1}H,^{6}Li} = \frac{4}{15}\left(\frac{\mu_0}{4\pi}\right)^2\left(\frac{h}{2\pi}\right)^2\frac{\gamma_H^2\gamma_{Li}^2}{r_{H-Li}^6}\tau_C\left[\frac{6}{1+(\omega_H+\omega_{Li})^2\tau_C^2}-\frac{1}{1+(\omega_H-\omega_{Li})^2\tau_C^2}\right] \quad (1)$$

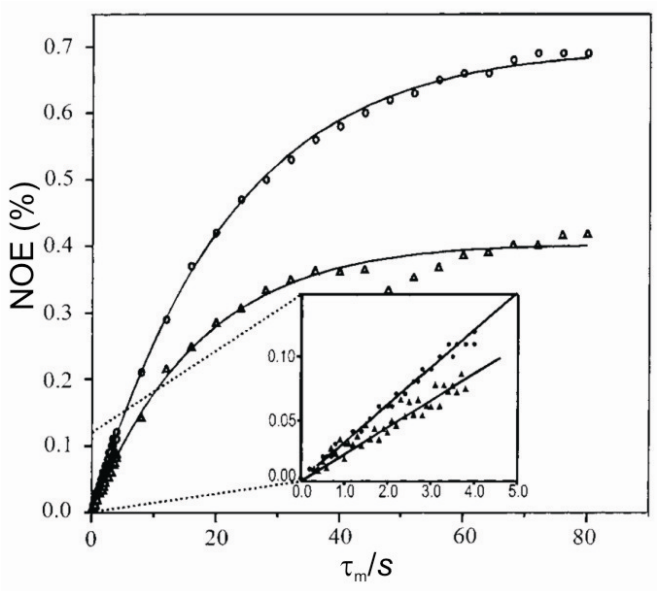

Figure 1. $^{1}H,^{6}Li$ buildup curves of Me_2CuLi•LiCN (△, **1**•LiCN) and Me_2CuLi (○, **1**), both 0.72 M in diethyl ether at 239 K. The initial buildup region is enlarged.[87]

The determination of homonuclear ^{1}H-^{1}H NOE buildup curves in highly symmetric molecules sometimes requires a determination of NOEs between chemically equivalent groups. In these structures the symmetry problem can be solved by using the two different isotopomers ^{1}H-^{13}C and ^{1}H-^{12}C (Figure 2a). The basic experiments for this purpose are the HMQC-ROESY[89] and the HSQC-NOESY pulse sequences.[90] However, in the case of long inter proton distances, even with a 20% ^{13}C labelling the sensitivity of these two methods is too low, because mixing times up to 1s have to be used, which lead to an extreme diffusion-like signal attenuation caused by the applied pulsed field gradients.

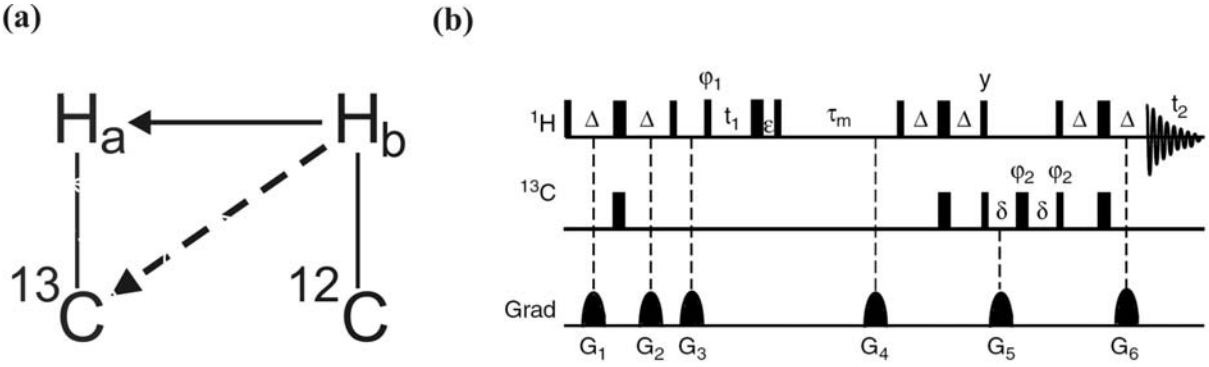

Figure 2. (a) Schematic description of the two different isotopomers, which are used in (b) the NOESY-HSQC to determine $^{1}H,^{1}H$ NOEs between chemically equivalent groups.[91]

To circumvent this obstacle, a NOESY-HSQC pulse sequence was developed, in which the gradients for coherence selection are separated only by short refocusing delays and diffusion effects are minimised (Figure 2b). This approach was successfully applied to organocuprates.[87,91] The pulse sequences used in exchange spectroscopy (EXSY) are closely related to the basic NOESY experiments. Both pulse sequences are identical and only the length of the mixing time is varied. The EXSY experiments can be used to detect and quantify exchange processes, which are slow on the NMR time scale, without applying temperature dependent NMR, which would be disadvantageous in case of temperature sensitive compounds.

A NMR spectroscopic method for the determination of the size of supramolecular assemblies is the diffusion ordered spectroscopy (DOSY).[84,86,92-96] In DOSY experiments the spatial molecular motion in solution by virtue of thermal energy is used for the determination of self diffusion coefficients. In the 1960´s Stejskal and Tanner[97] carried out the first PFG-SE-Experiment (Pulsed-Field-Gradient Spin-Echo). Due to the change of the spatial position within a distinct time interval between two pulsed gradients, an attenuation of the signal is observed, which can be used to calculate the self diffusion coefficient. The obtained diffusion coefficient D is inversely correlated to the hydrodynamic radius r_H, which is a measure of the size of supramolecular assemblies. For an accurate calculation of the hydrodynamic radius from the experimental diffusion coefficients a modified Stokes-Einstein equation (equation 2) has to be applied, which considers the relative solvent/solute size (c) and the shape of the molecules (f_S).[93,98]

$$D = \frac{kT}{c(r_{solv}, r_H)\, f_S \pi \eta r_H} \quad (2)$$

In equation 2, k represents the Boltzmann constant, T the temperature, and η the viscosity of the solvent. For reliable, reproducible and quantitative DOSY measurements, variations in the viscosity and possible contributions of thermal convection have to be especially considered. Viscosity changes, e.g., due to variable sample composition or concentration have to be eliminated via viscosity standards.[93,99] Convection in the NMR tube can falsify the diffusion value dramatically, because of the principal translational character of the self diffusion coefficient. Convection effects are significantly present in high or low temperature measurements and strengthen with increasing difference from room temperature. To compensate contributions from ideal convection, a convection compensating pulse sequence,

developed by Jerschow and Müller, is a reliable method.[100] Later on, attempts were made to circumvent the low sensitivity of this method by shorter and more sensitive pulse sequences.[101]

For the stabilisation of reaction intermediates rapid injection NMR (RI-NMR) is a very promising technical approach, which was developed in the last twenty years.[102,103] An insert inside the NMR spectrometer allows to inject substances directly into the NMR tube, while the tube remains in the probe ready for the next experiment. This technique affords minimal dead times between injection and NMR detection and is therefore ideal for the observation of reaction intermediates with short life times.

2.2 NMR Structure Determination of Organocopper Reagents

2.2.1. Stoichiometric Organocopper Reagents, an Introduction

The chemistry of stoichiometric organocopper(I) compounds is mostly covered by the chemistry of organocuprates. Since the first observations of Gilman and Straley,[104] who found soluble organocopper reagents after treatment of copper(I)salts with two equivalents of organolithium reagents, organocuprates have become a widely used organometallic reagent in organic synthesis. The general synthesis of homoleptic organocuprates is given in Scheme 1a. The reaction of 1 equivalent Cu(I) salt and 2 equivalents of organolithium compound yield the desired Gilman-type cuprate.[104] Using Grignard or organozinc reagents, instead of alkyllithium, Normant-type[105,106]or Knochel-type[107] cuprates are derived, respectively.

Scheme 1. Schematic description of the synthesis of (a) homoleptic Gilman cuprates (b) heteroleptic cyano cuprates and (c) heteroleptic amidocuprates.

In case that only one equivalent of alkylation agent is used, heteroleptic organocuprates (Scheme 1b) or amidocuprates (Scheme 1c) are obtained, which are sometimes of higher synthetic importance, due to the non-transferable ligand.[108] Especially the amidocuprates provide the introduction of chiral information via substituted chiral amido ligands.[109] Considering the three equations in Scheme 1, it is obvious that the exact ratio of copper(I) salt

to the alkylation agent is crucial, when the structures of free organocuprate reagents are discussed. In comparison to the synthetically highly valued heteroleptic cuprates, the Gilman-type dimethyl cuprates Me_2CuLi (**1**) have become a generally accepted model for mechanistic and structural studies on copper mediated reactions. The structure elucidation of these Gilman cuprates caused the famous and long standing scientific discussion about "higher order" and "lower order" organocuprates,[110] which could be finalized in favour of the Gilman cuprates,[110] and continued with numerous theoretical and spectroscopic studies about the structures and reaction intermediates of dimethyl cuprates.[19,111,112]

Synthetically, it was early recognized that dialkylcuprates (Scheme 1a) are able to form highly chemo- and diastereoselectively C-C bonds and this property is used throughout organic synthesis.[108,113-115] Scheme 2 shows schematically the three standard reaction types of organocuprates, addition reactions to unsaturated carbonyl compounds (Scheme 2a), S_N2-like substitution reactions (Scheme 2b), and S_N2' allylic substitutions (Scheme 2c).

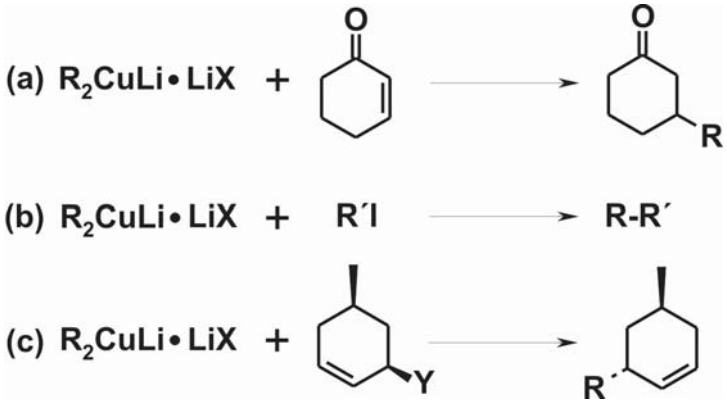

Scheme 2. Schematic description of (a) the 1,4-addition to α,β-unsaturated Michael acceptors, (b) S_N2-like substitution reactions and (c) S_N2' allylic substitution reactions of Gilman cuprates (X = CN, I; Y = halide, OAc).

Amidocuprates are also frequently used reagents in synthesis.[108,116-119] If additional redox agents, e.g. chloranil, are used, even coupling reactions between the alkyl- and the amido substituents are possible and therefore amidocuprates provide access to tertiary amines.[116-118]

The famous discussion about "higher order" organocuprates started, because Lipshutz and coworkers had reported higher reactivities of cyanocuprates than of iodocuprates.[120,121] Also later on, strong salt and solvent dependencies were found in synthetic studies of various organocuprate reactions.[108,122] Even the only two detailed studies with experimental setups enabling a direct comparison of the reactivities of cyano- versus iodocuprates show deviating results. In a study using logarithmic reactivity profiles similar reactivities were reported for

iodo- and cyanocuprates,[123] whereas a combined kinetic and spectroscopic study showed higher reactivities of the cyanocuprate in pure diethyl ether.[124] The identification of the Gilman type cuprates as the dominating monomer structure in solution for all dialkylcuprates[110] shifted the focus to possibly different supramolecular cluster structures of cyano- and iodocuprates as the reason for the deviating reactivities. Especially in diethyl ether, colligative measurements,[125-127] broad line widths in ^{13}C and ^{15}N spectra,[128] crystal structures,[129,130] and mass spectrometric investigations[131] consistently indicated supramolecular aggregation to be present. In 2005, the deviating reactivity of cyanocuprates and iodocuprates (Figure 3) as well as salt-free cuprates were explained by different supramolecular structures in solution by using combined kinetic and NMR spectroscopic studies of 1,4-addition reactions (Scheme 2a).[132] This study revealed that the variations in the reaction rates of **1**•LiI (Figure 3a) and **1**•LiCN (Figure 3b) in diethyl ether upon addition of THF correlate with a disaggregation of the supramolecular structure or solvent induced changes in the supramolecular cluster structures (see Section 2.2.3).

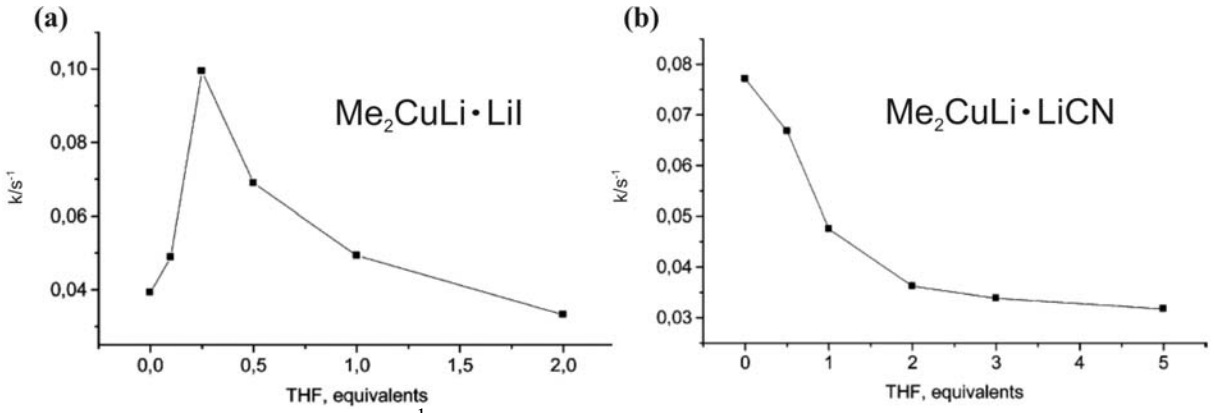

Figure 3. Rate constants k (s^{-1}) of the 1,4-addition reaction of (a) Me_2CuLi•LiI and (b) Me_2CuLi•LiCN to 4,4-dimethylcyclohex-2-enone in diethyl ether upon addition of THF.[124]

Also in the stabilisation and structure elucidation of organocuprate intermediates, impressive progress has been made during the last decade. Investigations on reaction intermediates of addition reactions revealed Cu(I) π-complexes as important intermediate structures[62,63,133-135] and in the past few years even the detection of decisive Cu(III) intermediates in addition, as well as in S_N2-like/S_N2' substitutions had been successful.[57-59,64,65]

In the course of structure determination of the supramolecular complexes and the intermediates of organocuprates in solution, NMR spectroscopy turned out to be a very powerful method even for complicated and highly symmetric aggregate structures. Especially,

a step by step NMR analysis of small structural aspects in combination with results from theoretical calculations and X-ray analyses allowed solving structural details of organocuprates and their intermediates, a knowledge, which is crucial for further developments in organocopper chemistry.

2.2.2. Diorganocuprates – The Free Reagent

2.2.2.1 Monomer structure

The reliable determination of the monomer structure was the basis for the structure elucidation of the free organocuprate reagent and its supramolecular structures in solution. At first, δ chemical shift values served as a source for structure information. However, with the chemical shifts as sole structural parameters, the differentiation of homoleptic and heteroleptic organocuprates was difficult and the influence of solvent, aggregation and temperature on organocuprates could not be explained for decades. Hence, the discussion about "higher order" ($R_2Cu(CN)Li_2$) and "lower order" ($R_2CuLi•LiCN$) cuprates had not been finalized for a long time.[110]

"Higher order" cuprates were proposed to have three ligands attached to one Cu(I) centre in contrast to the "lower order" cuprates, in which two ligands are bound to Cu(I). To detect these differences in the coordination sphere of copper the measurement of $^2J_{C,C}$ coupling constants across copper is a powerful method. The existence of scalar couplings directly reveals the connectivity in the complexes and the number and arrangements of the substituents is evident from the multiplicity pattern and the absolute coupling constant value of the signals. For this purpose $^2J_{C,C}$ coupling constants were determined in samples with and without cyanide containing cuprates to give evidence for either "higher order" or "lower order" cuprates. First, $^2J_{C,C}$ coupling constants in 1D ^{13}C spectra were observed in heteroleptic RCu(CN)Li cuprates in THF, with phenyl, ethyl and methyl groups as substituents (Table 2).[136] The fact that one cyanide and one alkyl substituent are bound to the same Cu-centre was proven upon ^{13}C labelling of the cyanide, which caused a doublet splitting of the alkyl group. Exemplarily, temperature dependent ^{13}C chemical shifts and $^2J_{C,C}$ of heteroleptic MeCu(CN)Li (**2**) and EtCu(CN)Li (**3**) are listed in Table 2. Interestingly, the coupling constants in Table 2 show strong temperature dependencies, that is, starting from a minimum value of 12.3 Hz, the absolute values increase with decreasing temperature, indicating similar

structures at low temperature and a partial decoupling at higher temperatures due to exchange processes.

Table 2. ^{13}C NMR chemical shift values and $^{2}J_{C,C}$ coupling constants of selected heteroleptic cuprates at different temperatures in THF or diethyl ether as solvent.[136]

cuprates	solvent	T/°C	C1, (ppm)	$^{2}J_{C,C}$/Hz	CN, (ppm)
$^{13}CH_3Cu(^{13}CN)Li$ (**2***)	THF-d_8	-78	-12.85		149.34
	THF-d_8	-100	-12.60		149.13
	THF-d_8	-110	-12.46	20.8	148.97
$CH_3Cu(^{13}CN)Li$ (**2**)	ether-d_{10}	-78	-12.58		151.01
	ether-d_{10}	-100	-12.25		150.20
	ether-d_{10}	-110	-12.10	12.3	149.95
	ether-d_{10}	-120	-11.93	21.6	149.78
$CH_3CH_2Cu(^{13}CN)Li$ (**3**)	THF-d_8	-78	1.64	21.6	149.11
	THF-d_8	-100	1.74	22	148.96
	ether-d_{10}	-78	1.85		150.86
	ether-d_{10}	-100	1.89	20.8	150.10

For example, at -110 °C, the $^{2}J_{C,C}$ coupling constant of **2** in diethyl ether is significantly smaller than that of **2*** in THF. But a temperature reduction of a sample of **2** to -120 °C causes a $^{2}J_{C,C}$ coupling constant even slightly larger than that of **2*** at -110 °C. A comparison of $^{2}J_{C,C}$ of **3** in THF at -78 °C (21.6 Hz) and -100 °C (22 Hz) suggests a maximum of the experimental coupling constant at the range of $^{2}J_{C,C}$ = 20.8 - 24.2 Hz. These results showed that it is principally possible to determine the number and kind of organic substituents on copper by measuring scalar couplings across copper. Therefore, this approach was ideal to prove or disprove the existence of "higher order" or cyano-Gilman cuprates in solution. For this purpose, the scalar coupling patterns of ^{13}C labelled Me_2CuLi (**1**) and Me_2CuLi•LiCN (**1**•LiCN) were measured in THF (Figure 4).[137]

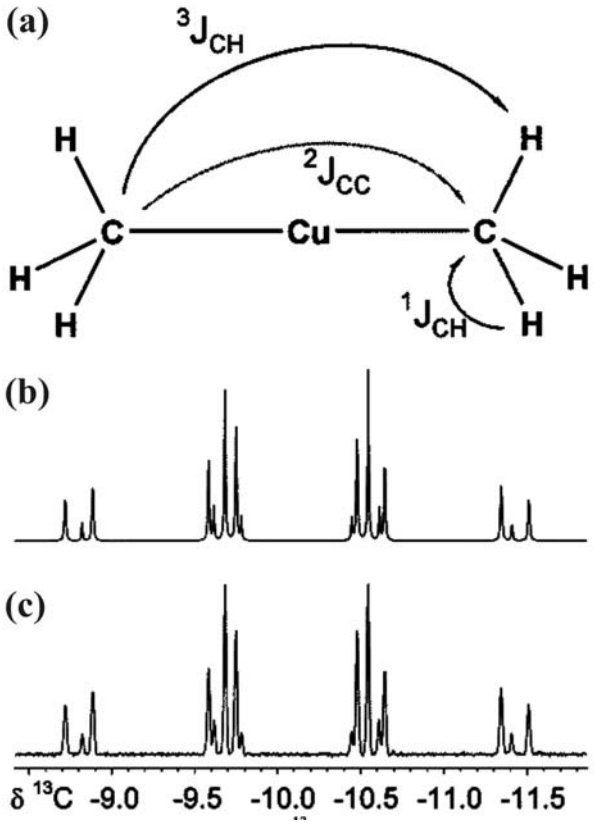

Figure 4. (a) Monomeric cuprate unit with the observed scalar couplings indicated by arrows; (b) simulated and (c) experimental ^{13}C spectrum of Me_2CuLi (**1**) in THF. The detection of identical $^1J_{C,H}$, $^2J_{C,C}$, and $^3J_{C,H}$ scalar coupling constants in 1D ^{13}C spectra of Me_2CuLi•LiCN showed that the Gilman cuprate is the general structure for all dialkylcuprates.[137]

The salt free cuprate Me_2CuLi (**1**) was used to provide the coupling constants of the basic Gilman dimethyl cuprate unit (Figure 4a) and interestingly for both salt containing cuprates Me_2CuLi•LiCN (**1**•LiCN) and Me_2CuLi•LiI (**1**•LiI) an identical multiplicity pattern compared to **1** (Figure 4c) was detected. A comparison with simulated spectra (Figure 4b) showed clearly the existence of an $A_3XX'A_3'$ spin system, which reveals identical "lower order" cuprate structures for **1**•LiCN and **1**•LiI.[137] In addition, the simulation provided the scalar coupling constants of $^1J_{C,H}$ = 109.5 Hz, $^2J_{C,C}$ =21.0 Hz, and $^3J_{C,H}$ = -0.8 Hz. A comparison of the $^1J_{H,C}$ scalar coupling with the one of MeLi ($^1J_{H,C}$ = 98 Hz) reveals the metal bound character of the methyl group and the value of $^2J_{C,C}$ = 21 Hz is in accordance with the maximum $^2J_{C,C}$ values of the heteroleptic organocuprates in Table 2. From these results, a linear structure with either two alkyl substituents or alkyl/cyanide (1:1) can be concluded for homoleptic cuprates and cyanide containing heteroleptic cuprates, which was also confirmed by various other theoretical and spectroscopic results.[110]

2.2.2.2 Solvent separated ion pairs (SSIPs) vs. contact ion pairs (CIPs)

Numerous synthetic studies revealed a strong solvent dependence of reactions with organocuprates, which hinted at the existence of supramolecular structures in solution being relevant for their reactivity.[122,123,138-140] The first investigations of the aggregation level of organocuprates started with colligative measurements in diethyl ether,[125,126,141] followed by mass spectrometric investigations,[131] NMR spectroscopic measurements,[129,142,143] and theoretical calculations.[111,144-146] Especially theoretical calculations proposed a dimer as minimal cluster, necessary for conjugate addition reactions of organocuprates.[145] In NMR spectroscopic investigations, Li coordinating agents, such as HMPA and crown ethers, influenced the $^{2}J_{C,C}$ coupling constants in heteroleptic cuprates across copper and this effect was attributed to the complexation of the Li cation.[136] Another obvious NMR spectroscopic hint of aggregation was the observation of broad line widths in ^{13}C and ^{15}N spectra of organocuprates in diethyl ether.[128] In addition, a study on phenyl- and diphenylcopper(I) species with variable temperature ^{13}C NMR spectra revealed some details about aggregation. An examination of δ(*ipso*-C) showed that for differently aggregated PhLi and Ph_2CuLi complexes the chemical shift of the *ipso*-C decreases with an increasing number of metal atoms bound to it (Figure 5),[143] an effect which can be attributed to the paramagnetic shielding term.[147]

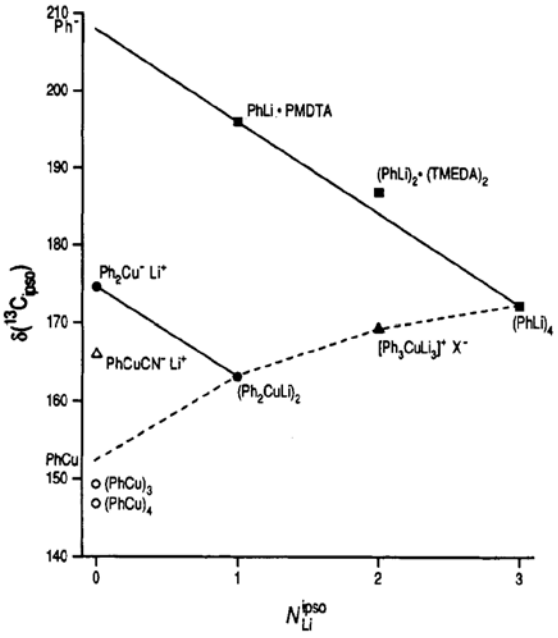

Figure 5. Plots of $\delta(^{13}C_{ipso})$ *vs* $N_{ipso}(Li)$, the number of Li atoms per ipso-C. Note that the $(Ph_2CuLi)_n$ line (●) is parallel to the $(PhLi)_n$ line (■).[143]

Figure 5 shows that for PhLi a chemical shift decrease of approximately 25 ppm is observed upon aggregation to $(PhLi)_4$, and the aggregation from Ph_2CuLi to $(Ph_2CuLi)_2$ causes a decrease of approximately 15 ppm.[143] But this useful correlation seems to be only valid for diphenylcuprates, because the homoleptic and heteroleptic alkylcuprates **1**, **1**•LiI, **1**•LiCN, **2,** and **3** (Table 2) show only small and even increasing chemical shift difference switching from THF (monomers) to diethyl ether (supramolecular aggregates).

Another NMR spectroscopic approach was initiated by the observation of different aggregation levels in crystal structures. Polar solvents like THF and Li coordinating agents force the cuprate to form solvent separated ion pairs (SSIPs, Figure 6b), while diethyl ether, which is a less coordinating, supports the formation of contact ion pairs (CIPs), in which the Li atom is a part of the supramolecular assembly (Figure 6a).

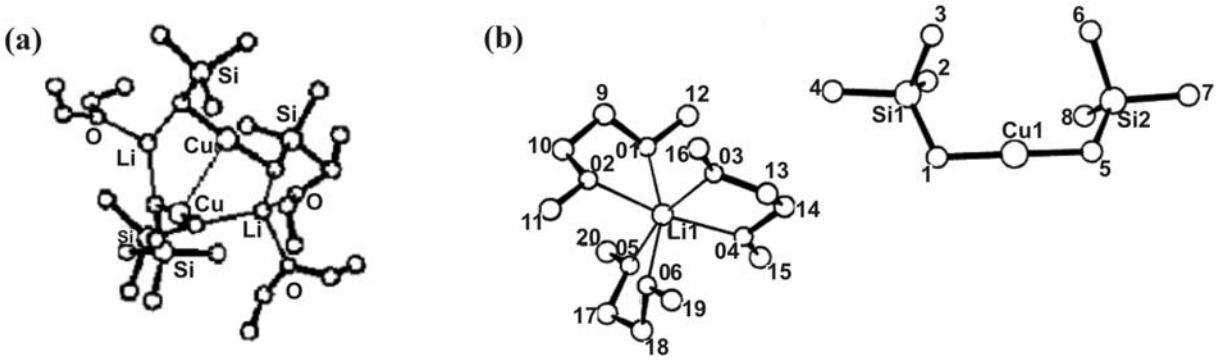

Figure 6. Two examples showing the principle structure of (a) CIPs in $[Li_2Cu_2(CH_2SiMe_3)_4(Et_2O)_3$[129] and (b) SSIPs in $[Li(dme)_3]^+[(Me_3SiCH_2)_2Cu]^-$.[129]

In general, a transfer of structure information from crystal structures to the situation in solution has to be done with great care. In studies of organolithium compounds, it was shown that completely different structures can be present either in solution or in the solid state.[148-151] But with selected NMR measurements, structural aspects of crystal structures can be verified in solution. Traditionally, aggregation studies on Li containing complexes are performed by determination of scalar couplings between Li and the heteroatom, as it is done for lithium amidocuprates (see later this section). However, in the case of homoleptic organocuprates, $J_{Li,C}$ scalar couplings have not been detected up to now. Therefore, in solution aggregation trends and supramolecular structures of organocuprates can only be derived via the measurement of diffusion coefficients and various dipolar interactions. Using Heteronuclear Overhauser Spectroscopy (HOESY), the quite good spectroscopic properties of ^{6}Li and ^{7}Li allow determining qualitative and sometimes even quantitative distances in solution. From

crystallographic[129,130] and theoretical studies[111,144,146,152,153] it was known that in organocuprate CIPs the distances between the Li ions and the alkyl substituents are less than 250 pm, i.e. quite intense HOE cross peaks can be detected. In contrast, in SSIPs the Li atom and the organocuprate units are separated more than 500 pm, which is beyond the cut off limit of HOEs. Therefore, no HOE cross peaks can be detected in SSIPs, if alternative magnetisation transfers via solvent molecules, chemical exchange or concentration dependent background signals can be excluded as accomplished for organocuprates.[142] Consequently, qualitative HOE measurements of organocuprates can be used to reveal the amount of SSIPs and CIPs in different samples, as it was shown for the model reagent Me_2CuLi (**1**) in THF and diethyl ether (Figure 7).[129]

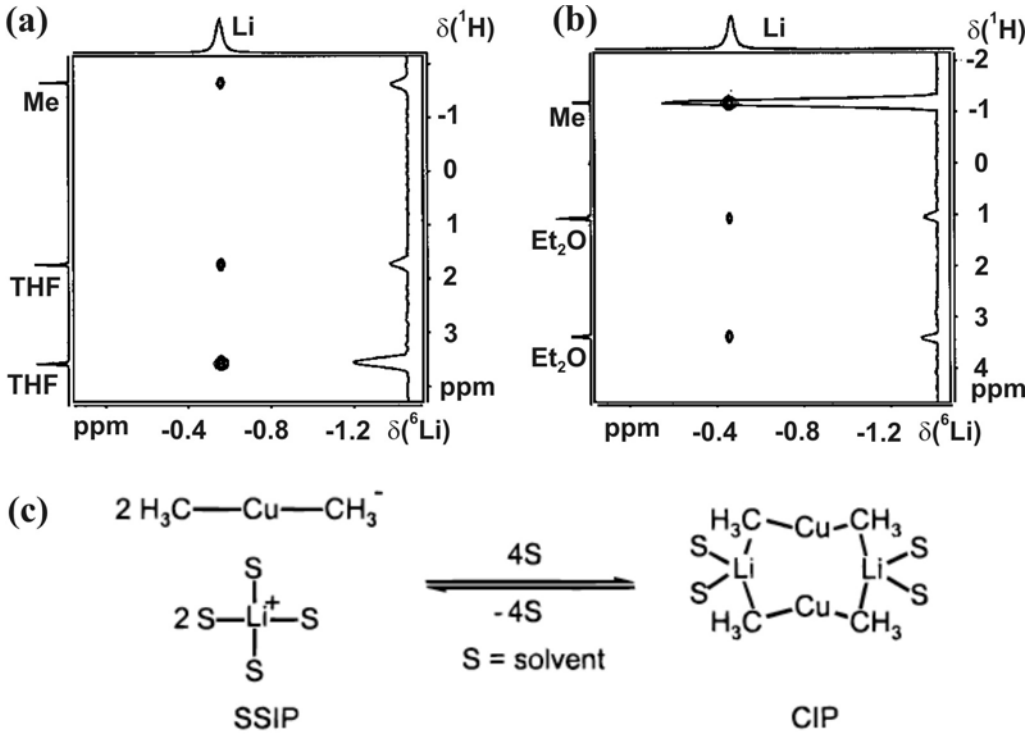

Figure 7. $^1H,^6Li$ HOESY spectra of **1** in (a) THF and (b) diethyl ether and (c) the corresponding equilibrium of solvent separated ion pairs (SSIPs) and contact ion pairs (CIPs); the Me/Li cross peak intensity in (a) indicates only small amounts of CIPs in THF, whereas in diethyl ether (b) mainly CIPs exist.[142]

In THF, a weak interaction between Li and dimethylcuprate and strong cross signals between Li and THF are detected (Figure 7a). In contrast, in diethyl ether the interaction between Li and dimethylcuprate is strong and that between Li and diethyl ether reduced (Figure 7b). To visualise these intensity differences, the 1D projections of the cross peaks are additionally given on the right side of the spectra in Figure 7. These $^1H,^6Li$ HOESY data

clearly indicate that in THF only a small amount of CIPs exist, whereas in diethyl ether the formation of CIPs is preferred. Thus, for organocuprates a solvent dependent equilibrium between SSIPs and CIPs was established in solution. This equilibrium could be correlated with the reactivity of organocuprates in 1,4-addition reactions and in accordance with theoretical calculations,[111] the CIPs were identified as the reactive species.[129]

In order to identify the structure of these synthetically so important CIPs in solution, quantitative ^{1}H, ^{7}Li HOEs and ^{1}H, ^{1}H NOEs of dimethylcuprates were measured in diethyl ether.[87] Salt free Me_2CuLi was used as archetype of organocuprate homodimers and cyanide containing Me_2CuLi•LiCN was used as model for the heterodimer structures, which were proposed in several theoretical calculations.[111,154-160] Based on crystal structures and theoretical calculations, the $^{1}H,^{1}H$ NOE and $^{1}H,^{6}Li$ HOE ratios between homo- and heterodimers were calculated (Figure 8) and the pronouncedly different values, especially for the $^{1}H,^{1}H$ NOE, show that a structure differentiation is possible, if these NMR parameters can be observed.

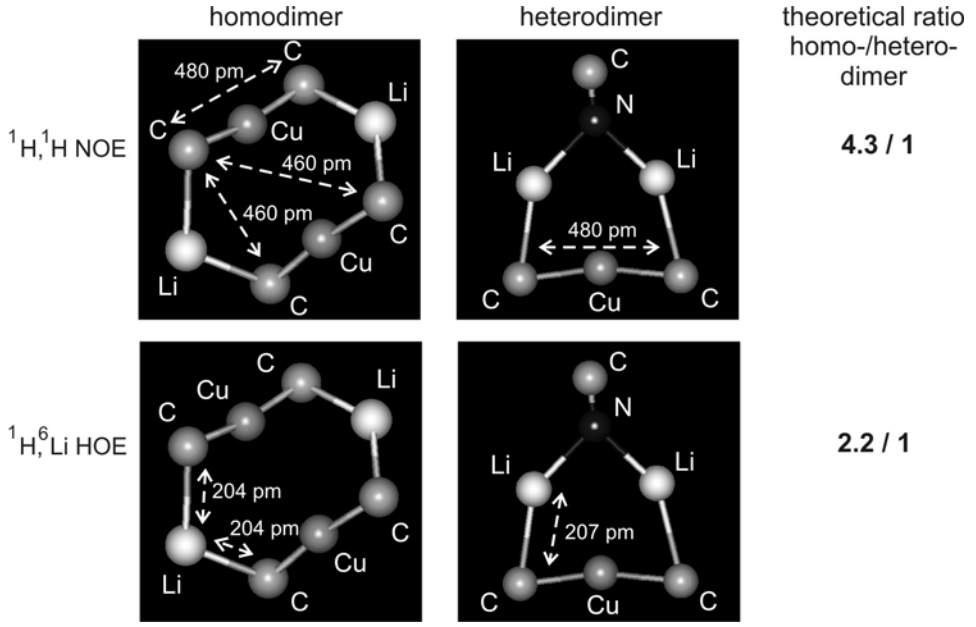

Figure 8. Homodimer, $(Me_2CuLi)_2$, and heterodimer structures (Me_2CuLi•LiCN) of organocuprates with the characteristic distances resulting in differently strong $^{1}H,^{1}H$ NOEs and $^{1}H,^{6}Li$ HOEs.[87]

As evident from Figure 8, the symmetric structures of organocuprates only allow for a detection of $^{1}H,^{6}Li$ HOE, both in homodimers and in heterodimers. This means that no reference distance is available. As a consequence, the correlation time (τ_C) had to be measured and the Solomon equations[88] were used to quantify the 1D HOE build up rates.[87] In

the case of dimethylcuprates, the maximum $^{1}H,^{6}Li$ HOE was used for the determination of τ_C as the most appropriate method.[87] The subsequent analysis of the $^{1}H,^{6}Li$ HOE build up curves revealed similar NOE intensities for both cuprates and H-Li distances of 243 ±3 pm and 242 ±9 pm for **1** and **1**•LiCN, respectively. This indicates very similar homodimer structures of both **1** and **1**•LiCN in diethyl ether. To confirm this conclusion, additionally $^{1}H,^{1}H$ NOE measurements were performed. In the case of **1** and **1**•LiCN, this means that NOEs between chemically equivalent protons has to be detected. Therefore, solutions of 20% ^{13}C labelled cuprates were prepared to differentiate the chemically equivalent groups by means of the different isotopomers ^{1}H-^{12}C and ^{1}H-^{13}C (Figure 9a).

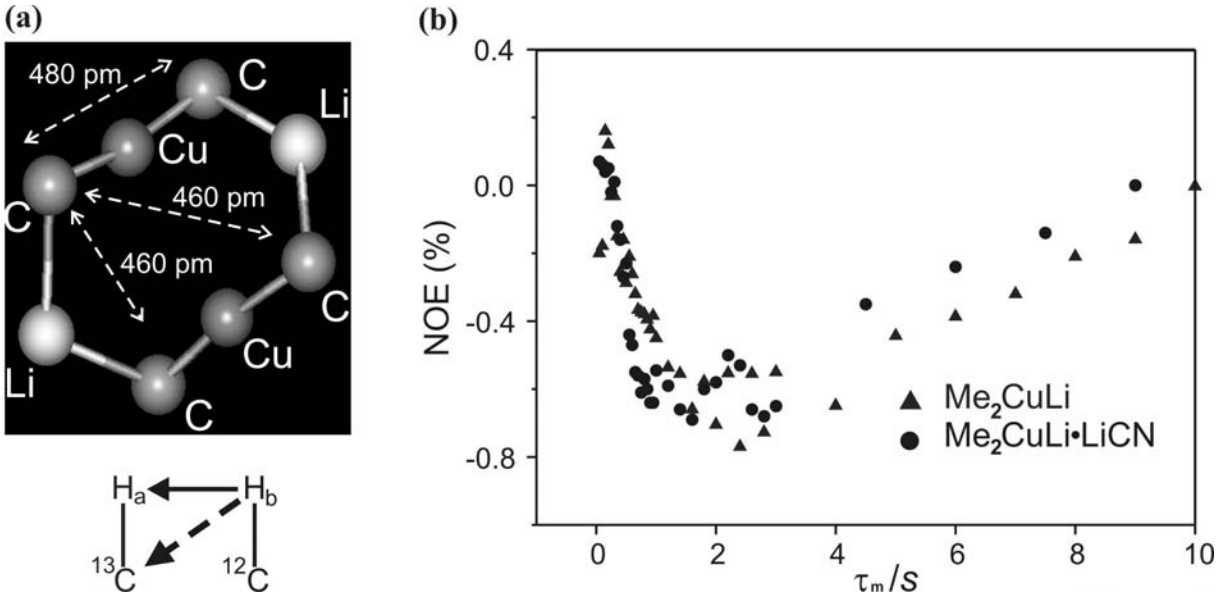

Figure 9. (a) ^{1}H, ^{1}H NOEs between chemically equivalent groups can be detected using the different isotopomers ^{1}H-^{13}C and ^{1}H-^{12}C; (b) ^{1}H, ^{1}H NOE-HSQC build up curves of Me_2CuLi (▲) and Me_2CuLi•LiCN (●) in diethyl ether show a similar structure of both compounds.[87]

This allows to measure NOE build up curves from the central ^{1}H signal (^{1}H-^{12}C) to the ^{13}C satellites (^{1}H-^{13}C isotopomer) with a sensitivity improved 1D NOESY-HSQC pulse sequence.[87] The results for **1** and **1**•LiCN in diethyl ether are displayed in Figure 9b. The build up curves of **1** and **1**•LiCN show a similar curve progression, which corroborates a homodimer structure of both **1** and **1**•LiCN.

In contrast to homoleptic alkylcuprates with lithium exchange rates being fast on the NMR time scale, in the case of lithium amidocuprates slow chemical exchange rates of Li are observed. This enables the detection of different Li signals as well as separated proton signals

in amidocuprates with a reduced symmetry and facilitates the structure elucidation of lithium amidocuprates, because a more classical NMR spectroscopic approach can be applied.

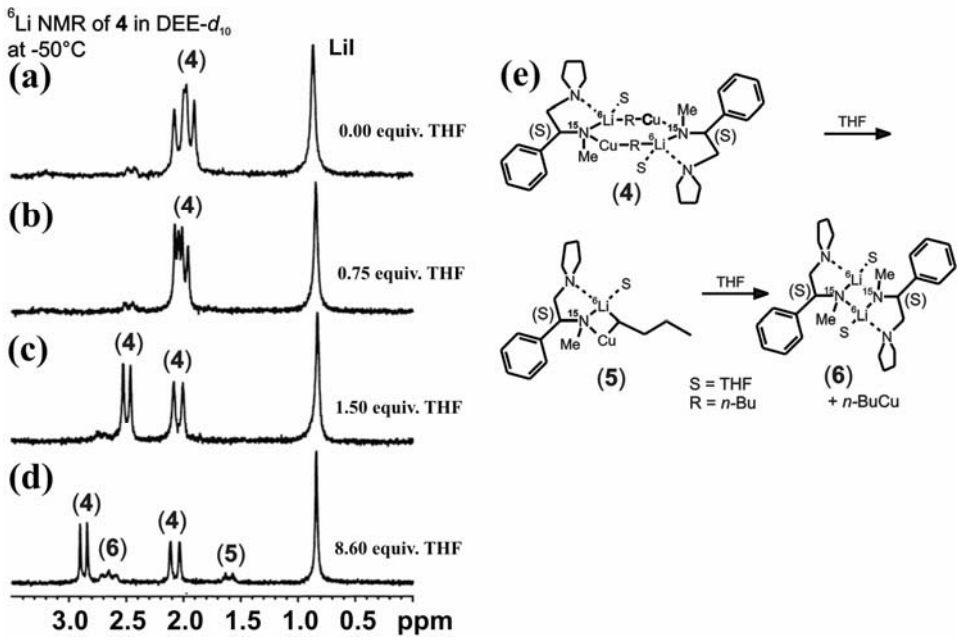

Figure 10. ^{6}Li spectra of **4** in (a) diethyl ether (DEE) and with additional (b) 0.75 equiv, (c) 1.5 equiv, and (e) 8.60 equiv THF; (e) schematic disaggregation process of the dimer upon addition of THF.[109]

As a result, the structure elucidation of amidocuprates is primarily based on different $^{6/7}$Li signals, which allow a detailed interpretation of $J_{Li,N}$ scalar coupling constants and multiplicity patterns (Figure 10a–d), [161-163] and of ^{1}H,$^{6/7}$Li HOESY spectra (Figure 11a) in the classical manner. As an example the ^{6}Li spectra of the amidocuprate **4** are shown in Figure 10, for which $J_{Li,N}$ values and multiplicity patterns in combination with 1D and 2D NMR spectroscopy suggest a dimer structure in diethyl ether, which is disaggregated upon addition of THF.[109] In Figure 10e the proposed disaggregation is shown from the dimer **4** to the monomer **5** and finally to **6**, which consists of separated Li amide and *n*-BuCu compounds. In further studies on $[Cu_2Li_2Mes_2(N(CH_2Ph)_2)_2]$ (**7**), indirectly detected ^{1}H,^{7}Li HOESY spectra[164,165] revealed several species in toluene, which are obvious from different Li signals (Figure 11a). With the aid of lithium chemical shift data,[166-168a] the different species were assigned to the Schlenk-like equilibrium shown in Figure 11b. Recently, similar NMR studies were performed to investigate the influence of THF on the structures and reactivities of these amidocuprates.[168b]

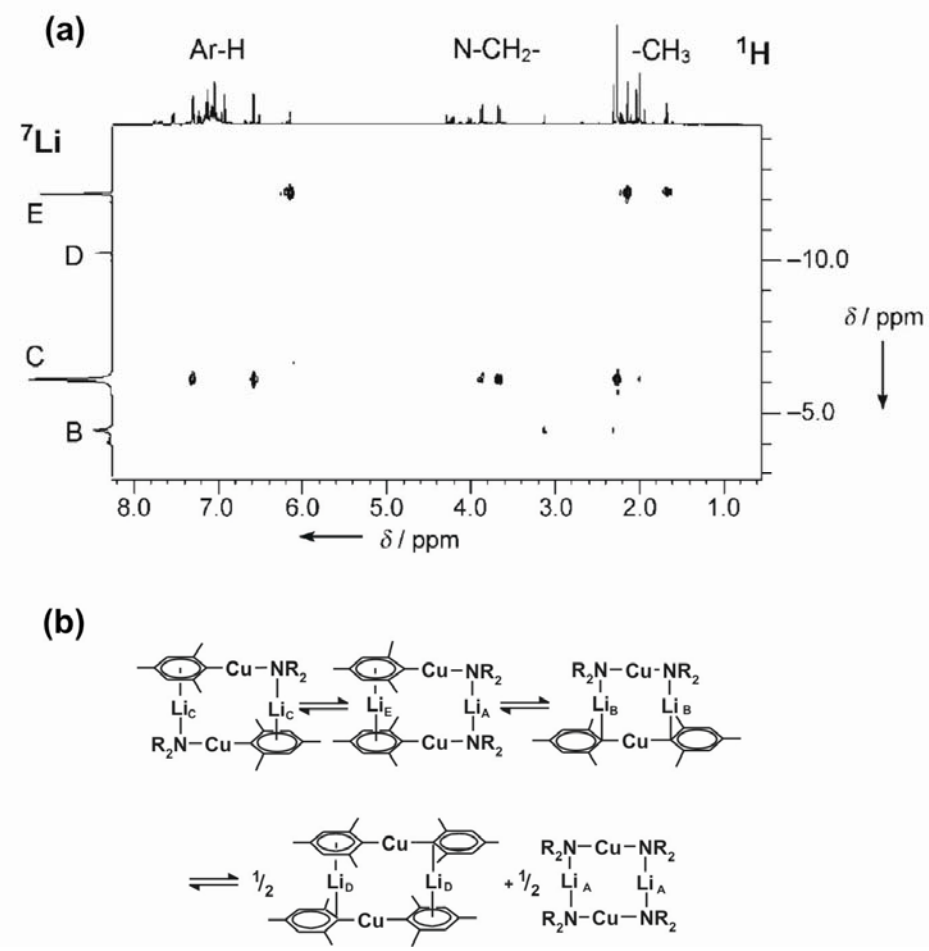

Figure 11. (a) $^{1}H,^{7}Li$ HOESY spectrum of **7**, showing different species in toluene, which are in accordance with (b) a Schlenk-like equilibrium of **7**. The signal of Li_A (~1ppm, not shown) does not show HOE signals, due to broad line width.[167a]

2.2.3. Supramolecular Aggregation

After the homodimeric core structure was elucidated as main structural motif of dialkylcuprates in diethyl ether and the CIPs were identified as the reactive species in 1,4-addition reactions to enones, the question arose whether there possibly exist even higher supramolecular assemblies with impact on the reactivity of these reagents. In the case of the homoleptic dimethylcuprates, **1** and **1**•LiCN, the negative sign of the $^{1}H,^{1}H$ NOE buildup curves (Figure 9b) indicated larger assemblies than homodimers in solution[87] and polymeric structures were found in crystal structures, e.g., that of $[Li_2Cu_2(CH_2SiMe_3)_4(SMe_2)_2]_\infty$ (Figure 12).[130]

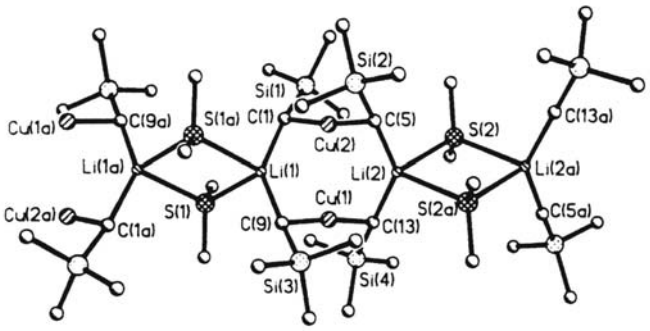

Figure 12. Solid state structure of $[Li_2Cu_2(CH_2SiMe_3)_4(SMe_2)_2]_\infty$ ($[\mathbf{8}_2 \bullet (SMe_2)_2]_\infty$.[130]

Aggregation tendencies beyond the formation of homodimers were additionally indicated by mass spectrometric investigations[131]and broad line width of ^{13}C and ^{15}N signals of organocuprate reagents in diethyl ether.[128] In synthetic studies, an influence of different copper salts, concentrations, and varying alkyl substituents on the reactivity and selectivity of organocuprates was observed.[108] As discussed in detail in Section 2.1.2, pulsed field gradient (PFG) DOSY experiments can be used to measure the diffusion coefficient D of supramolecular aggregates in solution, which can be correlated to the hydrodynamic radii and the aggregation level of these assemblies. One great advantage of DOSY measurements is that no special sample preparation is necessary, but correctly applied DOSY experiments (see Section 2.1.2 and references therein) can be used to monitor the influence of different concentrations, temperatures, and alkyl substituents on the aggregation level.

The tendency of organocuprates to form supramolecular structures in diethyl ether is shown in Table 3 by experimental and theoretical diffusion coefficients. Depending on the steric hindrance of the alkyl residues and the presence and kind of copper salts, aggregation levels between dimers and oligomers are found. For $(Me_3SiCH_2)_2CuLi$ (**8**), an example for sterically hindered cuprates, a slight trend towards higher diffusion values D, i.e. smaller aggregates, is observed. The diffusion data of cuprates with the same alkyl substituent, but different or no Li salt units attached, show that salt free **1** and **8** and iodide containing **1**•LiI and **8**•LiI have similar diffusion values, while **1**•LiCN and **8**•LiCN reveal much lower diffusion coefficients, which indicate larger assemblies.

Table 3. Diffusion coefficients D ($10^{-9}m^2s^{-1}$), molecular radii $r_C(10^{-10}$ m)[a], length indices n and n_{mf}[b], solvation indices n_{solv}, and theoretical solvation indices $n_{solv}(t)$ of different organocuprates in diethyl ether.[169]

complex		r_c[a,c]	D	n_{mf}[b]	n[c]	n_{solv}	$n_{solv(t)}$[c]
$(Me_3SiCH_2)_2CuLi$	**(8)**	5.39	0.59	1.3	1.7	4.8	3.2
$(Me_3SiCH_2)_2CuLi$ •LiI	**(8**•LiI)	6.05	0.54	1.1	1.4	7.5	5.4
		(6.39)			(1.3)		(7.5)
$(Me_3SiCH_2)_2CuLi$ •LiCN	**(8**•LiCN)	6.01	0.35	4.5	3.6	6.9	4.6
		(6.35)			(3.2)		(6.6)
Me_2CuLi	**(1)**	4.22	0.53	4.4	3.1	2.4	2.6
Me_2CuLi•LiI	**(1**•LiI)	5.20	0.51	2.2	2.3	6.3	4.9
		(5.64)			(1.9)		(7.0)
Me_2CuLi•LiCN	**(1**•LiCN)	5.14	0.33	9.0	5.2	5.1	4.4
		(5.58)			(4.5)		(6.4)

[a] r_c = radius of the core units calculated by molecular hard-sphere volume increments.
[b] n_{mf} is the aggregation number calculated by a model-free approach (see text for details).
[c] For salt-containing complexes, two sets of values are given: those obtained from model c) (without brackets) and from model d) (in brackets) of Figure 13.

For an accurate quantitative interpretation of the diffusion values in terms of aggregation numbers, presumptions and/or measurements of the solvent shell, the chemical composition and, especially in organometallic chemistry, possible exchange contributions have to be done. In addition, for non-spherical molecules, such as organocuprate oligomers (see Figures 12 and 13), shape correction factors are necessary for a quantitative interpretation of diffusion coefficients (Section 2.1.2 and equation 2). Therefore, the models shown in Figure 13 were used for the interpretation of the diffusion values in Table 3 and their hydrodynamic radii and cylindrical shape factors were derived from crystal structures,[130] theoretical calculations[111,152,153] and hard sphere increments.[170,171]

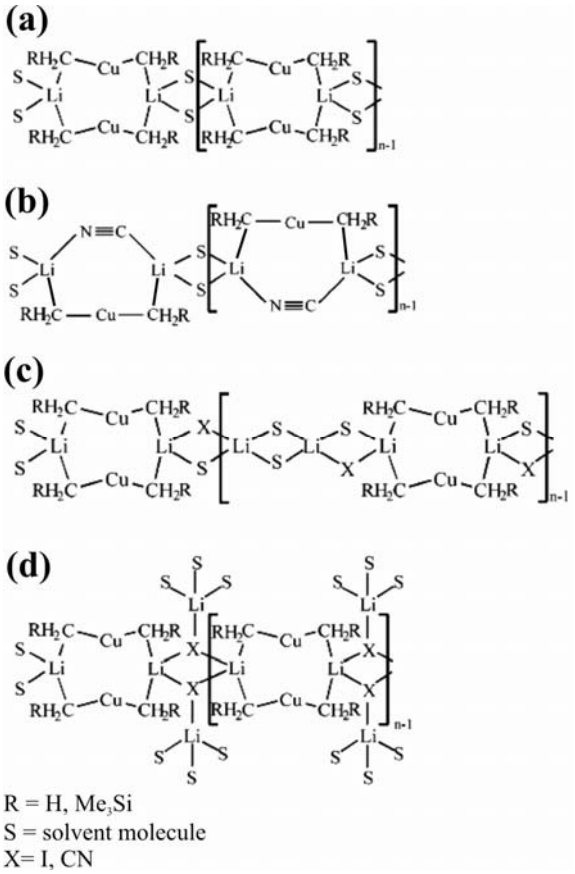

Figure 13. Structure models of dialkylcuprate aggregates beyond dimers; salt-free homodimers (a), salt-containing heterodimers (b), different salt-containing homodimers (c) and (d).[169]

In organometallic compounds, the properties of the solvent are often decisive for their structures in solution. In addition, the solvent shell usually has a significant size and is sometimes even larger than the organometallic compound itself. Therefore, it is crucial for the interpretation of DOSY data to determine and include the number of solvent molecules attached to the complex, i.e., the solvation index n_{solv}. In principle, the solvation of organometallic complexes can be calculated from the normalised diffusion constant of the pure solvent D_{free} and that of the solvent in the reagent sample D_{obs} according to equations 3 and 4 (D_{cup} represents the diffusion coefficient of the cuprate and α the percentage of coordinated solvent out of the total amount of solvent n_{tot}).

$$D_{obs} = \alpha D_{cup} + (1-\alpha) D_{free} \qquad (3)$$

$$n_{solv} = \alpha n_{tot} \qquad (4)$$

Equation 3 shows that the diffusion coefficient of the solvent in the cuprate samples is averaged between free and complexed solvent molecules. Considering the usual error range of 2-5% in DOSY measurements, the determination of solvation is only possible in the case of large oligomers or highly concentrated samples. Applying the models of Figure 13 inclusive the amount of solvent molecules attached, aggregation numbers (length indices) n can be calculated (Table 3).[169,172] To evaluate the influence of the shape factors, which were derived from linear polymeric chains in crystal structures, also the aggregation indices based on spherical shapes, i.e., without any model (n_{mf}), are given in Table 3. These n_{mf} values have similar relative aggregation trends, but different absolute values and highly increased oligomerisation numbers for **1**•LiCN and **8**•LiCN. These data show that for an absolute quantification of the oligomerisation, reliable shape factors are necessary, but that independent of the model used the presence of LiCN leads to significantly larger oligomers.

DOSY measurements combined with kinetic investigations can also be used to test whether the degree or oligomerisation of organocuprates is correlated with their reactivity in 1,4-addition reactions to enones.[124] For this purpose, the oligomers were stepwise disaggregated by using different solvent mixtures of diethyl ether and THF and parallel kinetic measurements were performed (see Figure 3 for kinetic and Figure 14 for diffusion results). A disaggregation of **1**•LiCN upon increasing equivalents of THF was indeed detected by normalised diffusion coefficients (Figure 14b), whereas in **1**•LiI samples no disaggregation effect was observed within an experimental error range of 5% (Figure 14a). The parallel kinetic data of **1**•LiCN showed significantly reduced rate constants upon addition of THF and, thus, the supramolecular structures of **1**•LiCN were found to be essential for its reactivity in 1,4-additions.

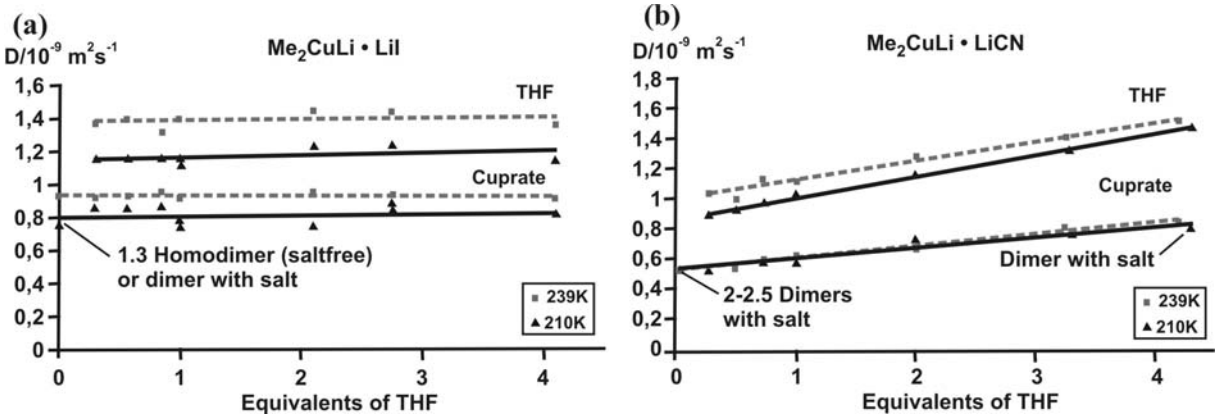

Figure 14. Diffusion coefficients of (a) Me_2CuLi•LiI and (b) Me_2CuLi•LiCN in different solvent mixtures of diethyl ether and THF.[124]

The kinetic data in Figure 3 clearly show a pronounced effect of THF on the reactivity of **1**•LiI, which is not detectable by DOSY-experiments. Therefore, $^{1}H,^{7}Li$ HOE and $^{1}H,^{1}H$ NOE experiments were applied, because dipolar interactions are more sensitive towards small structural changes due to the r^{-6} dependence of the NOE/HOE and the maximum range of approximately 5 Å.[124] From a NMR spectroscopic point of view, it is difficult for these highly symmetrical and flexible oligomers to find reliable reference distances to interpret the observed cross peak intensities of a number of HOE/NOE signals originating from different samples. Based on the result that homodimeric core structures exist in diethyl ether (Section 2.2.2.2) all $^{1}H,^{7}Li$ cross signals could be calibrated relative to the known cuprate $^{1}H,^{7}Li$ HOE cross signal. With this method, the effect of increasing amounts of THF on the structures of **1**•LiCN and **1**•LiI was elucidated. In the case of **1**•LiCN (Figure 15c), the HOE between Li and diethyl ether is decreasing in the same manner as the HOE between Li and THF is increasing upon addition of increasing amounts of THF. In samples of **1**•LiI, the HOE to THF increases dramatically, while the HOE to diethyl ether remains constant (Figure 15d). These HOE patterns indicate that in **1**•LiCN solvent molecules are exchanged from diethyl ether to THF, while the general supramolecular structure of **1**•LiCN remains and is disaggregated as a whole. In contrast, the addition of THF to **1**•LiI causes additional coordination sites for solvent molecules at Li, which can be interpreted as dissociation of salt units from the homodimer, which is schematically shown in Figure 15a and b.

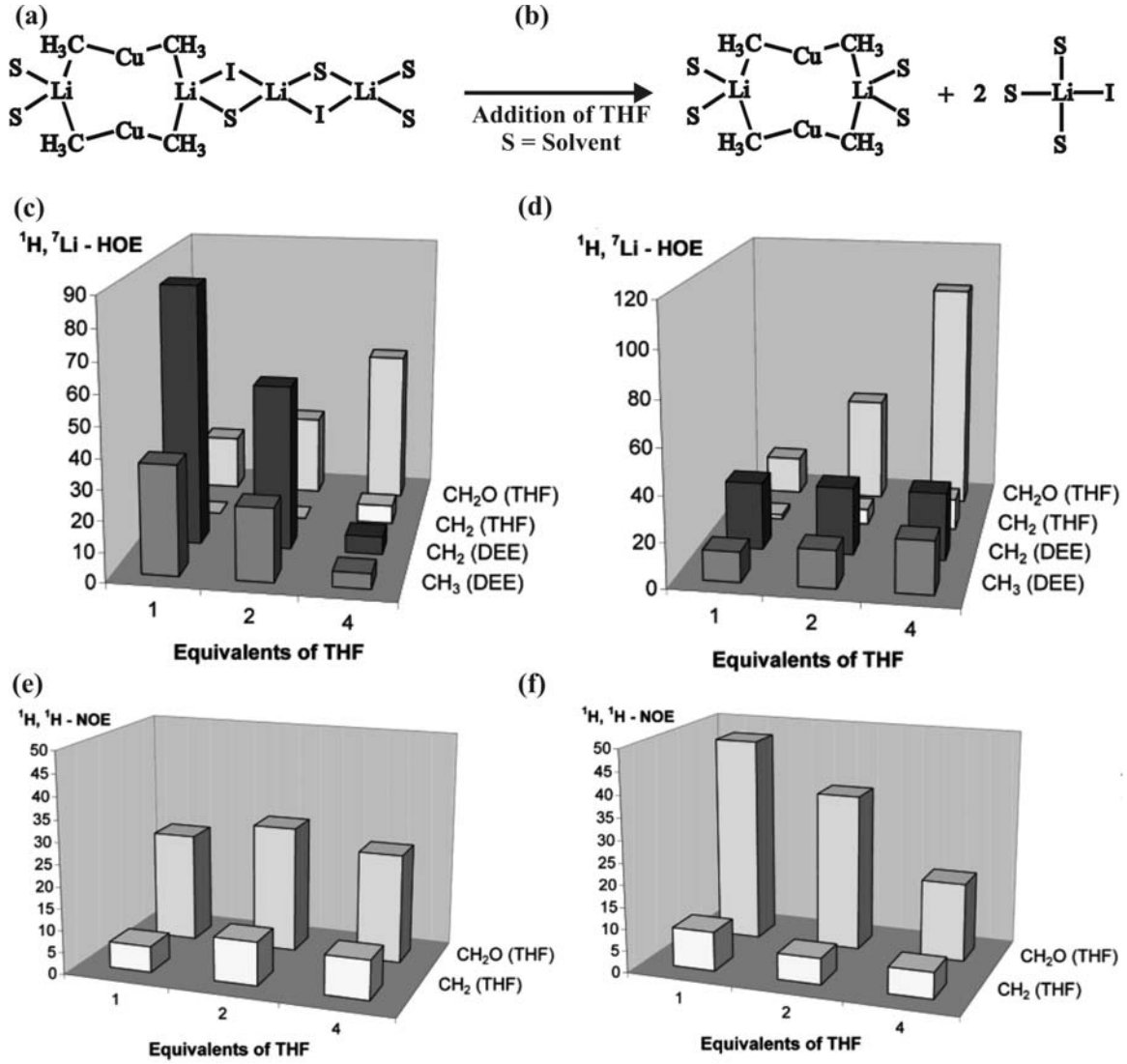

Figure 15. (a) Postulated aggregate structure and (b) disaggregation in the case of **1**•LiI. In addition, bar charts are displayed summarizing the ^{1}H, ^{7}Li HOE volume integrals of the cross-peaks between lithium and the protons of diethyl ether (DEE) and THF for (c) Me_2CuLi•LiCN and (d) Me_2CuLi•LiI and bar charts summarizing the ^{1}H, ^{1}H NOEs between the methyl groups of the cuprate and the CH_2-groups of THF for (e) Me_2CuLi•LiCN and (f) Me_2CuLi•LiI.[124]

Both structural interpretations were confirmed by $^{1}H,^{1}H$ NOE experiments, in which the distance between the two CH_2 groups of THF was chosen as reference distance, after normalisation of the increasing amounts of THF. In **1**•LiCN, the $^{1}H,^{1}H$ NOE between the methyl groups of the cuprate and THF remains constant (Figure 15e), as expected for an unmodified core structure. In contrast, in **1**•LiI, the $^{1}H,^{1}H$ NOEs between cuprates and THF decrease upon addition of THF (Figure 15f), which is in accordance with THF solvated Li ions dissociating from the cuprate unit. The previously discussed studies show that certain combinations of $^{1}H,^{1}H$ NOE and $^{1}H,^{7}Li$ HOE measurements are a sensitive method to

elucidate even the structural changes of disaggregation processes in supramolecular aggregates. However, these studies do not reveal the absolute position of the anion, either iodide or cyanide, in the supramolecular core structure.

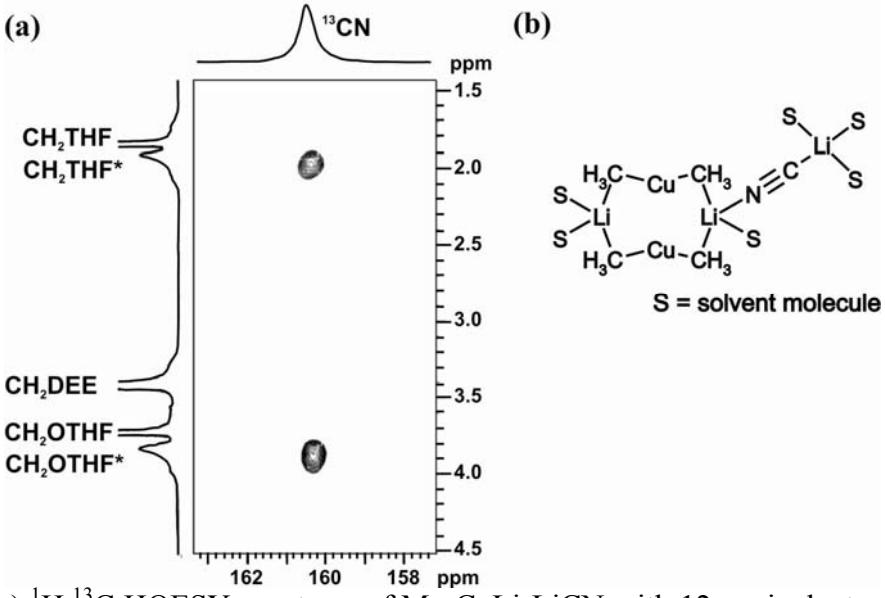

Figure 16. (a) ^{1}H,^{13}C HOESY spectrum of Me_2CuLi•LiCN with 12 equivalents of THF. Two sets of signals are observed for THF: THF in the solvent bulk and THF* bound to the cuprate aggregate; the observed ^{1}H,^{13}C HOE cross peaks indicate the orientation of CN shown in (b).[124]

For this purpose, ^{13}C-labelled Cu^{13}CN was used to elucidate the position of ^{13}CN by ^{1}H,^{13}C HOEs. In a sample in which the exchange between cuprate coordinated THF (THF* in Figure 16a) and bulk THF was slow on the NMR time scale, it was possible to detect ^{1}H,^{13}C HOEs between ^{13}CN and the cuprate bound THF molecules, but none to the cuprate itself (Figure 16a). This surprising result was interpreted as an orientation of the ^{13}C away from the cuprate moiety (Figure 16b).

2.3 NMR Spectroscopy of Intermediate Complexes of Organocuprates

The results presented for the free organocuprate reagents in the previous section show impressively that NMR spectroscopy is a powerful method for the structure determination of organometallic compounds in solution, even in the case of flexible and oligomeric aggregates. NMR is also the method of choice for the structure elucidation of reaction intermediates. However, the basic prerequisite for any NMR investigation of transient species is to stabilize sufficient amounts of it for a certain time period, because NMR is a very insensitive and slow

method. Consequentially, the NMR methods applicable to reaction intermediates are limited by the existing lifetime and amount of the intermediate and isotope labelling is often used to increase sensitivity.

2.3.1. Cu(I) Organocuprate Intermediates

In conjugate addition reactions of organocuprates to Michael acceptors, π-complexes between cuprates and Michael acceptors were proposed theoretically as first reaction intermediates[111,112,173-179] and were experimentally confirmed (e.g., Figure 17).[62,134,135,180-189] Furthermore, in copper mediated click reactions of copper acetylides with azides, a π-complex formation between Cu and the acetylene is reported as the initial step, too.[190] In these intermediate π-complexes, the π-bond carbons are expected to experience the highest chemical shift variations and can be used as sensors for the formation of π-intermediates. In one of the first literature available NMR studies of organocuprate intermediates,[134] a organocuprate π-complex was stabilized by using low temperature NMR in combination with cinnamic ester as quite inreactive Michael acceptor.

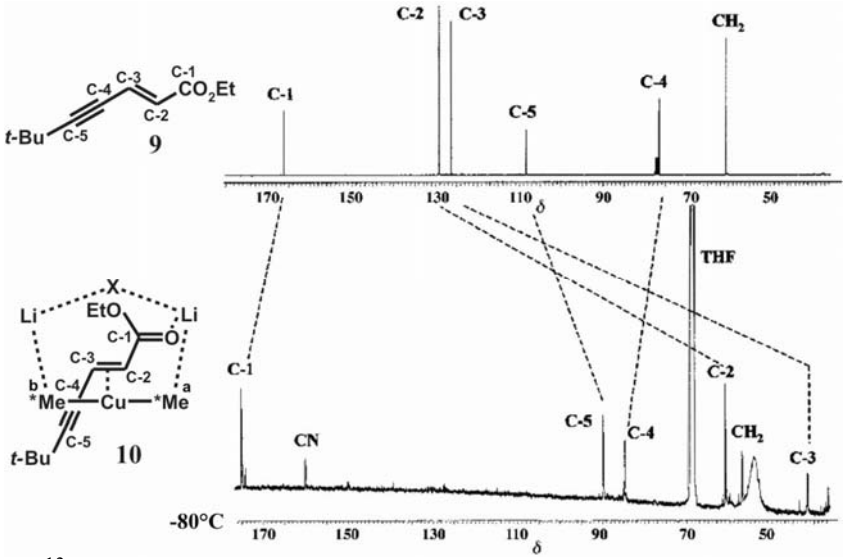

Figure 17. The ^{13}C NMR spectra of the ethyl 2-en-4-ynoate **9** and its cuprate-enyne π-complex **10** show typical ^{13}C chemical shift changes upon carbonyl complexation and π-complex formation.[62]

In the ^{13}C spectra of cinnamic ester and its organocuprate π-complex, upfield shifts of the π-bond carbons of $\Delta\delta$ = -67.2 ppm and -82.6 ppm were detected. In addition, a small downfield shift of the carbonyl carbon indicates a Li coordination at the carbonyl oxygen. Later on, also in further studies of organocuprate π-complexes, these characteristic ^{13}C

chemical shift differences were detected and used as evidence for π-complexation in organocuprate intermediates (for a typical example see Figure 17).[62,180-183,185,186]

Similar to the chemical shifts, scalar couplings as second fundamental NMR parameter can also be used for the detection and structure elucidation of intermediate complexes. However, especially in organocopper complexes, line broadening due to quadrupolar relaxation often hampers the detection of scalar couplings. In addition, exchange processes may lead to a reduction of the detected scalar coupling constant, as already mentioned for heteroleptic cuprates in Table 2 (Section 2.2.2.1). Dealing with this problem, elaborate intermediate stabilisation strategies, low temperature NMR, and specific isotope labelling rendered not only magnetisation transfers via scalar couplings but also the quantitative determination of scalar coupling constants possible in various intermediate species. Information from both methods allowed impressive insights into bonding orders and structures of organocuprate intermediates.

The first $J_{C,C}$ coupling constants in organocuprate π-complexes were detected in the cuprate ynoate complex **11** (Figure 18).[135] To enable the detection of $^1J_{C,C}$ scalar couplings, compound **9** was ^{13}C labelled at C-2, C-3, and C-5. The $^1J_{C,C}$ coupling constants of free **9** were determined with the aid of the INADEQUATE technique. After addition of the sterically demanding *t*-Bu_2CuLi•LiCN, the π-complex **11** and the corresponding $^1J_{C,C}$ coupling constants were detected (Figure 18).

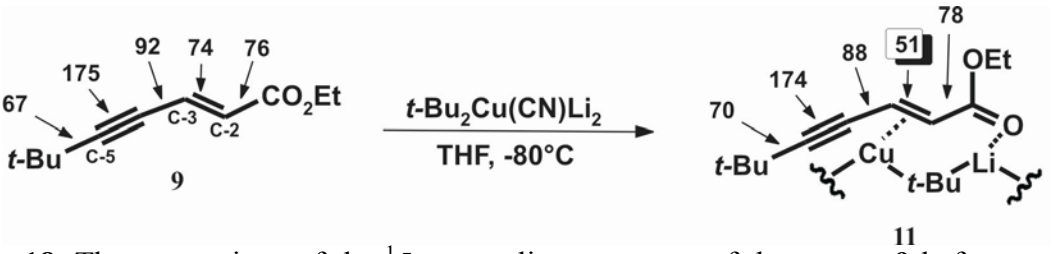

Figure 18. The comparison of the $^1J_{C,C}$ coupling constants of the ynoate **9** before and after formation of the π-complex **11** show the exclusive coordination of the cuprate to the former double bond.[135]

Comparing the coupling constants in **9** and **11**, it is evident that the most varying $^1J_{C,C}$ coupling constant is $^1J_{C,C}$ between C-2 and C-3, which decreases from 74 Hz to 51 Hz and indicates the interaction of the cuprate with the π-bond. As $^1J_{C,C}$ scalar couplings imply information about hybridisation and bond orders, the significant decrease of the $^1J_{C,C}$ shows that the hybridisation and bond order of C-2 and C-3 in the π-complex is similar to sp^2-carbons, which are connected via a single bond. For comparison, in 1,3-butadiene the $^1J_{C,C}$

coupling constant of the single bond, which is connecting the two sp^2-carbons, is 53.7 Hz.[135] Later studies showed that in organocuprate intermediates scalar couplings between the cuprate and the enone moiety can also be detected. For this purpose, samples with specifically ^{13}C labelled **9** and completely ^{13}C-labelled **1**•LiCN were prepared and the ^{13}C spectra of either C-2* or C-3* labelled intermediates (Figure 19b and 19c) were compared with that of completely unlabelled **9** in the π-complex **10** (Figure 19a). Introducing a ^{13}C label in the C3 position, the methyl group $^{*}Me^{a}$ at -6.9 ppm is split into a doublet with a coupling constant of 12 Hz. Consequently, the ^{13}C signal of C3 is also a doublet with 12 Hz.[62] In contrast, the labelling in position C2 produces no observable coupling pattern (Figure 19c). This difference in the scalar coupling constants within the π-complex is in accordance with a bent structure of the cuprate moiety in the intermediate (Figure 19d).

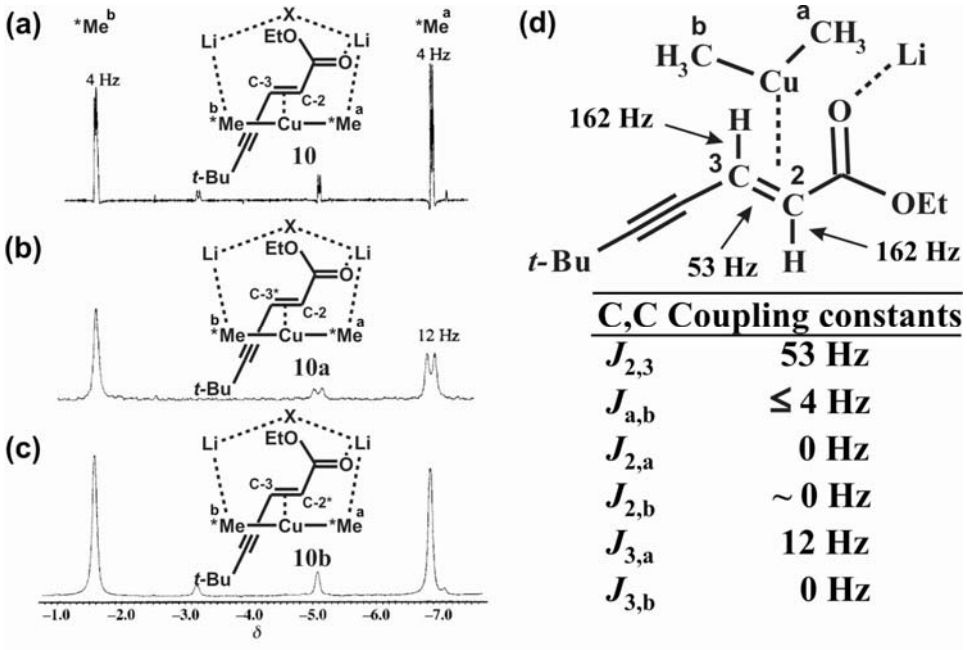

Figure 19. ^{13}C NMR spectra of the π-complexes (a) **10,** (b) **10a,** (c) **10b** with completely labelled **1**•LiCN (methyl groups termed a and b) and selectively labelled Michael acceptors. Labels are marked with asterisks. (d) The detected coupling constants of the π-complex demonstrate the partly covalent connection of cuprate and enone and the bent structure of the cuprate moiety.[62]

The orientation of the two methyl groups $^{*}Me^{a}$ and $^{*}Me^{b}$ in these intermediates was confirmed by NOESY cross signals to the vinyl protons H-2 and H-3 (Figure 20). The cross peak intensities show that the methyl group $^{*}Me^{b}$ at -0.6 ppm is directed towards the *t*-butyl group and the methyl group $^{*}Me^{a}$ at ~-1.1 ppm towards the carbonyl function (Figure 20).

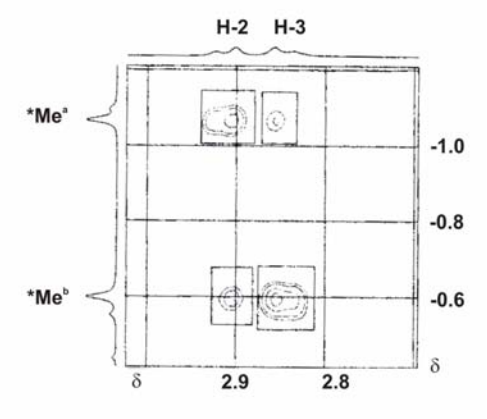

Figure 20. ^{1}H,^{1}H NOESY section of the vinyl protons and the cuprate methyl groups of the cuprate intermediate **10**, which confirms the orientation of the methyl groups shown in Figure 19d.[62]

The described general characteristic of organocuprates in THF to form π-complexes as first detectable intermediate in 1,4-addition reactions was also confirmed in intermediate studies with diethyl ether as solvent. From the studies of the organocuprate reagents it was known that oligomeric supramolecular assemblies exist in diethyl ether, which could be correlated to their different reactivity (see Section 2.2.1). Consequently, the question arose, whether these supramolecular assemblies persist in the π-intermediates. Extremely broad line widths and the gel like textures of concentrated π-complexes in diethyl ether indicated high supramolecular structures, but did not allow any detailed NMR investigations.[63,132] Therefore, distinct amounts of THF was used to disaggregate the supramolecular assemblies until spectroscopically acceptable line widths were observed, a strategy which was based on the studies of oligomeric aggregates of the free organocuprates (Section 2.2.3). In order to slow down the reaction rates compared to unsubstituted 2-cyclohexenone and in attempt to stabilize the π-intermediates, additionally different substitution patterns were used in the cyclic enones **12**, **13**, **14** and **15** (Scheme 3).[63,132,191]

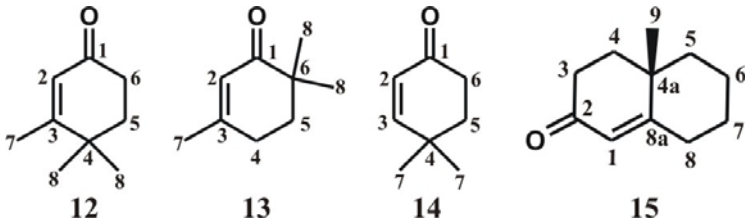

Scheme 3. Selected sterically demanding achiral enones **12**, **13**, and **14** and chiral enone **15**, which build NMR observable enantiomeric (**12**, **13**, **14**) and diastereomeric (**15**) π-complexes in diethyl ether.[63]

In investigations of the π-complexes of 4,4a,5,6,7,8-hexahydro-4a-methylnaphthalen-2(3H)-one (**15**) it could be shown, that diastereomeric complexes are formed due to an α- and β-face coordination of the cuprate (Figure 21a). This significantly complicates the NMR spectra of the resulting π-intermediates, because two sets of signals exist in varying amounts due to the two diastereomeric complexes (Figure 21c). The resulting problems of signal overlap and sensitivity were solved by using achiral enones, in which α- and β-face coordination of the cuprate leads to enantiomeric complexes producing only one set of signals (Figure 21b and d).[63]

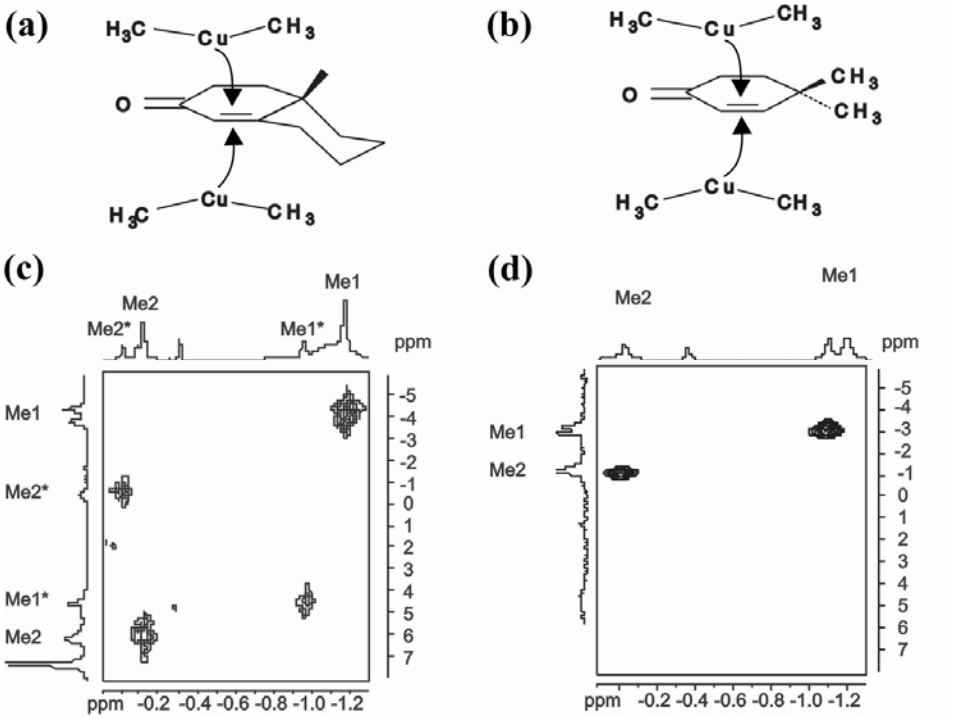

Figure 21. Schematic representation of the α- and β-face complexation of (a) chiral **15** and (b) achiral **14** and π-complex cuprate sections of the corresponding $^{1}H,^{13}C$ HMQC spectra in diethyl ether at 180 K. Diastereomeric π-complexes with chiral enones show (c) two sets of signals, while (d) enantiomeric π-complexes produce only one set of signals.[63]

Using disaggregation with THF and achiral enones, the NMR spectroscopic foundations were laid to demonstrate that the π-complexes described in THF, including their bended structure, are a general structural motif also in diethyl ether as solvent. In the example of **14** with 2 equivalents of **1**•LiI, the characteristic ^{13}C and ^{1}H chemical shift differences before (Figure 22a,b) and after (Figure 22c,d) π-complexation are shown in diethyl ether.

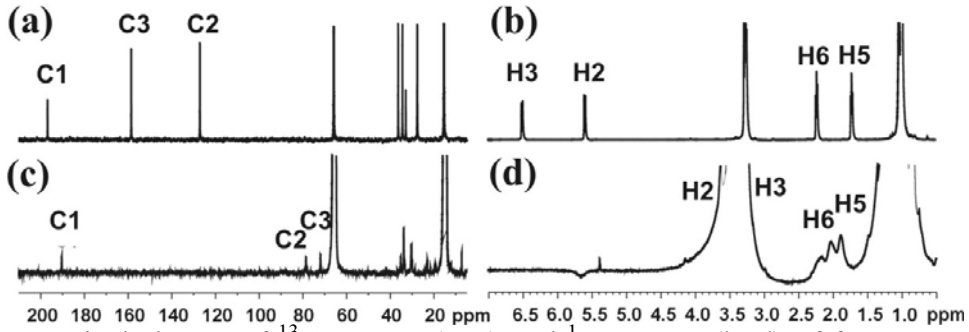

Figure 22. Typical change of ^{13}C spectra (a, c) and ^{1}H spectra (b, d) of free enone **14** (a, b) and upon π-complexation (c, d) with 2 equivalents of **1**•LiI in diethyl ether at 170 K.[63]

Interestingly, in diethyl ether the carbonyl carbon C1 experiences a small upfield shift upon π-complexation (Figure 22a,c), whereas in THF a downfield shift was observed, which was assigned to a Li coordination (Figure 17).[62] This observation indicates that in diethyl ether more complex species than a single Li ion are responsible for the carbonyl complexation.[63]

The most impressive result of the described optimization of the experimental conditions was the detection of scalar couplings in π-complexes even without ^{13}C labelling. By applying a HMBC magnetisation transfer across copper from the methyl groups of the cuprate to the enone, it was possible without specific ^{13}C labelling of the enone to adduce direct evidence for π-complexation and the bended cuprate structure in these intermediates also in diethyl ether (Figure 23).

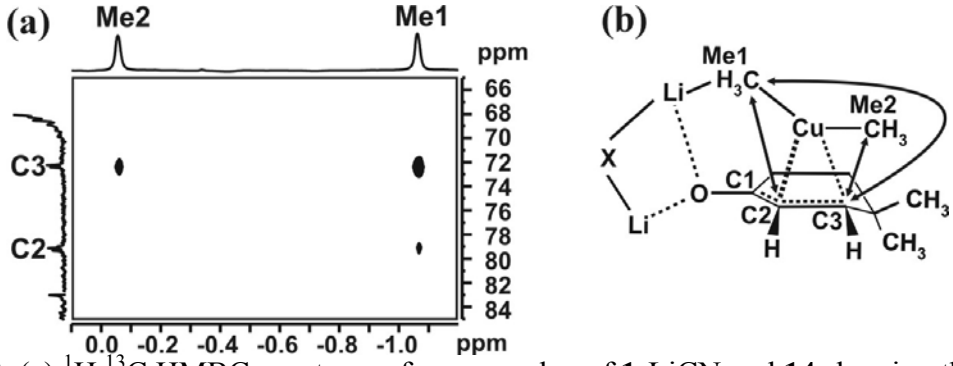

Figure 23. (a) $^{1}H,^{13}C$ HMBC spectrum of a π-complex of **1**•LiCN and **14** showing the cuprate section in the ^{1}H dimension and the coordinated double bond section in the ^{13}C dimension. The cross signals indicate scalar couplings, which are illustrated by arrows in the schematic π-complex (b).[63]

Previously, it was discussed for π-complexes in THF that different scalar coupling constants were used to deduce the bent structure of the cuprate moiety (Figure 19). Despite the described extensive improvements of the experimental conditions, in diethyl ether a

similar approach was not applicable, because the scalar couplings were smaller than the linewidths. In such cases an indirect approach can be used, because in HMBC spectra the integrals of the cross peaks are qualitatively correlated with the coupling constants.[192-195] Therefore, in principle qualitative coupling constants can be derived from HMBC spectra and e.g., the cross peak pattern shown in Figure 23a confirms the bent structure of the cuprate unit also for organocuprate π-intermediates in diethyl ether (Figure 23b). As additional structural feature in diethyl ether compared to THF, DOSY experiments revealed that the π-complexes also form supramolecular assemblies and that the oligomeric cuprate aggregates even increase after addition of enones.[63]

In synthetic studies about conjugate addition reactions of cuprates, high and sometimes unexpected diastereoselectivities were obtained for a variety of chiral cyclic enones.[108] For example the chiral enone **15** (Scheme 4a) yields almost exclusively the β-methyloctalone, which means that surprisingly a cis-selective 1,4-addition reaction takes place.

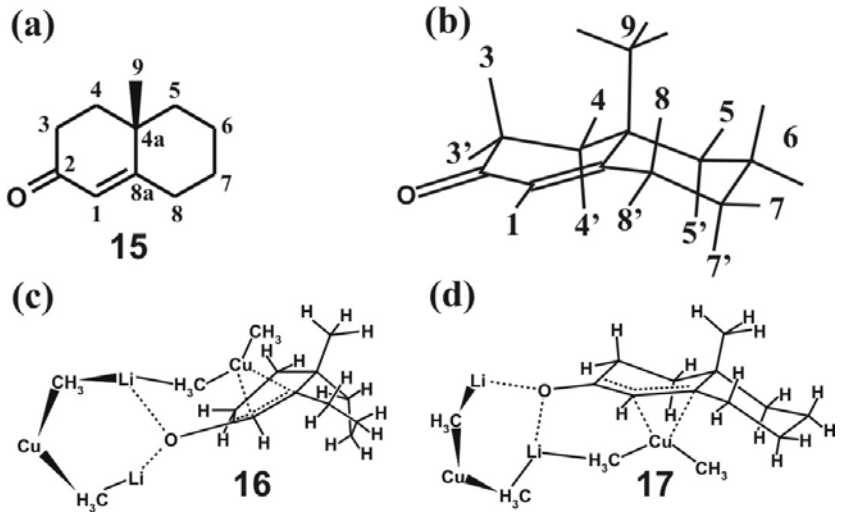

Scheme 4. (a) 4,4a,5,6,7,8-Hexahydro-4a-methylnaphthalen-2(3H)-one (**15**), (b) the differentiation of the protons within the CH_2 groups, (c) the major conformation or β-face complexation (**16**) and (d) the minor conformation or α-face complexation (**17**) of the π-complex composed of **15** and Me_2CuLi and $Me_2CuLi{\bullet}LiI$.[63]

In order to test whether this unexpected and high diastereoselectivity is caused by a conformational preference of the π-intermediate, π-complexes of **15** and methyl cuprate were prepared in diethyl ether and revealed two sets of signals due to diastereomeric α- and β-face complexes (see above).[63] The ^1H and ^{13}C chemical shifts were assigned via a combination of $^1H,^{13}C$ HSQC, $^1H,^{13}C$ HMBC, $^1H,^1H$ NOESY and $^1H,^{13}C$ INEPT INADEQUATE experiments, including a diastereotopic assignment of the CH_2 groups (Scheme 4b). With the aid of INEPT INADEQUATE experiments,[196,197] in both π-intermediate conformations scalar

couplings between the cuprate Me1 and C8a in **15** were detected even without ^{13}C labelling of the enone, indicating the bent cuprate structure in both intermediate conformations (Figure 24).

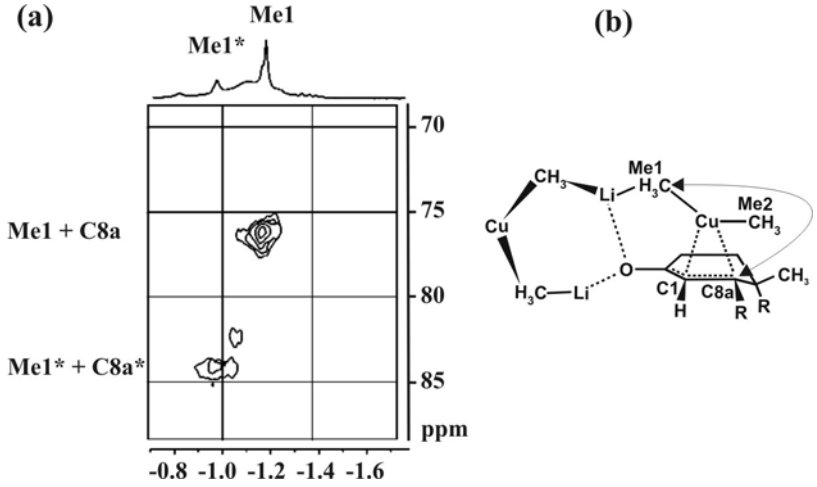

Figure 24. (a) Section of a ^{1}H, ^{13}C INEPT-INADEQUATE spectrum of the π-intermediates composed of **15** (natural abundance) and ^{13}C labelled **1**•LiI in diethyl ether at 180 K. The cross signals appearing at ^{13}C chemical shifts equal to $\delta^{13}C_{Me1(*)} + \delta^{13}C_{C8a(*)}$ are the result of $^{2}J_{C,C}$ scalar couplings across copper as indicated by the arrow in (b).[63]

From the schematic drawings of the α- and β-face π-complexes of **15** in Scheme 4 it is evident that the β-face π-complex is the precursor of the detected cis-addition and the α-face π-complex is the precursor of a possible anti-addition. Therefore, the further structural features of the two π-complexes of **15,** i.e. identification of α– and β-face complex and determination of the enone conformations in both complexes, were performed with NOESY experiments. Based on the qualitative interpretation of the $^{1}H,^{1}H$ NOESY spectrum shown in Figure 25 and the theoretically calculated conformations of pure **15**,[198] the major π-complex could be identified as the β-face π-complex shown in Scheme 4c and the minor π-complex was assigned to the α-face complex shown in Scheme 4d. These results indicate impressively that the conformational preferences of the enone change significantly upon cuprate complexation. In addition, the β-face complex is already the major π-intermediate species. This means that the nearly exclusive cis-selective formation of β-methyloctalone in the product, is to some extent already preformed in the α-/β-face ratio of the π-intermediates (Scheme 4, **16** and **17**) and further enhanced by the subsequent reaction pathway via the Cu(III) intermediates.

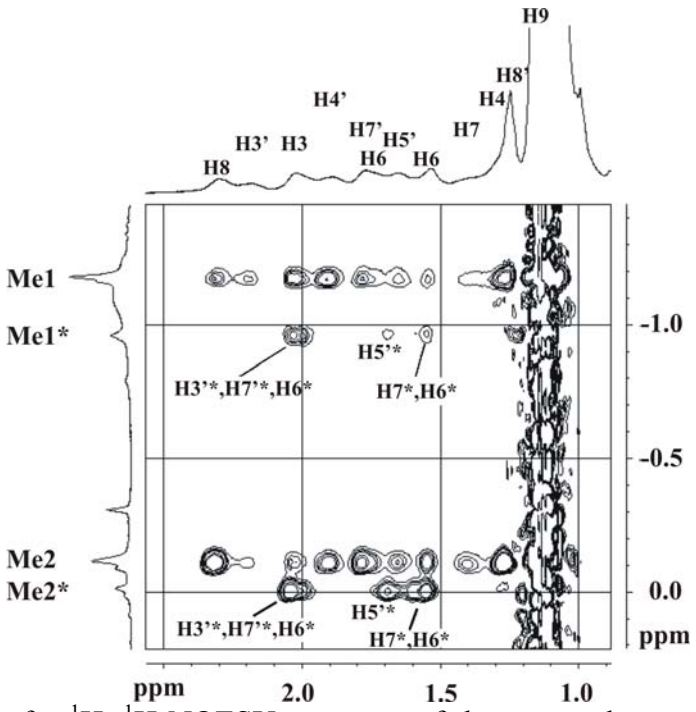

Figure 25. Section of a ^{1}H, ^{1}H NOESY spectrum of the π-complexes composed of **15** and **1**•LiI in diethyl ether at 180 K. The different patterns of the cross signals indicate the different structures presented in Scheme 4c,d. The minor intermediate is labelled with an asterisk, for a visualization of the numbers see Scheme 4b.[63]

The second principal technique used for the stabilization of organocuprate intermediates is the RI-NMR technique,[102,103] which reduces the dead time before the first NMR scan to a minimum and allows 1D NMR spectra within the first seconds of a reaction. After the very first scan, the starting time for the second experiment is limited by the relaxation properties of the sample and typical repetition times are between 1-2 s. For classical 2D NMR experiments, e.g. COSY or NOESY, also in RI equipped NMR spectrometers a stable equilibrium state is necessarily induced by low temperatures or with slowly reacting compounds.

A typical series of spectra, performed with RI-NMR, is shown in Figure 26 for the reaction of **1**•LiI and 2-cyclohexenone in THF at -100°C.[133] The assignment of the different detected species was based on 2D COSY and NOESY experiments after equilibrium was reached.

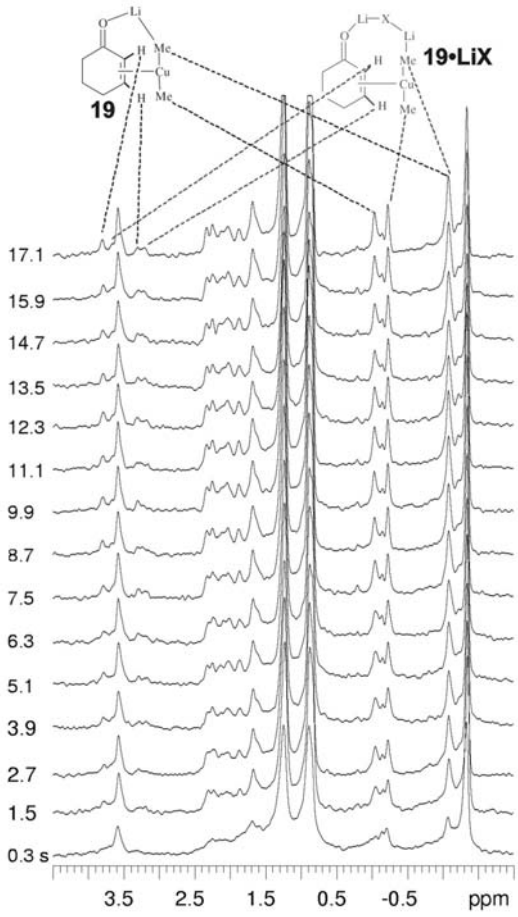

Figure 26. Stacked plot of rapid injection ^{1}H spectra of the reaction of **1**•LiI with 2-cyclohexenone at -100°C in THF.[133]

From the integrals of the signals presented in Figure 26, the rate constants for the formation of the individual π-complexes **19** and **19**•LiX can be determined. Such a measurement of reaction rates is a typical and powerful application of RI- and standard NMR on reacting systems. In the case of **19** and **19**•LiX, the observed rate constants in combination with EXSY measurements were used to propose the exchange equilibria of organocuprate reagents and intermediate species shown in Figure 27.[133]

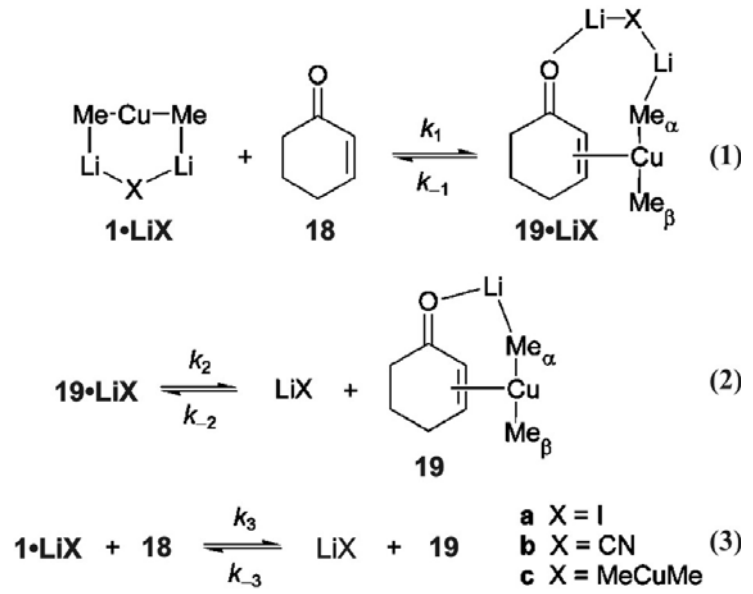

Figure 27. Equilibria in the reaction of **1**•LiI with 2-cyclohexenone in THF at -100°C based on experimental reactions rates and exchange equilibria.[133]

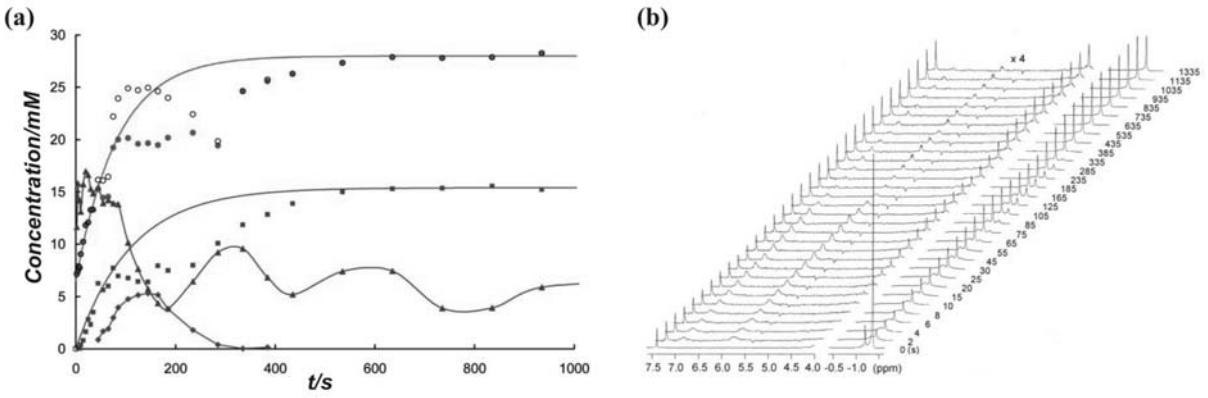

Figure 28. (a) Concentration vs. time plots for the reaction of cyano-Gilman reagent Me_2CuLi•LiCN (♦) with 2-cyclohexenone (▲) at -70° C. Additionally, the enolate product (■) and residual copper species (●) are displayed. (b) Stacked plots of ^{1}H NMR spectra for the addition of cyclohexenone to Me_2CuLi•LiCN at -70°C. The first spectrum shows the cuprate solution before injection.[184]

The importance of low temperature stabilization even in RI-NMR is impressively demonstrated in the following example. For the RI ^{1}H spectra shown in Figure 26 and the intensities derived from RI ^{1}H spectra shown in Figure 28, similar experimental setups were used (2-cyclohexenone, THF) and the temperature was raised from -100° C to -70° C. At -70° C (see Figure 28), the amount of π-complex is too low for detection but the enolate product is observed.[184] Additionally, an interesting ocillatory process becomes obvious. While directly after the injection of cyclohexenone (▲), no free Me_2CuLi•LiCN (♦) is detected, later on its

concentration rises again and reaches a maximum at 145 s. The curve of cyclohexenone (▲) in turn, shows an unexpected oscillating behaviour during the whole measurement.

2.3.2. Cu(III) Organocuprate Intermediates

Numerous theoretical calculations predicted Cu(III) species as second essential intermediate in the prototypical reactions of organocuprates, such as conjugate additions to α,β-unsaturated carbonyls, S_N2-like cross couplings, and S_N2' allylic substitutions.[111,173-176,199-202] In contrast to this extensive theoretical work, experimental evidence of these elusive Cu(III) species has been missing for decades. Therefore, it was a real breakthrough that recently the first Cu(III) intermediates were detected by NMR spectroscopy.[57-59,64,65] Later on, additional Cu(III) containing organometallic complexes were reported.[203] In 2007, Bertz and Ogle succeeded in the very first experimental detection of a Cu(III) intermediate in organocuprate reactions. In these experiments the Cu(III) intermediate of a 1,4-addition reaction was detected with the aid of rapid injection NMR and TMSCN as stabilising agent for the Cu(III) enolate species (Figure 29).[58]

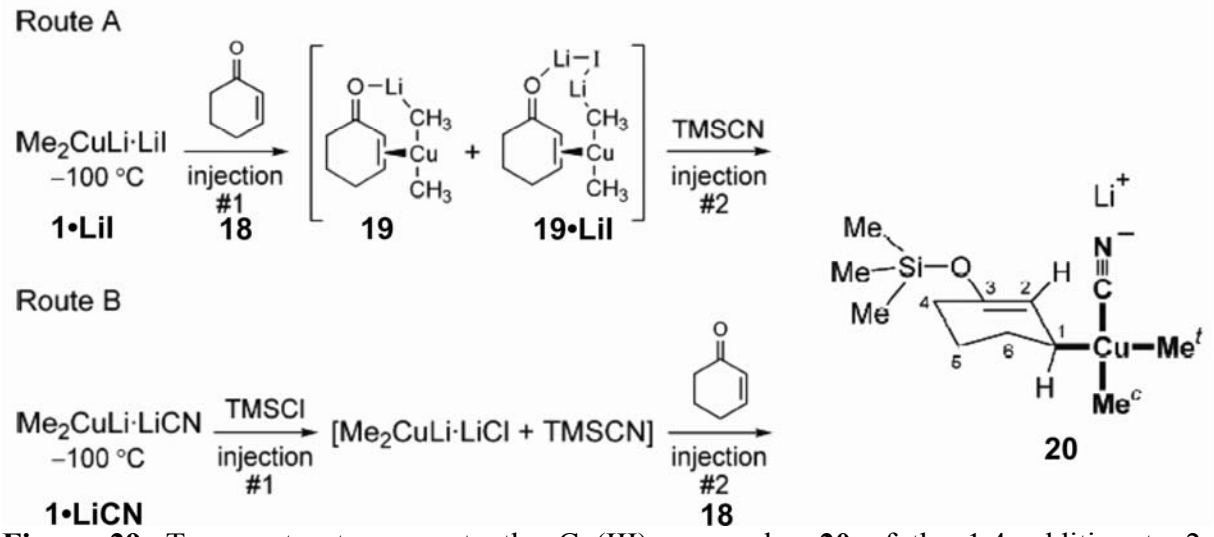

Figure 29. Two routes to generate the Cu(III) σ-complex **20** of the 1,4 addition to 2-cyclohexenone in THF.[58]

The intermediate Cu(III) enolate was trapped by the formation of a stable silyl enol ether (compound **20** in Figure 29) and this stabilisation trick allowed extensive NMR investigations of the Cu(III) intermediate. With a double application of the rapid injection technique it was even possible to show experimentally that neither the kind of starting cuprate (**1**•LiI or **1**•LiCN) nor the injection sequence influences the formation of the Cu(III) compound. Route A first allows the detection of π-complexes **19** and **19**•LiI, whereas the further injection of

TMSCN leads to the formation of the Cu(III) σ-complex (**20** in Figure 29). In route B the injection sequence starts with TMSCl and the identical Cu(III) σ-complex is observed immediately after the injection of the cyclohexenone.

In Table 4 the observed chemical shifts for the different compounds of Figure 29 are listed. The chemical shifts of the cuprates (**1**•LiI or **1**•LiCN) and the Cu(III) species **20** can be distinguished by an appreciable downfield shift of the methyl groups in **20**. While **1**•LiI (-9.12 ppm/-1.40 ppm for $^{13}C/^{1}H$) and **1**•LiCN (-9.04 ppm/-1.35 pm) show common cuprate chemical shifts, **20** exhibits a striking chemical shift combination of the ^{13}C and ^{1}H methyl signals (12.43 ppm/0.05ppm for Me^{t} and 25.31 ppm/0.53 ppm for Me^{c}). These numbers denote that the ^{13}C signals of the Cu(III) species shift dramatically downfield in the range of 20 to 35 ppm compared to cuprates. The observation of two distinguishable methyl resonances Me^{t} and Me^{c} in compound **20** (trans and cis to the ring) is caused by the asymmetric chemical environment in the Cu(III) complex and was confirmed by NOE spectra.

Table 4. Comparison of ^{13}C and ^{1}H (parenthesis) chemical shifts[a] for organocuprate Cu(I) π-complexes and Cu(III) σ-complexes.[58]

group	18	1•LiI	1•LiCN	19	19•LiI	19•LiCN	20
CH_3 (CH_3^{t})[b]		**-9.12** (-1.40)	**-9.04** (-1.35)	**-5.02** (-1.12)	**-5.56** (-1.16)	**-5.76** (-1.15)	**12.43** (0.05)
CH_3 (CH_3^{c})[b]		**-9.12** (-1.40)	**-9.04** (-1.35)	**-0.57** (-0.10)	**-1.85** (-0.24)	**-2.14** (-0.21)	**25.31** (0.53)
CN			158.89			159.20	**153.78**
C_1 (C_3)[b]	198.65			194.75	193.34	193[c]	144.73
C_2-H (C_2-H)[b]	130.12 (5.90)			**77.45** (3.77)	**75.82** (3.68)	**75.27** (3.71)	116.28 (5.02)
C_3-H (C_1-H)[b]	151.65 (7.08)			**61.50** (3.26)	**61.50** (3.19)	**61.51** (3.17)	**39.68** (2.74)

[a] Parts per million from TMS. Values for C atoms attached to Cu are in boldface. [b] Labeling for **20**. Note that C_1 of **18** becomes C_3 of **20** and C_3 of **18** becomes C_1 of **20**. [c] Shift could not be measured accurately, owing to broadening.

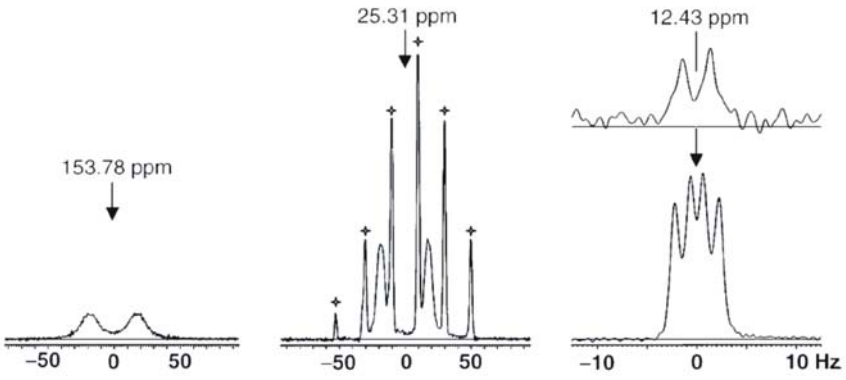

Figure 30. ^{13}C NMR sections for labelled **20** with solvent (+). In the upper spectrum ^{13}CN is ^{13}C labelled and in the lower spectra both, $^{13}CH_3$ and ^{13}CN, are ^{13}C labelled.[58]

The connectivity in **20** was directly proven using $^{2}J_{C,C}$ coupling patterns across copper. For this purpose, a sample with ^{13}C labelled methyl groups and labelled Cu^{13}CN was prepared and 1D ^{13}C measurements were performed (Figure 30). In the resulting spectra, all $^{2}J_{C,C}$ scalar couplings across copper were detected, which were expected for the connectivity in **20** ($^{2}J_{C,C}$ ring methine carbon (C_1), Me^t = 38.1 Hz, $^{2}J_{C,C}$ cyano substituent, Me^c = 35.4 Hz). Additionally, Me^t is coupled to the cyano group with $^{2}J_{C,C}$ = 5.4 Hz and to Me^c with $^{2}J_{C,C}$ = 2.9 Hz. The ^{13}C chemical shifts and $^{2}J_{C,C}$ coupling constants in **20** were consistent with theoretical calculations of **20**, which confirmed the proposed square planar structure of the Cu(III) σ-complex **20**.[199]

Shortly after the detection of the first Cu(III) σ-complex in 1,4-additions, the preparation and NMR spectroscopic detection of the first Cu(III) σ-complexes in cross coupling reactions was also successful.[59,65] During the investigation of organocuprate π-complexes conventional low temperature NMR, ^{13}C labelling of the cyanide and diethyl ether as solvent were standard experimental tools for stabilizing the Cu(I) intermediates.[63] Surprisingly, with this experimental setup an additional Cu(III) species was also detected in various $^{1}H,^{13}C$ HMBC spectra, which later turned out to be the intermediate of cross coupling reactions.[59] This species showed cross signals of two chemically non-equivalent methyl groups and one cyanide group attached to the same copper. Initially, the amount of this species was so low that in the corresponding proton spectra no signal could be detected even at a high number of scans and only the $^{3}J_{H,C}$ coupling between the methyl groups and the ^{13}C labelled cyanide led to a signal enhancement allowing its detection in the $^{1}H,^{13}C$ HMBC spectra (Figure 31c). By variations in the ratio of Cu^{13}CN to MeLi and the presence of small amounts of MeI, it was possible to increase the concentration of this Cu(III) species to such an extent that not only the detection of ^{1}H signals (Figure 31a), but also extensive HMBC (Figure 31b, c) and NOESY NMR measurements were possible. The two methyl signals Me_{trans} ($\delta(^{1}H)$ = 0.57 ppm) and Me_{cis} ($\delta(^{1}H)$ = -0.06 ppm) in the ^{1}H spectrum, their integral ratio of 1:2, respectively, and the HMBC coupling pattern shown in Figure 31b,c directly indicate the formation of the square planar Me_3Cu(III)(CN)Li complex (**21**) presented in Figure 31d. In contrast, in a tetrahedral Cu(III) complex only one signal would be observable for all three methyl groups in the ^{1}H spectrum. Considering the supramolecular assemblies as general feature of organocuprates and Cu(I) intermediates in diethyl ether, it is interesting that up to now $^{1}H,^{1}H$ NOESY spectra have not revealed any hint for supramolecular aggregates of the Me_3Cu(III)(CN)Li intermediate in cross coupling reactions in diethyl ether.

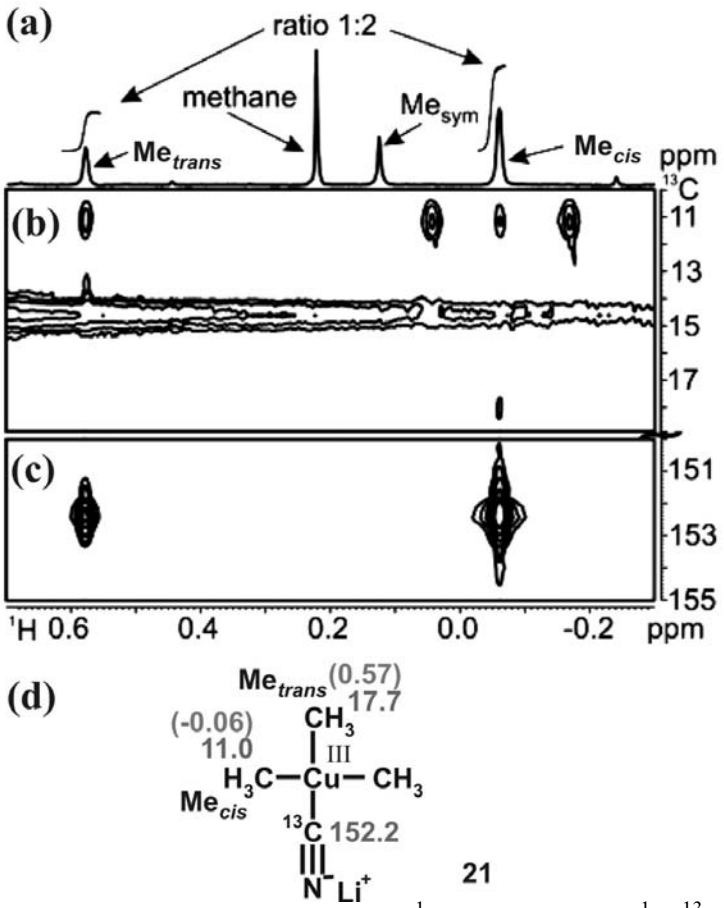

Figure 31. Selected high field section of (a) a 1D ^{1}H and (b), (c) a $^{1}H,^{13}C$ HMBC spectrum, which prove the existence of (d) a square planar lithium trimethylcyanocuprate(III) **21** due to cross signals between (b) the different methyl signals (^{1}H chemical shifts in parenthesis in d) and (c) cross signals between the methyl signals Me_{trans}/Me_{cis} and the cyanide. Me_{sym} is a separate, symmetrical species.[59]

Simultaneously to the described investigation of **20**, further Cu(III) intermediates of organocuprate substitution reactions were reported by applying rapid injection NMR in THF as solvent.[65] In Figure 32, exemplarily the time dependent intensity developments of the ^{1}H signals of the cyano Cu(III) and the iodo Cu(III) intermediates are shown. These Cu(III) intermediates were formed immediately after the injection of ethyl iodide into a cuprate/THF solution at -100°C and could be assigned via 1D ^{1}H, ^{13}C, 2D NOESY and HMQC spectra.

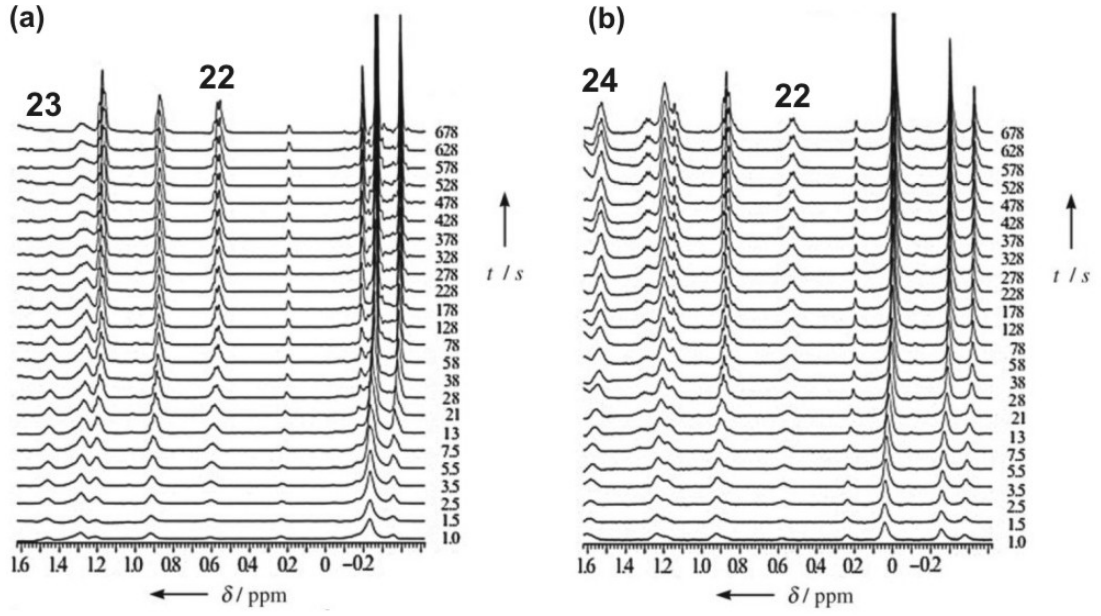

Figure 32. Time dependent ^{1}H NMR spectra from the rapid-injection treatment of (a) **1**•LiI and (b) **1**•LiCN with ethyl iodide. In (a) Me_2EtCuI (**23**) and (b) $Me_2EtCu(CN)$ (**24**) are observed, and both samples show signals assigned to Me_3EtCu (**22**).[65]

This experiment was repeated with various cuprates, Me_2CuLi•LiI (**1**•LiI), Me_2CuLi•LiCN (**1**•LiCN), Me_2CuLi•LiSCN (**1**•LiSCN) and Me_2CuLi•LiSPh (**1**•LiSPh) and yielded quite a number of different Cu(III) σ-complexes (Table 5).[65] Throughout all of these Cu(III) species, $^{2}J_{C,C}$ coupling constants were used to confirm the connectivity. With ^{13}C labelled cuprates and $CH_3{}^{13}CH_2I$, several coupling constants were determined for these compounds (Table 5), with the coupling constants across copper being consistent with the stereochemistry ($^{2}J_{trans}$ >> $^{2}J_{cis}$).[65,204,205] Again the carbon chemical shifts of the Cu(III) species show very deshielded values in the range of 13 ppm to 20 ppm for the CH_3 substituents and 28 ppm to 39 ppm for the CH_2 group of the ethyl substituent. The proton chemical shifts reveal values in the range of -0.5 ppm to 0.8 ppm and 0.5 ppm to 1.8 ppm, respectively (Table 5). In contrast, in cuprates the ^{13}C chemical shifts vary only between -9.07 ppm and -9.50 ppm and those of ^{1}H between -1.31 ppm and 1.41 ppm (Table 5). These deviating chemical shift differences in Cu(I) and Cu(III) complexes reflect the different binding properties between the copper compound and the anions of the previous copper salts (e.g. CN^-, I^-, SCN^-). In the Cu(I) complexes mainly ionic interactions exist between these species, whereas in the Cu(III) complexes the salt anions are covalently bound.

Table 5. ^{13}C NMR (^{1}H NMR) chemical shifts[a] for tetracoordinate, square planar Cu(III) σ-complexes in THF.[65]

Complex	δ Me	δ Et (CH_2,CH_3)	δ Cuprate[b]
Me_3EtCu[c]	13.26, 16.03[d]	28.17, 16.13	[e]
(22)	(−0.42, −0.29[d])	(0.54, 1.15)	
Me_2EtCuI	16.03	33.67, ND	−9.07
(23)	(−0.07)	(1.48, 1.28)	(−1.39)
$Me_2EtCuCN$[f]	14.06	34.66, 16.03	−9.11
(24)	(0.00)	(1.54, 1.20)	(−1.41)
$Me_2EtCuSCN$	17.42	39.07, ND	−9.08
(25)	(−0.21)	(1.36, 1.26)	(−1.31)
trans-$Me_2EtCuSPh$	18.06	34.21, 17.53	−9.50
(26a)	(−0.31)	(1.83, 1.31)	(−1.31)
cis-$Me_2EtCuSPh$	14.83, 20.40	30.04, 15.60	−9.50
(26b)	(−0.50, 0.83)	(0.53, 1.14)	(−1.31)

[a] Chemical shifts d [ppm] vs. TMS. ND = not determined. [b] Shifts of starting cuprate, 1•LiX (X = I, CN, SCN,SPh), before injection. [c] Shifts for 22 from 24, see [e]. [d] 2 x area of other Me peak. [e] Prepared from 1•LiX. The shifts of the ^{13}C atom bonded to copper in 22 vary with Cu salt by ± 0.1 ppm. [f] Cyanide ^{13}C shifts are d = 152.66 ppm for 24 and d = 158.95 ppm for 1•LiCN.

In addition to the trialkyl Cu(III) species with iodide (**23**), cyanide (**24**), thiocyanate (**25**) or thiophenolate (**26a**, **26b**) attached, quite often also the tetra alkyl species Me_3EtCu **22** was detected in this study (Table 5, Figure 32).[65] Interestingly, the tetra alkyl species **22** is exceedingly stable, because after warming up the sample to -10°C and re-cooling to -100°C, the tetra alkyl species predominated in solution.[65] In the case of an injection of ethyl iodide to **1**•LiSPh, an isomerisation process between *trans*-$Me_2EtCuSPh$ (**26a**) and *cis*-$Me_2EtCuSPh$ (**26b**) was also detected. In further studies, in which Gilman cuprates were treated with different stabilising agents, e.g. pyridine or PBu_3, even neutral copper complexes were detected in THF.[64] In addition, the described Cu(III) investigations demonstrate impressively the influence of the solvent on the reaction rates of organocuprates even on the level of Cu(III) intermediates. In THF, the reaction rate of the cross-coupling with methyl iodide as alkyl halide is too fast to observe any intermediate signals even with rapid injection NMR. In contrast, in diethyl ether a long term stabilization of the Cu(III) intermediate **21**, which is produced from MeI, is possible.

For S_N2' substitution reactions of organocuprates and allylic substrates, a reaction mechanism including Cu(III) intermediates similar to that of classical substitution reactions was proposed[111,173,174] and recently theoretical calculations on the origin of the regio- and stereoselectivity in S_N2' reactions were published.[206] With rapid injection NMR, the reaction of allyl chloride with the Gilman cuprates Me_2CuLi•LiX (X=I, CN) was investigated and

Cu(III) species were found also for this allylic substitution reactions.[57] Interestingly, after injection of 1,3-^{13}C labelled allyl chloride (**27**) into a solution of **1**•Li^{13}CN in THF (Figure 33a), the ^{13}C chemical shifts of the allyl part indicate two different Cu(III) complexes being present in solution, a Cu(III) σ-complex and a Cu(III) π-allyl-complex (Figure 33b).

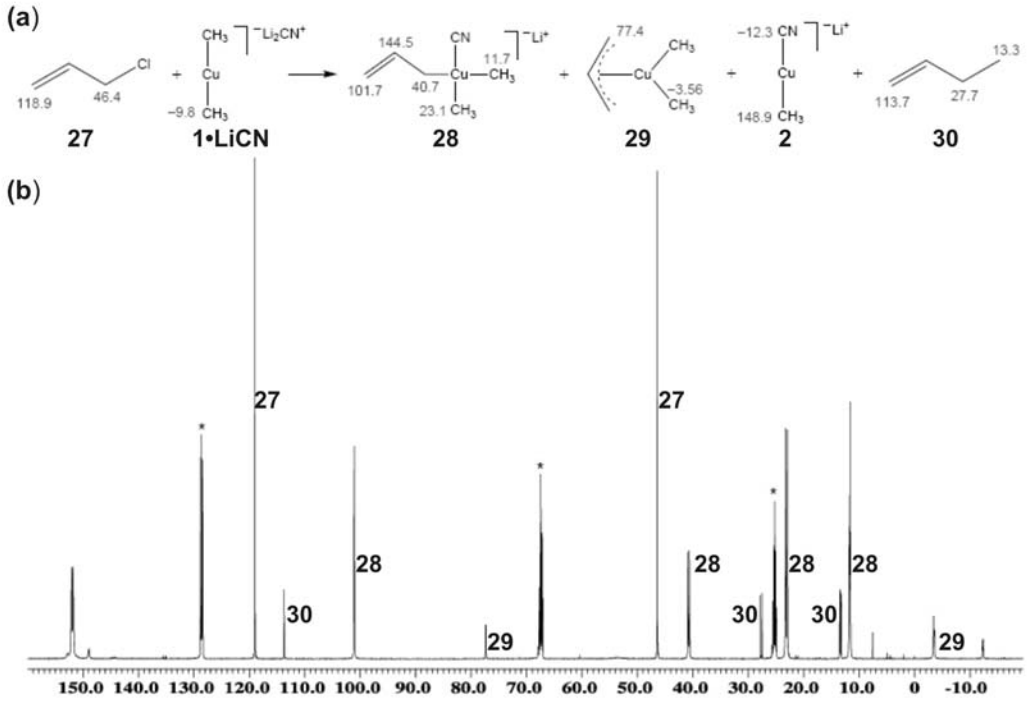

Figure 33. (a) Reaction of allyl chloride **27** (allyl-1,3-^{13}C chloride, 50 atom % at each position) with ($^{13}CH_3)_2$CuLi·Li^{13}CN (**1**•LiCN) and (b) ^{13}C NMR spectrum of products **28** (major) and **29** (minor) in THF-d_8 at –100° C. Asterisks denote solvent peaks.[57]

For compound **28** (Figure 33a), the methyl ^{13}C chemical shifts of 11.7 ppm and 23.1 ppm indicate the presence of a Cu(III) σ-complex in agreement with the previous Cu(III) NMR studies. For the π-allyl copper complex, identical ^{13}C chemical shifts (δ(^{13}C) = 77.4 ppm) of C1 and C3 of the allyl ligand (**29**, Figure 33a) and one chemical shift for the methyl groups bound to copper (δ(^{13}C) = -3.56 ppm) indicate an η_3 π-allyl-complex. Interestingly, the cuprate ^{13}C chemical shifts and $^2J_{C,C}$ coupling constants in this π-allyl-complex are quite similar to those observed in Cu(I) π-complexes of cuprates and α,β unsaturated Michael acceptors ($^2J_{C,C}$ = 12 Hz, see Figure 19). This is in accordance with theoretical calculations, which show that the formal Cu(III) π-allyl-complex has a binding situation similar to that of Cu(I) π-complexes.[57]

Rapid injection NMR spectra of these Cu(III) σ-allyl- and π-allyl-complexes show the time dependent interconversion of the two species (Figure 34b). The σ-allyl-complex is formed

directly after the injection of **27** (Figure 34a) and then its amount decreases in favour of the π-allyl complex. This suggests a thermodynamically higher stability of the π-allyl copper complex **29**.

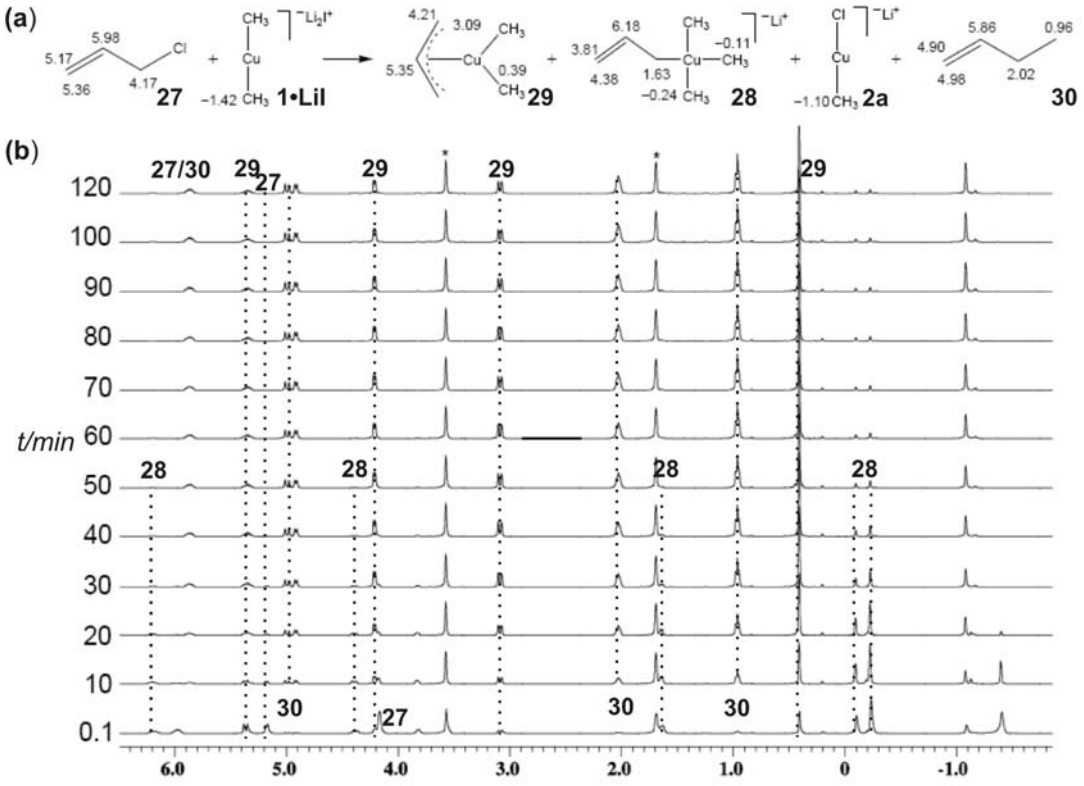

Figure 34. ^{1}H NMR spectra (b) of the products **29** and **28** at regular time intervals after injection of **27** into **1**•LiI (a).[57]

2.4 NMR Structure Elucidation in Cu(I) Catalysed Reactions

2.4.1. Catalytic Copper Complexes with Thiol-TADDOL Ligands

Nowadays, a multitude of catalytic metal/ligand combinations is accessible in organic synthesis. For copper and its catalytic properties, a recent series of reviews and the edition of this book describe the synthetic potential of copper catalyzed reactions in detail.[11-15,18,21,23] However, structure elucidation reports on catalytic copper systems are very rare and the amount not at all comparable to the numerous studies with e.g. Pt, Pd, or Rh as central transition metals. For example, in copper-catalyzed 1,4-addition reactions only a few crystal structures of precatalytic copper phosphoramidite complexes are published.[207,208] All of these crystal structures show a tetrahedral coordination on copper, which does not explain the

ligand accelerated catalysis observed in these reactions. Only in the last few years, NMR spectroscopic investigations revealed some structural details about precatalytic copper complexes in solution.[19] In the following, two examples will be discussed in detail, although diimine copper complexes[209-215] and ferrocene derived diphosphine copper complexes[216-218] have also been investigated.

A very remarkable study compares the structures of Cu(I) complexes with thiol-TADDOL ligands in the solid state and in solution.[219] In copper catalyzed enantioselective 1,4-additions of Grignard-reagents high *er* values are obtained in the presence of thiol-TADDOL ligands (Scheme 5). In this reaction, also an inversion of the *er* ratio can be achieved by applying the different derivatives **31**, **32** and **33**. Ligand **31** (Scheme 5a) catalyses the formation of (-)-(S)-3-butylcycloheptanone, whereas ligands **32** and **33** (Scheme 5a) form (+)-(R)-3-butylcycloheptanone.[220] Additionally, for ligands **31** and **32** a small non-linear effect was found, which suggests the participation of more than one ligand in the catalytically active complex.[219]

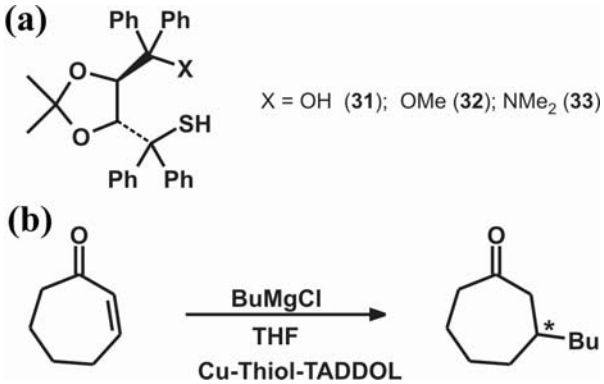

Scheme 5. (a) Thiol-TADDOL ligands **31-33**. (b) Copper-catalyzed conjugate addition: *er* = 92:8 (with **31**) and *er* = 8:92 (with **32** or **33**).[219]

For X-ray studies, crystals could be obtained by treating **31**, **32** or **33** with butyl lithium and adding afterwards CuCl. For each complex, the solid state structure shows a Cu_4S_4-unit, in which each sulfur atom is coordinated to two copper atoms. Interestingly, no interaction between the -OH, -OMe or -NMe_2 groups of the ligand and the metal centre is observed, that means, the thiol-TADDOL acts as a monodentate ligand.[219]

Subsequent NMR diffusion measurements of the pure ligands **31** and **32** (Scheme 5a) and the corresponding Cu_4L_4 complexes revealed that the Cu_4S_4-core unit remains intact in solution. Now the question arose, whether the Cu_4L_4 complex remains stable upon transmetalation. To model the transmetalation process and simultaneously to produce NMR

suitable samples, isocyanide was used as additional ligand and diffusion measurements indicated also Cu_4L_4 complexes for the isocyanide derivatives **34** – **36** (Figure 35).

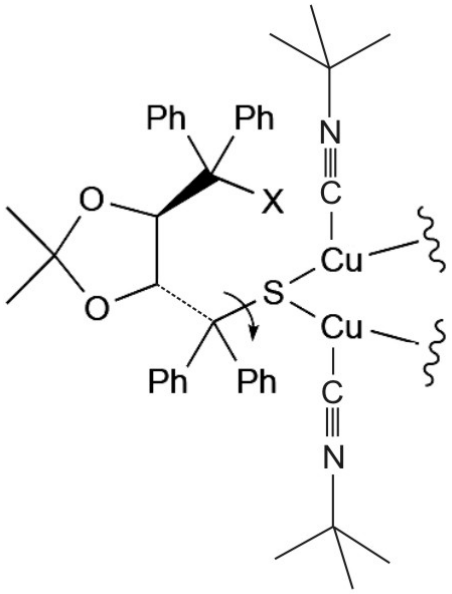

X = OH (**34**); OMe (**35**); NMe_2 (**36**)

Figure 35. Part of the Cu_4 (thiol-TADDOL)$_4$ structure, adopting a different conformation for **34** in contrast to **35** and **36**. This conformational change is indicated by an arrow.[219]

In addition, ^{1}H,^{1}H NOESY spectra of **34** (Figure 36a) and **35** (Figure 36b) were recorded in order to gain information, whether the observed inversion of enantioselectivity for **31** compared to **32**/**33** can be correlated with the 3-dimensional structures of their isocyanide complexes. Indeed, the NOESY cross peak sections of the isocyanide protons and the aryl protons of **34** and **35** show different signal intensities. For **34**, the methyl protons of the butyl group exhibit strong cross peaks to both sets of phenyl protons (Figure 36a), whereas in **35** the butyl protons have only a very weak interaction with the phenyl protons adjacent to the methoxy functional group (Figure 36b). This indicates a conformational change via rotation around the C-S bond (indicated in Figure 35 by an arrow), derivatising the free alcohol (**34**) into the methoxy substituent (**35**), and explains the observed inversion of enantioselectivity.

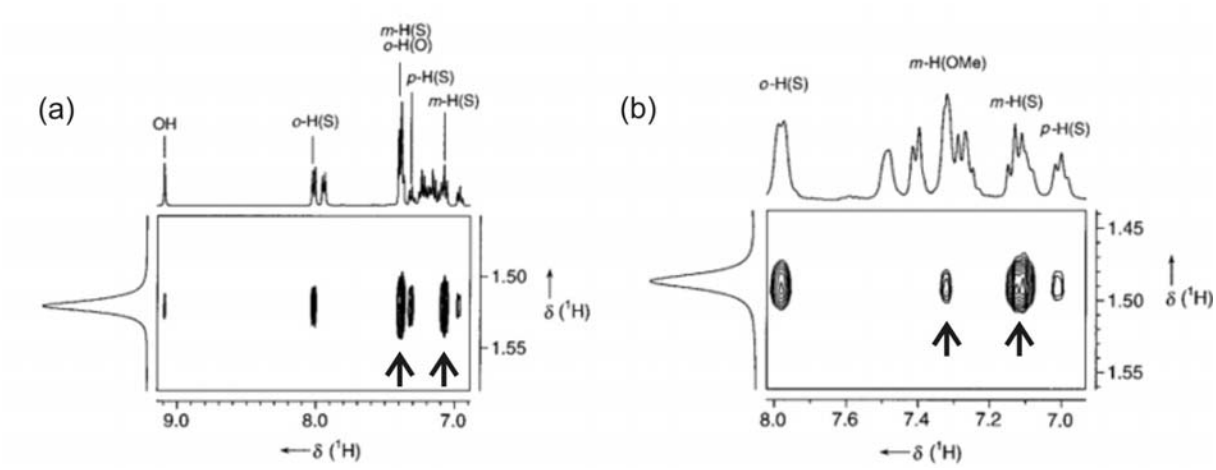

Figure 36. Sections of $^{1}H,^{1}H$ NOESY spectra of the complexes (a) **34** and (b) **35**. The labels O, S, and OMe in parenthesis refer to protons of the $Ph_2C(OH)$, $Ph_2C(S)$ and $Ph_2C(OMe)$ groups, respectively. Arrows indicate the significant cross peaks.[219]

2.4.2. Catalytic Copper Complexes with Phosphoramidite Ligands

In the past few years, the interest in chiral monodentate ligands has grown enormously.[221,222] In particular the biphenol- or binaphtol-based phosphoramidite ligands[223-226] are reported to yield high *ee*-values and tolerate a wide range of different reaction types and transition metals. Additionally, the phosphoramidites are applicable to a large variety of substrates, such as cyclic and acyclic enones, malonates, unsaturated nitro-olefins, unsaturated piperidones, and unsaturated imines or amines.[23] This broad range of applications suggests the existence of so called privileged ligand structures in the case of phosphoramidite ligands. In 1,4-addition reactions of dialkylzinc reagents, catalytic amounts of copper(I)salts (Scheme 6) in the presence of chiral monodentate phosphoramidites (Figure 37) yield excellent *ee*-values.[18,23,108,219,227-229] Two promising ligands, which combine atropisomerism with two stereogenic centres, are the binaphthol based (**37**) and biphenol based (**38**) phosphoramidites shown in Figure 37.

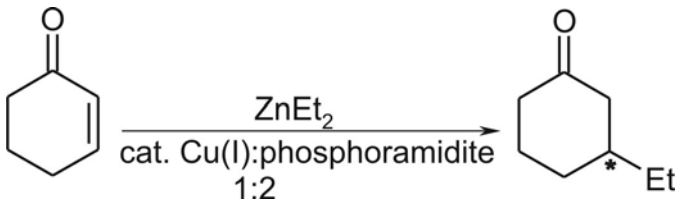

Scheme 6. Schematic description of the Cu(I)-catalyzed asymmetric 1,4-addition of non-stabilized carbon nucleophiles.[23]

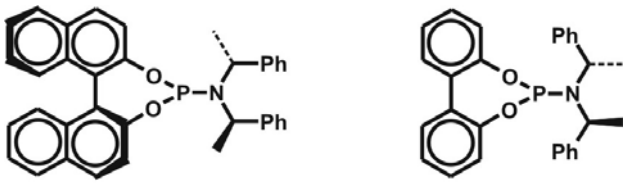

37 38

Figure 37. Two representative phosphoramidite ligands derived from binaphthol and biphenol.[228,230]

In 2002 Alexakis reported that highly enantioselective copper catalyzed 1,4-addition reactions of diethylzinc to cyclohexenone in the presence of **38** do not necessarily need toluene as solvent but are also possible in several other organic solvents and with a couple of different copper salts.[230] These synthetic results laid the basis for subsequent NMR spectroscopic investigations of precatalytic phosphoramidite copper complexes, because it was now possible to use several combinations of solvents and copper salts for the optimization of the spectroscopic properties (aggregation, linewidths, number of compounds, relaxation properties) without loosing relevance for the interpretation of synthetic results.

Under experimental conditions close to those used in synthetic 1,4-addition reactions, the ^{31}P spectra of 1:2 mixtures of different copper salts and **37** or **38** show the coexistence of free ligand and at least one copper phosphoramidite complex in solution (see Figure 38a). In the corresponding ^{1}H spectra the signals of the free ligand and the copper complexes show no separate signals but nearly completely overlapping chemical shifts. Therefore, 1D ^{31}P spectra are the key to distinguish different species of phosphoramidite Cu complexes in solution (for spectroscopic properties see Table 1) and were used to identify the solvent dependence of the complex species (Figure 38a).[231] In THF and toluene, broad signals of several complex species are observed, whereas in $CDCl_3$ and CD_2Cl_2 a single complex signal is detected (denoted as **C2**) besides the free ligand. By reducing the ligand to copper ratio from 2:1 to 1:1, one of the other complexes in Figure 38a could be assigned to the 1:1 phosphoramidite copper complex **C1** (Figure 38b). Based on these results, $CDCl_3$ and CD_2Cl_2 were chosen, because these solvents allow a separation of the two species **C1** and **C2** and simultaneously provide high *ee*-values in 1,4-addition reactions.

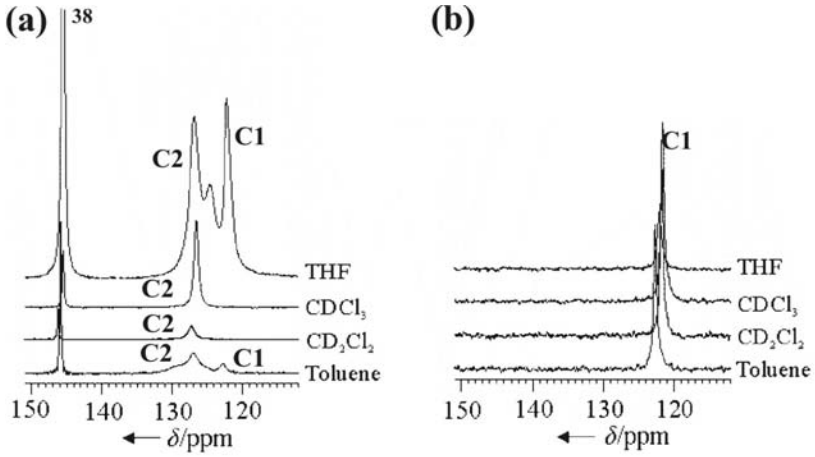

Figure 38. ^{31}P spectra of ligand **38** and CuCl in varying solvents and at a ratio of ligand:CuCl of (a) 2:1 and (b) 1:1 at 220 K.[231]

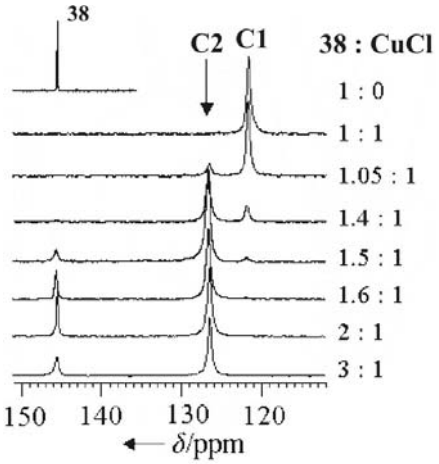

Figure 39. ^{31}P spectra of CuCl and ligand **38** at varying ratios in $CDCl_3$ at 220 K.[231]

From the synthetically optimized conditions it was proposed that a L_2Cu complex is the catalytically active species. Therefore, it was surprising that a 2:1 ratio of ligand to copper salt produced signals of **C2** plus free ligand. At this point, ^{31}P spectra with varying ratios of copper salt to ligand revealed the stoichiometry of **C2** (Figure 39). A 1:1 ratio exclusively produces **C1** (δ = 121.7 ppm). The addition of more ligand leads to the formation of **C2** (δ = 126.6 ppm) and to a decrease of **C1**. At 1.5:1 mainly **C2** is present besides small amounts of free ligand and **C1** and at higher ratios **C2** and increasing amounts of free ligand are detected. These spectra show that only in the case of a 1:1 ratio a single species (**C1**) exists in solution, which can be characterised directly with diffusion experiments. For all other ratios and especially for the diffusion characterisation of **C2**, separated signals for free and coordinated ligands would be necessary, which do not exist in the ^{1}H spectra due to severe signal overlap.

Also the well separated ^{31}P signals were not suitable for DOSY experiments, because quadrupole relaxation and exchange phenomena cause too short transversal relaxation times visible in extremely broad line widths. At this point serendipity helped to cut this Gordian knot. The internal dynamic of the phosphoramidite ligands is considerably influenced by its kind of complexation. As a result, the methine proton in **38** and **37** features different line widths in the free ligand, **C1** and **C2**, with the line width of **C2** being fortunately by far the smallest one at 220 K. This allows one to use the quite long convection compensating DOSY pulse sequence of Jerschow and Müller[100] as complex selective T_2 filter for the exclusive detection of the DOSY attenuation of **C2**.[231]

Table 6. Diffusion constants D ($10^{-10}m^2s^{-1}$) of the free ligands **37** and **38**, and the complexes **C1** and **C2** consisting of CuCl and ligands **37** or **38**.[231]

ligand	D(ligand)	D(**C1**)	D(**C2**)
37	2.30	1.60	1.62
38	2.68	1.81	1.83

The experimental diffusion constants of **C1** and **C2** with the identical ligand are very similar, while the free ligands, **37** and **38,** and the corresponding complexes with different ligands reveal well separated diffusion constants according to their size (Table 6). To interpret these experimental diffusion data, structural models were derived from crystal structures with ligand (L) to copper salt ratios between 1:1 and 3:1 and a maximum number of four ligands in the complex (Figure 40).

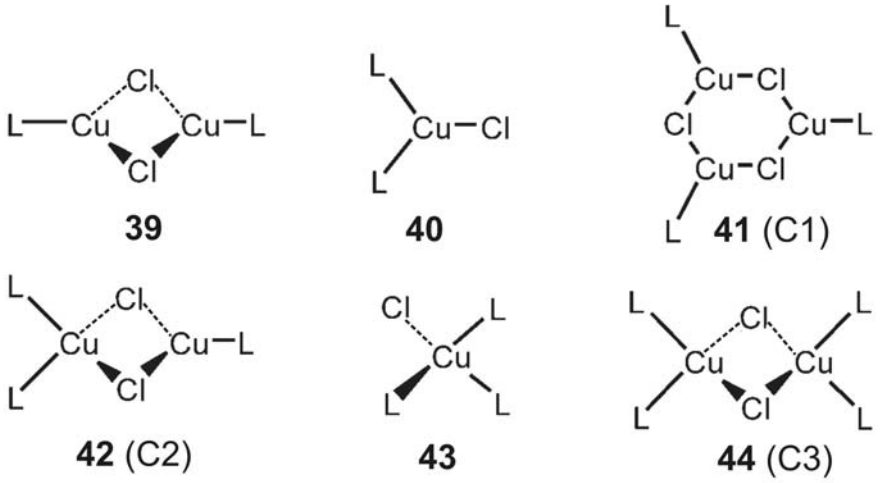

Figure 40. Schematic models of copper(I)complexes with one, two or three metal atoms based on crystal structures of phosphoramidite and phosphine Cu-complexes.[231]

From experimentally determined ligand volumes and hard sphere increments of the copper salts, the theoretical volumes of these models were derived and compared to the experimentally detected ones. With this method it could be shown that three phosphoramidite ligands exist in **C1** and **C2**. The volume of different amounts of copper salts in the two complexes is within the experimental error of the DOSY measurements. Therefore, this information was taken from the ^{31}P spectra shown in Figure 39 and **C1** could be proposed to be structure **41** and **C2** correlated with structure **42** (Figure 40). Due to the fact that in synthetic protocols the 2:1 ratio was reported to give the highest *ee*-values, and at a 2:1 ratio only **C2** is present besides free ligand (Figure 39), complex **C2** can be proposed to be the precatalytic complex.

A further NMR spectroscopic screening with three phosphoramidite ligands and four Cu(I)X salts (X = Cl, Br, I, thiophene-2-carboxylate) confirmed the mixed trigonal/tetrahedral Cu-coordination in **42** as basic structural motif of precatalytic phosphoramidite copper complexes with a free coordination site for transmetalation.[232]

Due to the fact that the above described structure elucidation process of **C2** does not conform to a classical NMR structure determination, additional low temperature ^{31}P spectra of phosphoramidite copper complexes were recorded. The resolved low temperature spectra of CuCl/**37** and CuI/**38** are shown in Figure 41, representing the two principal signal pattern found in the low temperature spectra of various phosphoramidite copper complexes.[61]

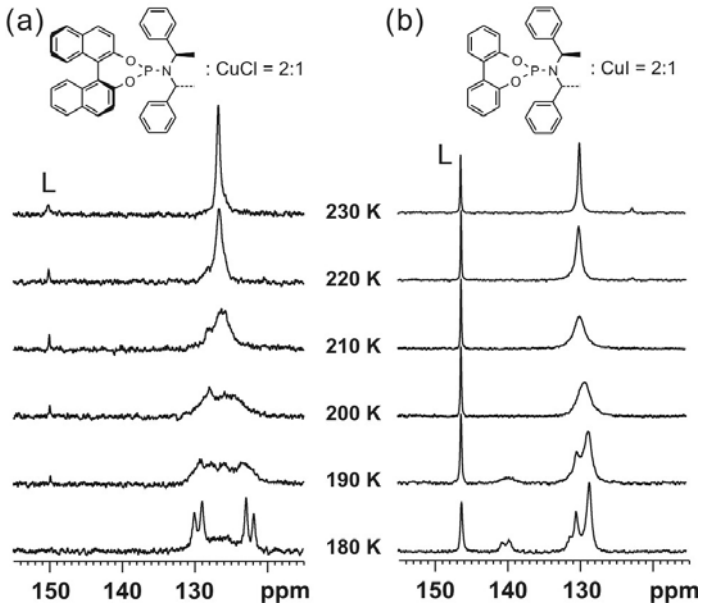

Figure 41. ^{31}P NMR spectra of the combinations (a) ligand **37**/CuCl and (b) ligand **38**/CuI at a ratio of 2:1 at different temperatures in CD_2Cl_2. L indicates the free ligand.[61]

The CuCl containing sample (Figure 41a and 42a) is the first example of phosphoramidite copper complexes, in which a resolved AA´BB´ signal pattern with a $^{2}J_{P,P}$ coupling of 260 Hz is detected.[61] This and cross signals in the low temperature $^{31}P,^{31}P$ COSY spectra indicate CuLL´ subunits, in which the two ligands have different three-dimensional orientations with chemically non-equivalent phosphorous atoms. Diffusion measurements of closely related complexes showed that these CuLL´ subunits are part of a $L_2L_2´Cu_2Cl_2$-complex (Figure 42) as already found in a phosphoramidite crystal structure.[208] Furthermore, dynamic NMR simulations indicate high ligand exchange rates in these complexes (Figure 42b).[61]

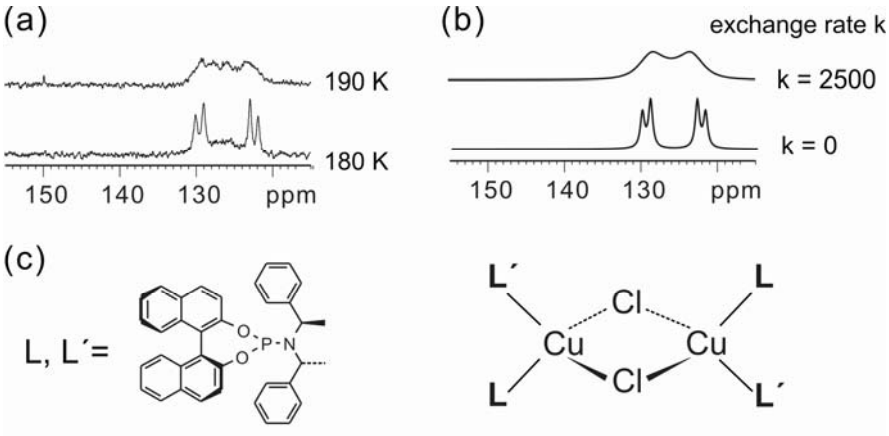

Figure 42. (a) Experimental and (b) simulated spectra of the low temperature complex composed of **37** and CuCl. (c) Schematic structures of the ligand and the $L_2L_2´Cu_2X_2$ complex are given. L and L´ represent the identical ligand in different sterical arrangements resulting in separated ^{31}P signals.[61]

A comparison of the spectrum of the $L_2L_2´Cu_2Cl_2$ complex of **37**/CuCl (Figure 41a) with that of **38**/CuI (Figure 41b) suggests for **38**/CuI a combination of two complex species with one part being the already identified type $L_2L_2´Cu_2X_2$. An intensity adapted simulation of the spectra reveal the second complex species to have two signals with an intensity ratio of 1:2, which fits perfectly to the previously proposed mixed trigonal/tetrahedral precatalyst. Hence, a separated simulation of the ^{31}P spectra of $L_2L_2´Cu_2I_2$ (Figure 43a) and of $LL_2´Cu_2I_2$ (Figure 43b) was the basis for the interpretation of the low temperature species of **38**/CuI at 180 K. An intensity-adapted superposition (Figure 43c) of the simulated spectra of $L_2L_2´Cu_2I_2$ (Figure 43a) and of $LL_2´Cu_2I_2$ (Figure 43b) shows a nearly perfect agreement with the experimental spectrum in Figure 43d. Thus, the existence of the mixed trigonal/tetrahedral complex **C2** was also proven by classical NMR spectroscopic methods.

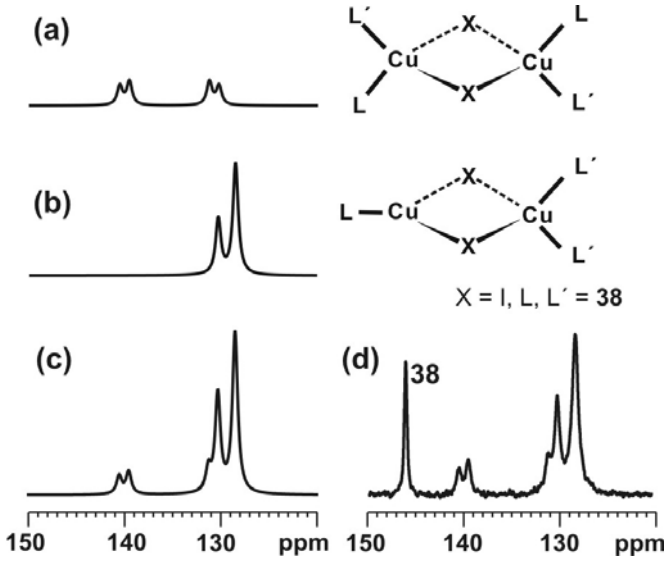

Figure 43. Simulated ^{31}P NMR spectra of (a) the $L_2L_2'Cu_2X_2$ complex, (b) the $LL_2'Cu_2X_2$ complex, and (c) an intensity adapted superposition of (a) and (b). The superposition (c) shows an excellent agreement with (d) the experimental ^{31}P spectrum of a 2:1 ratio of **38** to CuI at 180 K. L and L´ represent an identical ligand in different sterical arrangements resulting in separated ^{31}P signals.[61]

The combined interpretation of low temperature ^{31}P spectra and temperature dependent DOSY information of various phosphoramidite copper complexes hinted at a temperature dependent interconversion of different copper complex species in solution. For example, in DOSY measurements, CuL_2 complexes were detected at higher temperatures (300 K) and these copper complexes aggregate with decreasing temperature up to $L_4Cu_2X_2$ complexes at 180 K. A temperature dependent interconversion of different catalytic species in solution is of extreme interest for synthetic applications and would explain the observed temperature sensitivity of these reactions. However, from the low spectral resolution and the averaged signals of the temperature dependent ^{31}P spectra shown in Figure 44 it is obvious that a classical NMR quantification of the different complex species, for which well separated and well resolved signals are necessary, is not possible. Therefore, the well resolved and sharp ^{31}P signal of the free ligand was used as indicator for the existing copper species in solution. From the investigations described, the possibly different coexisting copper complexes were identified as **C1**, **C2**, and **C3** (for schematic models see Figure 40), possessing the different ligand to copper salt ratios of 1:1, 1.5:1, and 2:1, respectively. That means, in the case of a temperature dependent interconversion of **C1** into **C2** and then into **C3** that the free ligand is stepwise consumed and reflects the interconversion step as shown exemplarily in Figure 44a. The temperature dependent amounts of **C1**, **C2**, **C3**, and free ligand, which are derived from

the ^{31}P integrals of a 2:1 ratio of **38**/CuI, are displayed in Figure 44b. These graphs show that above 210 K small amounts of **C1** coexist beside the main complex **C2**. At 210 and 200 K **C2** exists exclusively in solution and it partially interconverts into **C3** at temperatures below 200 K. Interestingly, at a 1.5:1 ratio of ligand to copper, i.e., at the stoichiometry of the precatalytic complex **C2** ($L_3Cu_2X_2$), the stability of **C2** is reduced. This is obvious from Figure 44c showing a significantly reduced temperature range, in which **C2** exclusively exists. With this method, the amount of the different copper complexes can be detected even in temperature regions in which spectroscopically unresolved complex signals exist, because the free ligand is used as a spy for the interconversion of stoichiometrically deviating complexes.

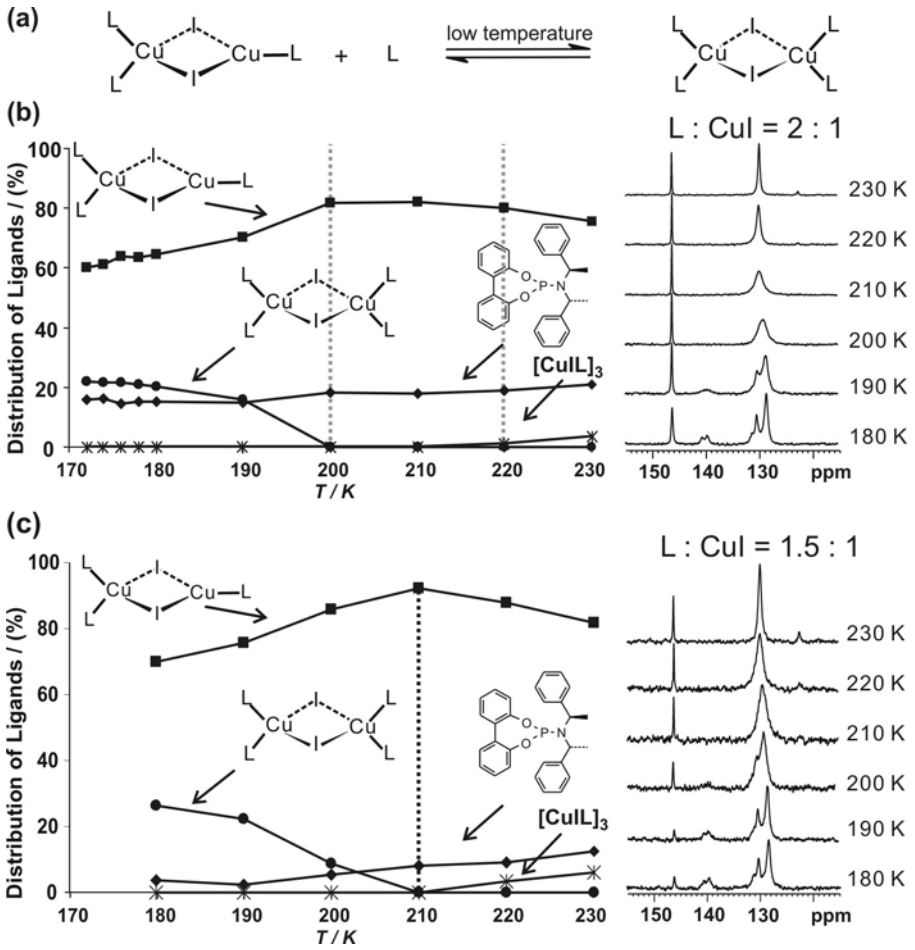

Figure 44. (a) Schematic representation of the temperature dependent interconversion of **C2** into **C3**. Relative ^{31}P integral values and experimental ^{31}P spectra of a **38**/CuI ratio of (b) 2:1 and (c) 1.5:1 at temperatures between 170 and 230 K; free ligand (♦), **C1** (x), **C2** (■), and **C3** (●).[61]

2.5 Conclusion

For decades, the disadvantageous properties of the two Cu isotopes, the presence of dynamic equilibria, and the complex supramolecular structures hampered the structure elucidation of organocopper complexes in solution. With continuous developments in NMR spectroscopic techniques, the switch to the NMR active nuclei in the ligands of organocopper complexes, and step–by-step structural approaches, it was recently possible to elucidate the supramolecular structures of stoichiometric and catalytically active copper reagents in solution. In these complexes, the high symmetry of the aggregates often hampers the application of classical NMR spectroscopic approaches. However, elaborate DOSY, HOE, and NOE NMR spectroscopic measurements, which are tailored to the specific structure problems, allow to gain insights into the structures and sizes of these supramolecular assemblies, which is still a challenging task.

For organocuprates, it could be shown that the linear cuprate units form homodimer core structures in diethyl ether solution, which tend to aggregate in a chain-like manner bridged by salt and solvent molecules. These supramolecular aggregates of organocuprates could be correlated with their reactivities in addition reactions to α,β-unsaturated enones. Furthermore, the two approaches of intermediate stabilisation, i.e., the rapid injection NMR at low temperatures and the preparative stabilisation in conventional low temperature NMR, in combination with isotopic labelling, allowed the detection of elusive intermediate structures of copper mediated reactions. Thus, it was experimentally proven via NMR spectroscopy that both π- and σ-complexes of the Cu(I)/Cu(III) redox system are the decisive intermediate complexes in copper mediated conjugate addition and S_N2/S_N2' reactions.

In the case of catalytic copper complexes, the continuous spectroscopic improvement allowed for a structure elucidation revealing multinuclear complexes. Again, via DOSY and NOE measurements, for both, TADDOL-like as well as phosphoramidite ligands, detailed structural information was derived from NMR in solution. Especially, for phosphoramidites and their precatalytic complexes, it was possible to obtain important information about the temperature dependent stability of the precatalytic copper complexes, which may be very helpful for a further design of catalytically active complexes. Thus, the recent progress in structure elucidation of organocopper compounds in solution by NMR spectroscopy shows impressively the capability of this method, which should encourage further research in the field of supramolecular assemblies throughout organocopper chemistry.

2.6 References

(1) Berners-Price, S. J.; Ronconi, L.; Sadler, P. J. *Prog. Magn. Res. Spectrosc.* **2006**, *49*, 65-98.

(2) Dybowski, C.; Neue, G. *Prog. Magn. Res. Spectrosc.* **2002**, *41*, 153-170.

(3) Ernsting, J. M.; Gaemers, S.; Elsevier, C. J. *Magn. Reson. Chem.* **2004**, *42*, 721-736.

(4) Johnels, D.; Guenther, H. *"Solid state NMR spectroscopy" in Organolithium Chemistry of Organolithium Compounds*; John Wiley&Sons: Chichester, UK, 2004 pp.137-203; Vol. 1.

(5) Penner, G. H.; Liu, X. *Prog. Magn. Res. Spectrosc.* **2006**, *49*, 151-167.

(6) Priqueler, J. R. L.; Butler, I. S.; Rochon, F. D. *Appl. Spectrosc. Rev.* **2006**, *41*, 185-226.

(7) Ramaprasad, S. *Prog. Magn. Res. Spectrosc.* **2005**, *47*, 111-121.

(8) Wrackmeyer, B. *Mod. Magn. Res.* **2006**, *1*, 457-459.

(9) Still, B. M.; Kumar, P. G. A.; Aldrich-Wright, J. R.; Price, W. S. *Chem. Soc. Rev.* **2007**, *36*, 665-686.

(10) Davies, J. A. In *The chemistry of the metal carbon bond*; Harley, F. R., Patai, S., Eds.; Wiley: 1982; Vol. 1, p 813.

(11) Yamada, K.-i.; Tomioka, K. *Chem. Rev.* **2008**, *108*, 2874-2886.

(12) Stanley, L. M.; Sibi, M. P. *Chem. Rev.* **2008**, *108*, 2887-2902.

(13) Shibasaki, M.; Kanai, M. *Chem. Rev.* **2008**, *108*, 2853-2873.

(14) Poulsen, T. B.; xf; rgensen, K. A. *Chem. Rev.* **2008**, *108*, 2903-2915.

(15) Meldal, M.; Torn; xf; e, C. W. *Chem. Rev.* **2008**, *108*, 2952-3015.

(16) Matsuo, Y.; Nakamura, E. *Chem. Rev.* **2008**, *108*, 3016-3028.

(17) Lipshutz, B. H.; Yamamoto, Y. *Chem. Rev.* **2008**, *108*, 2793-2795.

(18) Harutyunyan, S. R.; den Hartog, T.; Geurts, K.; Minnaard, A. J.; Feringa, B. L. *Chem. Rev.* **2008**, *108*, 2824-2852.

(19) Gschwind, R. M. *Chem. Rev.* **2008**, *108*, 3029-3053.

(20) Evano, G.; Blanchard, N.; Toumi, M. *Chem. Rev.* **2008**, *108*, 3054-3131.

(21) Deutsch, C.; Krause, N.; Lipshutz, B. H. *Chem. Rev.* **2008**, *108*, 2916-2927.

(22) Breit, B.; Schmidt, Y. *Chem. Rev.* **2008**, *108*, 2928-2951.

(23) Alexakis, A.; Bäckvall, J. E.; Krause, N.; Pamies, O.; Dieguez, M. *Chem. Rev.* **2008**, *108*, 2796-2823.

(24) Mason, J. *Multinuclear NMR*; Plenum Press: New York, 1987.

(25) Granger, P. *Transition Metal Nuclear Magnetic Resonace*; Elsevier: Amsterdam, 1991.

(26) Malito, J. *J. Annu. Rep. NMR Spectrosc.* **1999**, *38*, 265-287.

(27) Marker, A.; Gunter, M. J. *J. Magn. Reson.* **1982**, *47*, 118-32.

(28) Szymanska, I. *Polish J. Chem.* **2006**, *80*, 1095-1117.

(29) Irangu, J. K.; Jordan, R. B. *Inorg. Chem.* **2003**, *42*, 3934-3942.

(30) Kroneck, P.; Kodweiss, J.; Lutz, O.; Nolle, A.; Zepf, D. *Z. Naturforsch., Teil A.* **1982**, *37A*, 186-90.

(31) Kujime, M.; Kurahashi, T.; Tomura, M.; Fujii, H. *Inorg. Chem.* **2007**, *46*, 541-51.

(32) Ochsenbein, U.; Schlaepfer, C. W. *Helv. Chim. Acta* **1980**, *63*, 1926-31.

(33) Kitagawa, S.; Munakata, M.; Sasaki, M.; *Inorg. Chem. Acta* **1986**, *120*, 77-80.

(34) Kroneck, P.; Lutz, O.; Nolle, A.; Oehler, H. *Z. Naturforsch.* **1980**, *35A*, 221-5.

(35) Lutz, O.; Oehler, H.; Kroneck, P. *Z. Naturforsch.* **1978**, *33A*, 1021-4.

(36) Lutz, O.; Oehler, H.; Kroneck, P.; *Z. Physik A* **1978**, *288*, 17-21.

(37) Szlyk, E.; Szymanska, I. *Polyhedron* **1999**, *18*, 2941-2948.

(38) Black, J. R.; Levason, W.; Spicer, M. D.; Webster, M. *J. Chem. Soc., Dalton Trans.* **1993**, *20*, 3129-36.

(39) Fife, D. J.; Moore, W. M.; Morse, K. W. *Inorg. Chem.* **1984**, *23*, 1684-91.

(40) Berners Price, S. J.; Brevard, C.; Pagelot, A.; Sadler, P. J. *Inorg. Chem.* **1986**, *25*, 596-9.

(41) Doel, C. L.; Gibson, A. M.; Reid, G.; Frampton, C. *Polyhedron* **1995**, *14*, 3139-46.

(42) Mohr, B.; Brooks, E. E.; Rath, N.; Deutsch, E. *Inorg. Chem.* **1991**, *30*, 4541-5.

(43) Szlyk, E.; Kucharek, R.; Szymanska, I. *Polish J. Chem.* **2001**, *75*, 337-344.

(44) Szlyk, E.; Kucharek, R.; Szymanska, I. *J. Coord. Chem.* **2001**, *53*, 55-67.

(45) Szlyk, E.; Kucharek, R.; Szymanska, I.; Pazderski, L. *Polyhedron* **2003**, *22*, 3389-3393.

(46) Connor, J. A.; Kennedy, R. J. *Polyhedron* **1988**, *7*, 161-2.

(47) Endo, K.; Yamamoto, K.; Deguchi, K.; Matsushita, K. *Bull. Chem. Soc. Jpn.* **1987**, *60*, 2803-7.

(48) Geerts, R. L.; Huffman, J. C.; Folting, K.; Lemmen, T. H.; Caulton, K. G. *J. Am. Chem. Soc.* **1983**, *105*, 3503-6.

(49) Gill, D. S.; Byrne, L.; Quickenden, T. I. *Z. Naturforsch.* **1998**, *53a*, 1004-1008.

(50) Gill, D. S.; Kamp, U.; Doelle, A.; Zeidler, M. D. *Ind. J. Chem.* **2001**, *40A*, 693-699.

(51) Gill, D. S.; Rodehüser, L.; Delpuech, J. J. *J. Chem. Soc., Faraday Trans.* **1990**, *86*, 2847-52.

(52) Gill, D. S.; Rodehuser, L.; Rubini, P.; Delpuech, J. J. *J. Chem. Soc., Faraday Trans.* **1995**, *91*, 2307-12.

(53) Gill, D. S.; Singh, J.; Singh, R.; Zamir, T.; Quickenden, T. I. *Ind. J. Chem.* **1999**, *38A*, 913-920.

(54) Kitagawa, S.; Munakata, M. *Inorg. Chem.* **1984**, *23*, 4388-90.

(55) Nilsson, K. B.; Persson, I. *J. Chem. Soc., Dalton Trans.* **2004**, *9*, 1312-9.

(56) Goodfellow, R. *Post-Transition Metals, Copper to Mercury, in Multinuclear NMR, J. Mason Ed.*; Plenum Press: New York, 1987; Vol. 19.

(57) Bartholomew, E. R.; Bertz, S. H.; Cope, S.; Murphy, M.; Ogle, C. A. *J. Am. Chem. Soc.* **2008**, *130*, 11244-11245.

(58) Bertz, S. H.; Cope, S.; Murphy, M.; Ogle, C. A.; Taylor, B. J. *J. Am. Chem. Soc.* **2007**, *129*, 7208-9.

(59) Gaertner, T.; Henze, W.; Gschwind, R. M. *J. Am. Chem. Soc.* **2007**, *129*, 11362-11363.

(60) Tang, J. A.; Ellis, B. D.; Warren, T. H.; Hanna, J. V.; Macdonald, C. L. B.; Schurko, R. W. *J. Am. Chem. Soc.* **2007**, *129*, 13049-13065.

(61) Schober, K.; Zhang, H.; Gschwind, R. M. *J. Am. Chem. Soc.* **2008**, *130*, 12310-12317.

(62) Canisius, J.; Mobley, T. A.; Berger, S.; Krause, N. *Chem. Eur. J.* **2001**, *7*, 2671-2675.

(63) Henze, W.; Gärtner, T.; Gschwind, R. M. *J. Am. Chem. Soc.* **2008**, *130*, 13718-13726.

(64) Bartholomew, E. R.; Bertz, S. H.; Cope, S.; Dorton, D. C.; Murphy, M.; Ogle, C. A. *Chem. Commun.* **2008**, 1176-1177.

(65) Bertz, S. H.; Cope, S.; Dorton, D.; Murphy, M.; Ogle, C. A. *Angew. Chem. Int. Ed. Engl.* **2007**, *46*, 7082-5.

(66) Collum, D. B. *Acc. Chem. Res.* **1993**, *26*, 227-34.

(67) Corruble, A.; Davoust, D.; Desjardins, S.; Fressigne, C.; Giessner-Prettre, C.; Harrison-Marchand, A.; Houte, H.; Lasne, M.-C.; Maddaluno, J.; Oulyadi, H.; Valnot, J.-Y. *J. Am. Chem. Soc.* **2002**, *124*, 15267-15279.

(68) Fraenkel, G.; Fraenkel, A. M.; Geckle, M. J.; Schloss, F. *J. Am. Chem. Soc.* **1979**, *101*, 4745-7.

(69) Gregory, K.; Schleyer, P. v. R.; Snaith, R. *Adv. Inorg. Chem.* **1991**, *37*, 47-142.

(70) Lucht, B. L.; Collum, D. B. *Acc. Chem. Res.* **1999**, *32*, 1035-1042.

(71) Mulvey, R. E. *Chem. Soc. Rev.* **1991**, *20*, 167-209.

(72) Saspe, A.-M.; Schleyer, P. v. R. E. *Lithium Chemistry: A Theoretical and Experimental Overview*; Wiley: Chichester, 1995.

(73) Seebach, D.; Haessig, R.; Gabriel, J. *Helv. Chim. Acta* **1983**, *66*, 308-37.

(74) Sott, R.; Granander, J.; Hilmersson, G. *J. Am. Chem. Soc.* **2004**, *126*, 6798-6805.

(75) Avent, A. G.; Eaborn, C.; El-Kehli, M. N. A.; Molla, M. E.; Smith, J. D.; Sullivan, A. C. *J. Am. Chem. Soc.* **1986**, *108*, 3854-3855.

(76) Bauer, W.; Clark, T.; Schleyer, P. v. R. *J. Am. Chem. Soc.* **1987**, *109*, 970-977.

(77) Bauer, W.; Klusener, P. A. A.; Harder, S.; Kanters, J. A.; Duisenburg, A. J. M.; Brandsma, L.; Schleyer, P. v. R. *Organometallics* **1988**, *7*, 552-555.

(78) Bauer, W.; Müller, G.; Schleyer, P. v. R. *Angew. Chem., Int. Ed. Engl.* **1986**, *25*, 1103.

(79) Bauer, W.; Schleyer, P. v. R. *Magn. Reson. Chem* **1988**, *26*, 827-833.

(80) Bauer, W.; Schleyer, P. v. R. *Adv. Carbanion Chem.* **1992**, *1*, 89-175.

(81) Brand, T.; Cabrita, E. J.; Berger, S. *Prog. Magn. Reson. Spectrosc.* **2005**, *46*, 159-196.

(82) Günther, H.; Moskau, D.; Schmalz, D. *Angew. Chem.* **1987**, *99*, 1242-1250.

(83) Hilmersson, G.; Arvidsson, P. I.; Davidson, O.; Hakansson, M. J. *Am. Chem. Soc.* **1998**, *120*, 8143-8149.

(84) Macchioni, A. *Chem. Rev.* **2005**, *105*, 2039-2073 (Review).

(85) Mo, H.; Pochapsky, T. C. *Prog. NMR Spectrosc.* **1997**, *30*, 1-38.

(86) Pregosin, P. S.; Kumar, A. P. G.; Fernandez, I. *Chem. Rev.* **2005**, *105*, 2977-2998.

(87) Gschwind, R. M.; Xie, X.; Rajamohanan, P. R.; Auel, C.; Boche, G. *J. Am. Chem. Soc.* **2001**, *123*, 7299-7304.

(88) Neuhaus, D.; Williamson, M. *The Nuclear Overhauser Effect in Structural and Conformational Analysis*; VCH: Weinheim, 1989.

(89) Kawabata, J.; Fukushi, E.; J., M. *J. Am. Chem. Soc.* **1992**, *114*, 1115-1117.

(90) Wagner, R.; Berger, S. *Magn. Reson. Chem.* **1997**, *35*, 199-202.

(91) Gschwind, R. M.; Xie, X.; Rajamohanan, P. R. *Magn. Reson. Chem* **2004**, *42*, 308-312.

(92) Dehner, A.; Kessler, H. *ChemBioChem* **2005**, *6*, 1550-1565.

(93) Macchioni, A.; Ciancaleoni, G.; Zuccaccia, C.; Zuccaccia, D. *Chem. Soc. Rev.* **2008**, *37*, 479-89.

(94) Pregosin, P. S. *Prog. Nuc. Magn. Res. Spectrosc.* **2006**, *49*, 265-288.

(95) Stilbs, P. *Prog. NMR Spectrosc.* **1987**, *19*, 1-45.

(96) Cohen, Y.; Avram, L.; Frish, L. *Angew. Chem. Int. Ed. Engl.* **2005**, *44*, 520-54.

(97) Stejskal, E. O.; Tanner, J. E. *J. Chem. Phys.* **1965**, *42*, 288-292.

(98) Zuccaccia, D.; Macchioni, A. *Organometallics* **2005**, *24*, 3476-3486.

(99) Cabrita, E. J.; Berger, S. *Magn. Reson. Chem.* **2001**, *39*, S142-S148.

(100) Jerschow, A.; Muller, N. *J. Magn. Reson.* **1997**, *125*, 372-375.

(101) Sørland, G. H.; Seland, J. G.; Krane, J.; Anthonsen, H. W. *J. Magn Reson.* **2000**, *142*, 323-325.

(102) McGarrity, J. F.; Ogle, C. A.; Brich, Z.; Loosli, H. R. *J. Am. Chem. Soc.* **1985**, *107*, 1810-15.

(103) McGarrity, J. F.; Prodolliet, J. *J. Org. Chem* **1984**, *49*, 4465-70.

(104) Gilman, H.; Straley, J. M. *Recl. Trav. Chim. Pays-Bas* **1936**, *55*, 821.

(105) Normant, J. F. *Synthesis* **1972**, *2*, 63.

(106) Ashby, E. C.; Goel, A. B.; Smith, R. S. *J. Organomet. Chem.* **1981**, *212*, C47-C50.

(107) Yeh, M. C. P.; Knochel, P.; Santa, L. E. *Tetrahedron Lett.* **1988**, *29*, 3887-3890.

(108) Krause, N. *Modern Organocopper Chemistry*; Wiley-VCH: Weinheim, 2002.

(109) Eriksson, J.; Arvidsson, P. I.; Davidsson, O. *J. Am. Chem. Soc.* **2000**, *122*, 9310-9311.

(110) Krause, N. *Angew. Chem. Int. Ed.* **1999**, *38*, 79-81.

(111) Nakamura, E.; Mori, S. *Angew. Chem. Int. Ed.* **2000**, *39*, 3750-3771.

(112) Nakamura, E.; Yoshikai, N. *Bull. Chem. Soc. Jpn.* **2004**, *77*, 1-12.

(113) Krause, N. In *Metallorganische Chemie*; Spectrum Akademischer Verlag: Heidelberg, Germany, 1996, p 175-191.

(114) Lipshutz, B. H. In *Organometallics in Synthesis*; Schlosser, M., Ed.; Wiley: Chichester, U.K., 1994, p 283-382.

(115) *Organocopper Reagents: A practical approach*; Taylor, R. J. K., Ed.; Oxford University Press: Oxford, U.K., 1994.

(116) Boudet, N.; Dubbaka, S. R.; Knochel, P. *Org. Lett.* **2008**, *10*, 1715-1718.

(117) Dubbaka, S. R.; Kienle, M.; Mayr, H.; Knochel, P. *Angew. Chem. Int. Ed.* **2007**, *46*, 9093-9096.

(118) Kienle, M.; Dubbaka, S. R.; Brade, K.; Knochel, P. *Eur. J. Org. Chem.* **2007**, *2007*, 4166-4176.

(119) Bertz, S. H.; Ogle, C. A.; Rastogi, A. *J. Am. Chem. Soc.* **2005**, *127*, 1372-1373.

(120) Lipshutz, B. H.; Wilhelm, R. S.; Floyd, D. M. *J. Am. Chem. Soc.* **1981**, *103*, 7672-7674.

(121) Lipshutz, B. H.; Kozlowski, J. A.; Wilhelm, R. S. *J. Org. Chem.* **1984**, *49*, 3943-3949.

(122) Hallnemo, G.; Ullenius, C. *Tetrahedron* **1983**, *39*, 1621-1625.

(123) Bertz, S. H.; Chopra, A.; Eriksson, M.; Ogle, C. A.; Seagle, P. *Chem. Eur. J.* **1999**, *5*, 2680-2691.

(124) Henze, W.; Vyater, A.; Krause, N.; Gschwind, R. M. *J. Am. Chem. Soc.* **2005**, *127*, 17335-17342.

(125) Ashby, E. C.; Watkins, J. J. *J. Am. Chem. Soc.* **1977**, *99*, 5312-5317.

(126) Gerold, A.; Jastrzebski, J. T. B. H.; Kronenburg, C. M. P.; Krause, N.; van Koten, G. *Angew. Chem. Int. Ed. Engl.* **1997**, *36*, 755-757.

(127) Gregory, C. D.; Pearson, R. G. *J. Am. Chem. Soc.* **1976**, *98*, 4098-4104.

(128) Bertz, S. H.; Nilsson, K.; Davidsson, Ö.; Snyder, J. P. *Angew. Chem. Int. Ed.* **1998**, *37*, 314-317.

(129) John, M.; Auel, C.; Behrens, C.; Marsch, M.; Harms, K.; Bosold, F.; Gschwind, R. M.; Rajamohanan, P. R.; Boche, G. *Chem. Eur. J.* **2000**, *6*, 3060-3068.

(130) Olmstead, M. M.; Power, P. P. *Organometallics* **1990**, *9*, 1720-1722.

(131) Lipshutz, B. H.; Keith, J.; Buzard, D. J. *Organometallics* **1999**, *18*, 1571-1574.

(132) Henze, W. PhD Theses, Rheinische Friedrich-Wilhelms-Universität Bonn, 2005.

(133) Bertz, S. H.; Carlin, C. M.; Deadwyler, D. A.; Murphy, M. D.; Ogle, C. A.; Seagle, P. *J. Am. Chem. Soc.* **2002**, *124*, 13650-13651.

(134) Hallnemo, G.; Olsson, T.; Ullenius, C. *J. Organomet. Chem* **1985**, *282*, 133-144.

(135) Krause, N.; Wagner, R.; Gerold, A. *J. Am. Chem. Soc.* **1994**, *116*, 381-382.

(136) Bertz, S. H. *J. Am. Chem. Soc.* **1991**, *113*, 5470-5471.

(137) Mobley, T. A.; Müller, F.; Berger, S. *J. Am. Chem. Soc.* **1998**, *120*, 1333-1334.

(138) Bertz, S. H.; Dabbagh, G. *Tetrahedron* **1989**, *45*, 425-434.

(139) Ouannes, C.; Dressaire, G.; Langlois, Y. *Tetrahedron Lett.* **1977**, 815-818.

(140) Whitesides, G. M.; Fischer, W. F.; SanFilippo, J.; Bashe, R. W.; House, H. O. *J. Am. Chem. Soc.* **1969**, *91*, 4871-4882.

(141) Pearson, R. G.; Gergory, C. D. *J. Am. Chem. Soc.* **1976**, *98*, 4098-4104.

(142) Gschwind, R. M.; Rajamohanan, P. R.; John, M.; Boche, G. *Organometallics* **2000**, *19*, 2868-2873.

(143) Bertz, S. H.; Dabbagh, G.; He, X.; Power, P. P. *J. Am. Chem. Soc.* **1993**, *115*, 11640-11641.

(144) Mori, S.; Nakamura, E. *Chem. Eur. J.* **1999**, *5*, 1534-1543.

(145) Nakamura, E.; Mori, S.; Morokuma, K. *J. Am. Chem. Soc.* **1997**, *119*, 4900-4910.

(146) Nakamura, E.; Mori, S.; Nakamura, M.; Morokuma, K. *J. Am. Chem. Soc.* **1997**, *119*, 4887-4899 and references therein.

(147) Karplus, M.; Pople, J. A. *J. Chem. Phys.* **1963**, *38*, 2803-2807.

(148) Collum, D. B.; Kahne, D.; Gut, S. A.; DePue, R. T.; Mohamadi, F.; Wanat, R. A.; Clardy, J.; Van Duyne, G. *J. Am. Chem. Soc.* **1984**, *106*, 4865-9.

(149) Kaufman, M. J.; Streitwieser, A., Jr. *J. Am. Chem. Soc.* **1987**, *109*, 6092-7.

(150) Liou, L. R.; McNeil, A. J.; Ramirez, A.; Toombes, G. E. S.; Gruver, J. M.; Collum, D. B. *J. Am. Chem. Soc.* **2008**, *130*, 4859-4868.

(151) Xu, F.; Reamer, R. A.; Tillyer, R.; Cummins, J. M.; Grabowski, E. J. J.; Reider, P. J.; Collum, D. B.; Huffman, J. C. *J. Am. Chem. Soc.* **2000**, *122*, 11212-11218.

(152) Bertz, S. H.; Vellekoop, A. S.; Smith, R. A. J.; Snyder, J. P. *Organometallics* **1995**, *14*, 1213-1220.

(153) Böhme, M.; Frenking, G.; Reetz, M. T. *Organometallics* **1994**, *13*, 4237-4245.

(154) Huang, H.; Alveraz, K.; Liu, Q.; Barnhart, T. M.; Snyder, J. P.; Penner-Hahn, J. E. *J. Am. Chem. Soc.* **1996**, *118*, 8808-8816 and 12252 (correction).

(155) Huang, H.; Liang, C. H.; Penner-Hahn, J. E. *Angew. Chem. Int. Ed. Engl.* **1998**, *37*, 1564-66.

(156) Kronenburg, C. M. P.; Amijs, C. H. M.; Jastrzebski, J. T. B. H.; Lutz, M.; Spek, A. L.; van Koten, G. *Organometallics* **2002**, *21*, 4662 - 4671.

(157) Kronenburg, C. M. P.; Jastrzebski, J. T. B. H.; Boersma, J.; Lutz, M.; Spek, A. L.; van Koten, G. *J. Am. Chem. Soc.* **2002**, *124*, 11675-11683.

(158) Snyder, J. P.; Bertz, S. H. *J. Org. Chem.* **1995**, *60*, 4312-13.

(159) Snyder, J. P.; Spangler, D. P.; Behling, J. R.; Rossiter, B. E. *J. Org. Chem.* **1994**, *59*, 2665-2667.

(160) Stemmler, T. L.; Barnhart, T. M.; Penner-Hahn, J. E.; Tucker, C. E.; Knochel, P.; Böhme, M.; Frenking, G. *J. Am. Chem. Soc.* **1995**, *117*, 12489-12497.

(161) Armstrong, D. R.; Henderson, K. W.; Kennedy, A. R.; Kerr, W. J.; Mair, F. S.; Moir, J. H.; Moran, P. H.; Snaith, R. *J. Chem. Soc. Dalton Trans.* **1999**, 4063-4068.

(162) Aubrecht, K. B.; Lucht, B. L.; Collum, D. B. *Organometallics* **1999**, *18*, 2981-2987.

(163) Koizumi, T.; Morihashi, K.; Kikuchi, O. *Bull. Soc. J.* **1996**, *69*, 305-9.

(164) Alam, T. M.; Pedrotty, D. M.; Boyle, T. J. *Magn. Reson. Chem* **2002**, *40*, 361-365.

(165) Bauer, W. *Magn. Reson. Chem* **1996**, *34*, 532-537.

(166) Bauer, W. *in Lithium Chemistry: A Theoretical and Experimental Overview (Eds.: Sapse, A.-M., Schleyer, P. v. R.)*; Wiley: New York, **1995**, pp. 125-172.

(167) a) Davies, R. P.; Hornauer, S.; Hitchcock, P. B. *Angew. Chem. Int. Ed.* **2007**, *46*, 5191-5194. b) Dieter, R. K.; Hanks, T. W.; Lagu, B. *Organometallics* **1992**, *11*, 3549-3554.

(168) a) Günther, H. In *Advanced Applications of NMR to Organometallic Chemistry*; Gielen, M., Willem, R., Wrackmeyer, B., Eds.; Wiley & Sons: Chichester, 1996. b) Bomparola, R.; Davies, R. P.; Hornauer, S.; White, A. J. P. *Dalton Trans.* **2009**, 1104.

(169) Xie, X.; Auel, C.; Henze, W.; Gschwind, R. M. *J. Am. Chem. Soc.* **2003**, *125*, 1595-1601.

(170) Bondi, A. *J. Phys. Chem.* **1964**, *68*, 441 - 451.

(171) Marcus, Y.; Hefter, G. *Chem. Rev.* **2004**, *104*, 3405-3452.

(172) Bloomfield, V. A. In *On-Line Biophysics Textbook*; Schuster, T. M., Ed. 2000; Vol. Separation and Hydrodynamics, p 1-5.

(173) Norinder, J.; Baeckvall, J.-E.; Yoshikai, N.; Nakamura, E. *Organometallics* **2006**, *25*, 2129-2132.

(174) Yamanaka, M.; Kato, S.; Nakamura, E. *J. Am. Chem. Soc.* **2004**, *126*, 6287-6293.

(175) Yamanaka, M.; Nakamura, E. *Organometallics* **2001**, *20*, 5675-5681.

(176) Yoshikai, N.; Yamashita, T.; Nakamura, E. *Angew. Chem. Int. Ed.* **2005**, *44*, 4721-4723.

(177) Mori, S.; Nakamura, E.; Morokuma, K. *Organometallics* **2004**, *23*, 1081-1088.

(178) Mori, S.; Uerdingen, M.; Krause, N.; Morokuma, K. *Angew. Chem. Int. Ed.* **2005**, *44*, 4715-4719.

(179) Yamanaka, M.; Nakamura, E. *J. Am. Chem. Soc.* **2005**, *127*, 4697-4706.

(180) Bertz, S. H.; Smith, R. A. *J. Am. Chem. Soc.* **1989**, *111*, 8276-8277.

(181) Christenson, B.; Olsson, T.; Ullenius, C. *Tetrahedron* **1989**, *45*, 523-534.

(182) Krause, N. *J. Org. Chem* **1992**, *57*, 3509-3512.

(183) Lindstedt, E. L.; Nilsson, M.; Olsson, T. *J. Organomet. Chem* **1987**, *334*, 255-261.

(184) Murphy, M. D.; Ogle, C. A.; Bertz, S. H. *Chem. Commun.* **2005**, 854-856.

(185) Sharma, S.; Oehlschläger, A. C. *Tetrahedron* **1991**, *47*, 1177-1184.

(186) Ullenius, C.; Christenson, B. *Pure Appl. Chem.* **1988**, *60*, 57-64.

(187) Eriksson, J.; Davidsson, O. *Organometallics* **2001**, *20*, 4763-4765.

(188) Nilsson, K.; Ullenius, C.; Krause, N. *J. Am. Chem. Soc.* **1996**, *118*, 4194-4195.

(189) Vellekoop, A. S.; Smith, R. A. *J. Am. Chem. Soc.* **1994**, *116*, 2902-2913.

(190) Nolte, C.; Mayer, P.; Straub, B. F. *Angewandte Chemie* **2007**, *119*, 2147-2149.

(191) Nilsson, K.; Andersson, T.; Ullenius, C.; Gerold, A.; Krause, N. *Chem. Eur. J.* **1998**, *4*, 2051-2058.

(192) Bax, A.; Pochapsky, S. *J. Magn. Reson.* **1992**, *99*, 638-643.

(193) Bax, A.; Summers, M. F. *J. Am. Chem. Soc.* **1986**, *108*, 2093-2094.

(194) Ruiz-Cabello, J.; Vuister, G. W.; Moonen, C. T. W.; van Gelderen, P.; Cohen, J. S.; van Zijl, P. C. M. *J. Magn. Reson.* **1992**, *100*, 282-303.

(195) Willker, W.; Leibfritz, D.; Kerssebaum, R.; Bermel, W. *Magn. Reson. Chem.* **1993**, *31*, 287-292.

(196) Reif, B.; Köck, M.; Kerssebaum, R.; Kang, H.; Fenical, W.; Griesinger, C. *J. Magn. Reson., Series A* **1996**, *118*, 282-285.

(197) Weigelt, J.; Otting, G. *J. Magn. Reson., Series A* **1995**, *113*, 128-130.

(198) Aamouche, A.; Devlin, F. J.; Stephens, P. J. *J. Am. Chem. Soc.* **2000**, *122*, 7358-7367.

(199) Hu, H.; Snyder, J. P. *J. Am. Chem. Soc.* **2007**, *129*, 7210-7211.

(200) Mori, S.; Nakamura, E. *in Modern Organocopper Chemistry (Ed. Krause N.), Wiley-VCH, Weinheim,* **2002**, pp. 315-346 and references therein.

(201) Mori, S.; Nakamura, E.; Morokuma, K. *J. Am. Chem. Soc.* **2000**, *122*, 7294-7307.

(202) Snyder, J. P. *J. Am. Chem. Soc.* **1995**, *117*, 11025-6.

(203) Huffman, L. M.; Stahl, S. S. *J. Am. Chem. Soc.* **2008**, *130*, 9196-9197.

(204) Pregosin, P. S.; Kunz, R. W.; in *NMR-Basic Principles and Progress*, Springer: Berlin, 1979, p 28-46.

(205) Price, S. J. B.; DiMartino, M. J.; Hill, D. T.; Kuroda, R.; Mazid, M. A.; Sadler, P. J. *Inorg. Chem.* **1985**, *24*, 3425-3434.

(206) Yoshikai, N.; Zhang, S.-L.; Nakamura, E. *J. Am. Chem. Soc.* **2008**, *130*, 12862-12863.

(207) de Vries, A. H. M.; Meetsma, A.; Feringa, B. L. *Angew. Chem.* **1996**, *108*, 2526-2528.

(208) Shi, W.-J.; Wang, L.-X.; Fu, Y.; Zhu, S.-F.; Zhou, Q.-L. *Tetrahedron Asymmetry* **2003**, *14*, 3867-3872.

(209) Conry, R. R.; Striejewske, W. S. *Organometallics* **1998**, *17*, 3146-3148.

(210) Desvergnes-Breuil, V.; Hebbe, V.; Dietrich-Buchecker, C.; Sauvage, J.-P.; Lacour, J. *Inorg. Chem* **2003**, *42*, 255-257.

(211) Kunz, K.; Scholz, U.; Ganzer, D. *Synlett* **2003**, 2428-2439.

(212) Ley, S. V.; Thomas, A. W. *Angew. Chem.* **2003**, *42*, 5400-5449.

(213) Ouali, A.; Taillefer, M.; Spindler, J.-F.; Jutand, A. *Organometallics* **2007**, *26*, 65-74.

(214) Pianet, I.; Vincent, J.-M. *Inorg. Chem.* **2004**, *43*, 2947-53.

(215) Posset, T.; Bluemel, J. *J. Am. Chem. Soc.* **2006**, *128*, 8394-8395.

(216) Harutyunyan, S. R.; Lopez, F.; Browne, W. R.; Correa, A.; Pena, D.; Badorrey, R.; Meetsma, A.; Minnaard, A.; Feringa, B. L. *J. Am. Chem. Soc.* **2006**, *128*, 9103-9118.

(217) Lopez, F.; Harutyunyan, S. R.; Meetsma, A.; Minnaard, A. J.; Feringa, B. L. *Angew. Chem. Int. Ed.* **2005**, *44*, 2752-2756.

(218) Lopez, F.; Minnaard, A. J.; Feringa, B. L. *Acc. Chem. Res.* **2007**, *40*, 179-188.

(219) Pichota, A.; Pregosin, P. S.; Valentini, M.; Worle, M.; Seebach, D. *Angew. Chem. Int. Ed.* **2000**, *39*, 153-156.

(220) Seebach, D.; Jaeschke, G.; Pichota, A.; Audergon, L. *Helv. Chim. Acta* **1997**, *80*, 2515-2519.

(221) Komarov, I. V.; Börner, A. *Angew. Chem. Int. Ed.* **2001**, *40*, 1197-1200.

(222) Tang, W.; Zhang, X. *Chem. Rev.* **2003**, *103*, 3029-3070.

(223) Alexakis, A.; Rosset, S.; Allamand, J.; March, S.; Guillen, F.; Benhaim, C. *Synlett* **2001**, 1375-1378.

(224) Arnold, A. E., PhD thesis Rijksuniversiteit 2002.

(225) Mikhel, I. S.; Bernardinelli, G.; Alexakis, A. *Inorg. Chim. Acta* **2006**, 1826-1836.

(226) van den Berg, M.; Minnaard, A. J.; Schudde, E. P.; van Esch, J.; de Vries, A. H. M.; de Vries, J. G.; Feringa, B. L. *J. Am. Chem. Soc.* **2000**, *122*, 11539-11540.

(227) Alexakis, A.; Benhaim, C. *Eur. J. Org. Chem.* **2002**, 3221-3236.

(228) Arnold, L. A.; Imbos, R.; Mandoli, A.; De Vries, A. H. M.; Naasz, R.; Feringa, B. L. *Tetrahedron* **2000**, *56*, 2865-2878.

(229) Li, K.; Alexakis, A. *Tetrahedron Lett.* **2005**, *46*, 8019-8022.

(230) Alexakis, A.; Benhaim, C.; Rosset, S.; Humam, M. *J. Am. Chem. Soc.* **2002**, *124*, 5262-5263.

(231) Zhang, H.; Gschwind, R. M. *Angew. Chem. Int. Ed.* **2006**, *45*, 6391-6394.

(232) Zhang, H.; Gschwind, R. M. *Chem. Eur. J.* **2007**, *13*, 6691-6700.

3. Supramolecular Aggregation – An Additional Note

For these investigations, I synthesised the different organocuprate samples, while Stefanie Joseph measured the X-ray structures.

Tobias Gärtner, Stefanie Joseph, Ruth M. Gschwind

to be published as a note in Z. Naturforsch.

3.1 Discussion

Since the first synthesis of organocuprates, much effort was spent on the structure elucidation of organocuprates (see Section 2.2). Combined theoretical, NMR-spectroscopic and X-ray analyses helped to resolve the general linear structure motif for organocuprates (see Section 2.2.2). Furthermore, aggregation was found to play an important role for the reactivity of organocuprates. In an indirect NMR study (see Section 2.2.3 Figures 14, 15 and 16) it was observed, that for Me_2CuLi•LiI and Me_2CuLi•LiCN the supramolecular aggregates react differently on solvent variations (see Section 2.2.3 Figure 14), which was ascribed to the different salt units present in solution. After the measurement of an elaborate combination of DOSY, $^1H,^7Li$ HOESY and $^1H,^1H$ HOESY spectra it could be concluded that in the case of Me_2CuLi•LiI in diethyl ether upon addition of THF small salt units are separated from the cuprates, whereas for Me_2CuLi•LiCN the additional salt unit remains attached to the cuprate. Nevertheless, until now it was not directly possible to localise the position of the residual salt in the supramolecular structures of homoleptic organocuprates. As shown, via NMR spectroscopic investigations the salt units are only capable by indirect measurements, the crystal structures of the simplest homoleptic cuprates Me_2CuLi•LiI and Me_2CuLi•LiCN should help to solve the position of the salt units. Although the absence of crystal structures for these types of cuprates are said to be caused by the supramolecular aggregation, which suppresses crystallisation, not published results of our group encouraged for new crystallisation experiments.

In a screening of Me_2CuLi•LiI, Me_2CuLi•LiCN and Me_2CuLi•LiSPh as different cuprate reagents, THF, Et_2O and toluene as pure solvents or solvent combinations, it was possible to observe colourless needles. In Figure 1a the structure of LiI•THF_3 is given, which was obtained from a mixture of Me_2CuLi•LiI in Et_2O covered with THF. The crystal structure of LiI•$(THF)_3$ is already known[1] and shows a distorted tetrahedral coordination of Li. For our case, this observation directly confirms the NMR spectroscopic finding (see Section 2.2.3 Figure 15a and b) that upon addition of THF the LiI units are separated from the cuprate by a coordination of the Li with THF, although no cuprate crystal was found. The equivalent sample with Me_2CuLi•LiCN and Me_2CuLi•LiSPh did not show any similar behaviour and no crystals were observed. In further experiments with Me_2CuLi•LiCN and additional substrates

containing iodide, e.g. methyliodide, it was possible to repeat the crystallisation of LiI•$(THF)_3$ without any LiCN.

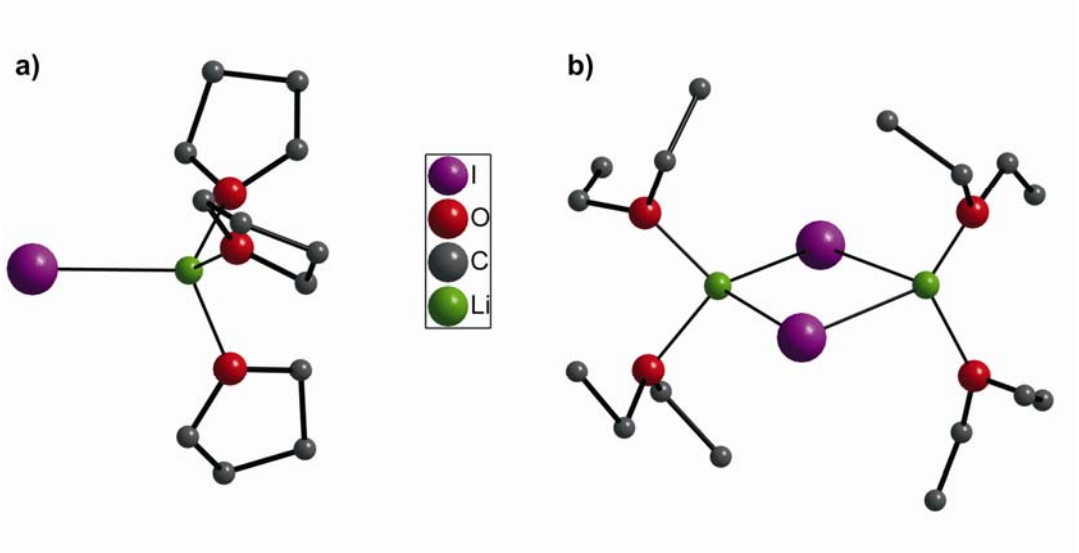

Figure 1. Observed structures of a) LiI•$(THF)_3$ obtained from Me_2CuLi•LiI in Et_2O, covered by THF and b) $(LiI)_2$•$(Et_2O)_4$ obtained after the reaction of Me_2CuLi•LiCN with MeI in the presence of 1 equivalent MeLi in pure Et_2O. H-atoms are omitted for clarity.

In a further sample, first crystallographic structures were observed, that in pure Et_2O without THF the LiI units are not separated, but show higher aggregates of the formal structure $(LiI)_2$•$(Et_2O)_4$ (Figure 1b). This observation also conforms to the NMR spectroscopic findings already discussed in Section 2.2.3. Although the crystal was treated under inert conditions at low temperatures, small temperature variations during the transfer to the IPDS led to a poor crystal quality. Therefore, larger crystals had to be taken for the measurement. The larger crystals in turn support the formation of crystals, which are grown together.

3.2 Experimental section

A Schlenk flask, equipped with a stirring bar and 0.5 mmol (1 eq) Cu(I)-salt (CuI, CuCN or CuSPh), was heated four times in vacuum to remove residual moisture. Then 5 mL of solvent (Et_2O or THF) were added and the Cu(I)-salt was suspended. Upon addition of 2 eq MeLi in Et_2O the mixture gave a colourless solution. After removal of the stirring bar, the solution was covered with either no solvent, Et_2O or THF or toluene. The flask then was stored at -80°C for several days.

(1) Nöth, H.; Waldhör, R. *Z. Naturforsch.* **1998**, *53b*, 1525-1527.

4. Organocuprate Conjugate Addition: The Structural Features of Diastereomeric and Supramolecular π-Intermediates*

Wolfram Henze, Tobias Gärtner, Ruth M. Gschwind

The spectra of diastereomeric and enantiomeric π-intermediates, which are shown in the publication, were measured by Wolfram Henze. My contribution was the assigment of additional symmetrical species as well as the separation of overlapping signals, belonging either to the π-intermediates or to the Cu(III)-intermediates.

---

*Wolfram Henze, Tobias Gärtner, Ruth M. Gschwind
J. Am. Chem. Soc. **2008**, 130, 13718-13726

4.1 Abstract

In the reaction pathway of conjugate additions with organocuprates reagents, Cu(I) π-complexes and Cu(III) σ-complexes have been identified as central, NMR detectable intermediate species. However, neither about the structures of π–intermediates with extensive chiral enones nor about the principle aggregation level and aggregate structure of π-complexes in diethyl ether experimental evidence has been available so far. Furthermore, the structural characteristics of π-complexes which are decisive for their high reactivities and diastereoselectivities have not yet been rationalized experimentally. Therefore, the π-intermediates of 4,4a,5,6,7,8-hexahydro-4a-methyl-naphthalen-2(3H)-one **1** and Me_2CuLi **2** or $Me_2CuLi{\cdot}LiX$ (X = I, CN) in diethyl ether are investigated in detail. For the first time the formation of two intermediate cuprate enone π-complexes on both sides of the double bond is observed. In addition, the conformation of the enone adopted in the major β-face π-complex rationalizes the exclusive syn addition observed in the synthetic product. For the investigation of the aggregation level and structure a NMR screening of π-complexes with $Me_2CuLi{\cdot}LiX$ (X = I, CN) and three achiral enones is performed which simplify the spectra by the generation of enantiotopic π-complexes. Thus, for the first time NMR diffusion experiments on cuprate intermediates and the detection of scalar couplings across copper without isotope labelling are possible. Extensive NMR studies including cyclohexanone complexes show that in principle saltfree dimethylcuprate is able to complex the carbonyl group. However, in the presence of salt the carbonyl complexing aggregates are composed of salt and cuprate moieties. These mixed aggregates cause the formation of large supramolecular π-intermediate structures which control their reactivity. The π-complexing cuprate units show a bent geometry as general structural feature unaffected by the presence or kind of salt and the type of enone. Thus, the high diastereoselectivity and the reactivity of organocuprate 1,4-addition reactions is for the first time rationalized on the basis of structural characteristics of selected π-intermediates.

4.2 Introduction

Organocopper reagents are among the most frequently applied transition metal reagents for the formation of C-C bonds in organic synthesis.[1-4] Despite their important role in organic reactions, the complicated structure determination of organocopper complexes in solution,

their potential self aggregation, and their sensitivity to solvent, salt, and concentration effects have been a hindrance to experimental structure elucidation so far. Therefore, a rational design capable of tapping the full potential of copper reagents, is still limited. However, in case of organocuprates which are generally accepted as mechanistic models for organocopper chemistry, a number of experimental investigations allowed some insight into their monomer and aggregate structures and identified organocuprate enone π-complexes as intermediates in 1,4-addition reactions.[5-8] Very recently even the first Cu(III) intermediates were detected by NMR spectroscopic studies in conjugate addition and substitution reactions of organocuprates.[9-12] In addition to these experimental studies, various theoretical calculations provide insight into the reaction pathways of organocopper reagents revealing open cluster structures and transition states in these impressively complex mechanisms.[13-15]

For the synthetically so important 1,4 addition reactions of organocuprates to enones combined NMR investigations and kinetic studies showed that in ethereal solutions the aggregation level of these reagents is decisive for their reactivity.[16,17] Thus, THF as solvent leads to a rigorous reduction of the reactivity in 1,4 additions to enones, because it supports the formation of solvent separated ion pairs[18] and only a small amount of the reactive contact ion pairs remains.[16,19] In contrast, in diethyl ether dimethylcuprates form oligomeric structures composed of homodimers connected by salt and solvent bridges,[20,21] which promote conjugate addition reactions. Recently, the aggregation degree and the composition of the supramolecular structures of the organocuprate reagents were correlated with the reactivities obtained in 1,4 addition reactions to cyclohexenones.[17] In case of $Me_2CuLi{\cdot}LiCN$ (**2**·LiCN) in diethyl ether, the addition of certain equivalents of THF leads to a disaggregation of its oligomeric structure into dimers with salt units attached. Simultaneously to this disaggregation the reactivity decreases corroborating the importance of the aggregated species in 1,4 addition reactions of organocuprates. In agreement with these experimental results also theoretical calculations suppose that the reactivity and the synthetic potential of organocuprate clusters are based on their ability to form supramolecular assemblies which are appropriate to allow cooperative interactions within the polymetallic clusters.[13] However, despite the impressive progress in the theoretical calculations of supermolecules, so far the computable cluster sizes have been small compared to the supramolecular organocuprate clusters which are experimentally observed in diethyl ether.

Regarding the intermediate species in conjugate addition reactions it has been possible to observe a couple of intermediate π-complexes in the reaction pathway of 1,4-, 1,6 and 1,8-

addition reactions of cuprates up to now.[22-34] However, despite the importance of aggregates in 1,4 addition reactions, most of these NMR studies have been performed in THF which allows only the observation of minimum cluster sizes as main species. These studies reveal congruently one cuprate unit attached to the π-system next to the carbonyl moiety. With the aid of isotopically labeled compounds two types of scalar couplings across copper were observed indicating a bent geometry of the cuprate unit in the π-complex.[23,33] Also the studies done in solvents, which in principle support the formation of contact ion pairs or higher aggregates, have been reported so far solely about one cuprate unit directly attached to the π-system.[22,30,35] The aggregation level and aggregate structure of the π-intermediates in diethyl ether, which is expected to be decisive for their reactivities, as well as the influences of the kind of enones or the type of salt on these intermediates, is entirely unknown up to now. In addition, the experimental intermediate studies published so far have not yet addressed the structural or conformational reasons for the high diastereoselectivities observed in many 1,4 addition reactions of cuprates, which should be related to the formation of α- or β-face π-complex intermediates. One of the famous examples in this direction is the 1,4 methylation of methyloctalones by organocuprates, which yields exclusively the syn addition product that means β-methyloctalones.[36]

Therefore, in this study the structures and aggregation trends of the intermediate π-complexes of 4,4a,5,6,7,8-hexahydro-4a-methyl-naphthalen-2(3H)-one (synonym: 10-methyl-$\Delta^{1,9}$-2-octalone) (**1**) and Me_2CuLi (**2**) or **2**·LiX (X = I, CN) in diethyl ether are investigated in detail. For the first time structural details of two intermediate cuprate enone π-complexes are elucidated and the diastereoselectivity of the reaction is rationalized experimentally. Furthermore, a NMR screening of intermediate π-complexes with **2**·LiX (X = I, CN) and three achiral enones is presented. The resulting enantiotopic π-complexes simplify the spectra to such an extend that it is possible for the first time to investigate the aggregate structure and the aggregation level of cuprate enone π-complexes as well as the influence of the type of salt on these intermediates.

4.3 Results and Discussion

4.3.1. π-complexes of 4,4a,5,6,7,8-hexahydro-4a-methyl-naphthalen-2(3H)-one

To investigate the structures of intermediate cuprate π-complexes with sterically hindered chiral enones, 10-methyl-$\Delta^{1,9}$-2-octalone (**1**) (see Figure 1a) and Me_2CuLi (**2**) or Me_2CuLi•LiI (**2**•LiI) in diethyl ether was chosen as model system. The synthetic approaches, the NMR spectroscopic results and the theoretical calculations known for this system allow a detailed interpretation of the NMR spectroscopic data to rationalize the high stereocontrol of 1,4 addition reactions of organocuprates to chiral, cyclic enones experimentally. Actually, 1,4 addition reactions of **1** with copper species yielded β-methyloctalones exclusively and without further additives diethyl ether is the best solvent for this reaction.[36-40]

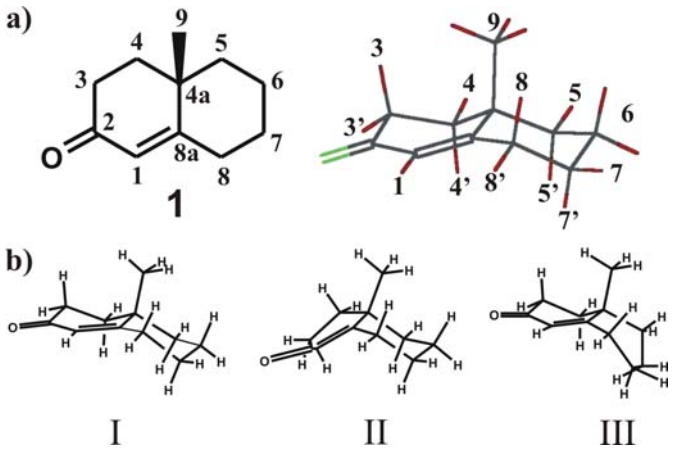

Figure 1. a) Schematic representation of 4,4a,5,6,7,8-hexahydro-4a-methyl-naphthalen-2(3H)-one (synonym: 10-methyl-$\Delta^{1,9}$-2-octalone) (**1**) and major conformation with the diastereoselective labeling of the protons; no diastereoselective assignment of the protons 6 possible; b) DFT structures of conformations I, II, and III of **1** according to Aamouche et al..[41]

In order to explain this syn addition with respect to the methyl substituent an enolate like geometry of the transition state was postulated,[36,38-40] in which **1** adopts a conformation similar to II in Figure 1b. In contrast, theoretical calculations of pure **1** proposed three conformations, "trans-chair" (I), "cis-chair" (II), and "trans-boat" (III) showing relative energies I<II<III (see Figure 1).[41] Furthermore, in the vibrational spectra of **1** only conformation I was definitively observed, which was attributed to the energy difference of I and II predicted to be ~1.8 kcal/mol. This reveals that conformation I is preferred for free **1** and conformation II does not contribute significantly in CCl_4 or CS_2. From NMR

investigations, the stabilization of several not further specified cuprate π-complexes in a mixture of **1** and **2** in diethyl ether was reported[22] showing the existence of different π-complex conformations as possible indications of the stereocontrol mechanism of this reaction.

In order to optimize the experimental conditions, the different cuprate enone complex species of **1** and **2**, reported previously as mixtures,[22] were prepared individually and their assignment reconfirmed. Exemplarily, typical ^{1}H and ^{13}C spectra of **1** complexed with 2 equivalents of **2** are shown in Figure 2. The formation of π-complexes is directly indicated by the characteristic upfield shifts ($\Delta\delta^{13}C$) of C1, C2, and C8a of the enone.[6,22] Despite the optimization procedure and the exclusive formation of cuprate olefine π-complexes (see Figure 2b), the cuprate section of the ^{1}H spectrum is still very overcrowded (see Figure 2a). Thus, the splitting of each presented ^{13}C signal of free **1** into at least two signals and the appearance of multiple proton signals in the cuprate section indicate the formation of several intermediate species (see Figure 2b).

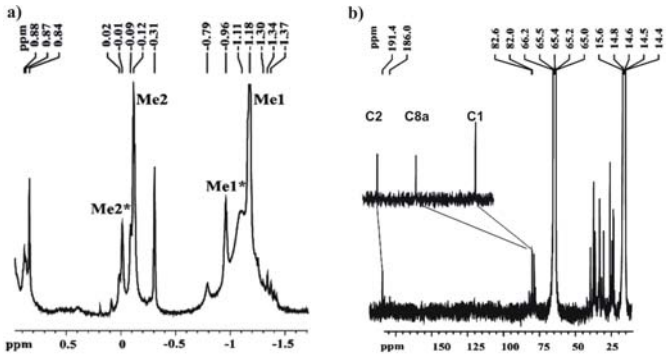

Figure 2. a) Cuprate section of the ^{1}H spectrum and b) enone section of the ^{13}C spectrum of the intermediate π-complexes composed of **1** and 2 equivalents of **2**•LiI in diethyl ether at 170 K. In b) the ^{13}C spectrum of free **1** is given as insert to show the chemical shift changes upon π-complexation. The minor intermediate is labeled with an asterisk.

Interestingly, with 2 equivalents of the lower order cyanocuprate MeCu(CN)Li no π-complexes, but only lithium carbonyl complexes are observable. Similar results are obtained for enone **4** (see below). In contrast, the NMR detection of a π-complex of *t*-BuCu(CN)Li attached to the alkine moiety of methyl phenylpropiolate in THF is reported,[28] and active substrate control was observed at the treatment of 5-oxygen-substituted cyclohexenones with the heteroleptic cuprates MeCu(CN)Li and *t*-BuCu(CN)Li.[42,43] These results reflect nicely the higher thermodynamic stability of π-complexes between electron poor transition metal

complexes and alkines. In case of alkyl substituted enones and electron poor heteroleptic cuprates, the resulting π-complexes are not sufficiently stabilized to allow for an NMR observation.

In case of the π-complex formation of **1** with 2 equivalents of dimethyl cuprates, two differently populated π-complexes were identified and their ^{1}H and ^{13}C chemical shifts assigned with the aid of $^{1}H,^{13}C$ HMQC, $^{1}H,^{13}C$ HMBC, $^{1}H,^{1}H$ NOESY, and $^{1}H,^{13}C$ –INEPT-INADEQUATE spectra as well as ^{13}C isotopically labelled dimethyl cuprates (for ^{1}H and ^{13}C chemical shift assignments see Tables S1 – S3 in the Supporting Information). Due to severe line broadening of the proton signals, it was not possible to use ^{1}H, ^{1}H scalar coupling constants to identify the individual methylene protons. Therefore, the diastereotopic assignment is based on NOE contacts. For both π-complexes the orientation of the two methyl groups named Me1/Me1* and Me2/Me2* (see Figure 3b) has been assigned by various NOESY cross peaks to the enone system. In addition, using INEPT-INADEQUATE[44,45] spectra it was for the first time possible to detect ^{13}C-^{13}C scalar coupling interactions between the cuprate moiety and an enone without ^{13}C labelling of the enone. The exclusive detection of scalar couplings between Me1/C8a and Me1*/C8a* (see Figure 3a) indicates a bent cuprate unit in both π-complexes (see Figure 3b), which is in accordance with previous NMR investigations of cuprate-enyne π-complexes[23,33] and theoretically predicted reaction pathways.[13-15]

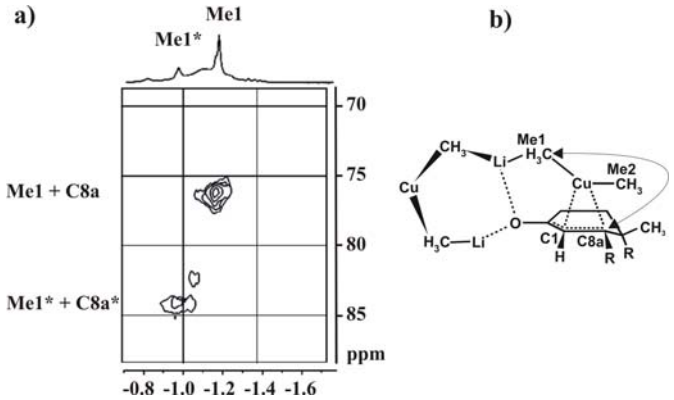

Figure 3. a) Section of a ^{1}H, ^{13}C –INEPT-INADEQUATE spectrum of **1** at natural abundance and ^{13}C labeled **2**•LiI in diethyl ether at 180 K. The cross signals appearing at ^{13}C chemical shifts equal to $\delta^{13}C_{Me1(*)} + \delta^{13}C_{C8a(*)}$ are the result of ^{13}C, ^{13}C scalar couplings across copper as indicated by the arrow in b.

The similarity of the cuprate units attached to the double bond in both conformations raises the question about their structural differences. For this purpose information is gained from the different cross peak patterns in the NOESY spectrum (see Figure 4). In the major conformation, the NOE cross peak between Me1 and H3' is smaller than that between Me1 and H8 and the cross peaks Me1/H3 and Me1/H4' show similar intensities. In addition, unexpectedly strong cross signals Me1/H7' and Me1/H6 are detected. In principle this pattern resembles a β -face π-complex for the major conformation (see Scheme 1a). However, for **1** in conformation I, a very strong NOE contact between Me1 and H3 would be expected and very weak or no NOE cross peaks for Me1/H7' and Me1/H6. In contrast, Me1/H3 shows a similar intensity as Me1/H4' and Me1/H3' is very small. Thus, the actual NOE pattern of the major conformation fits well to a β-face π-complex, in which the enone part of **1** has a conformation according to type II and the cyclohexyl ring adopts a conformation similar to III (for schematic representations of I, II, and III see Figure 1). In case of the minor conformation the observed NOE patterns differ significantly from that of the major π-complex. Despite the fact that severe signal overlaps build an obstacle for the interpretation, some cross peaks are very informative: Even for the low signal intensities of the minor conformation a cross signal between Me1* and H7*/H6* is detected. Furthermore, the cross signal Me2*/(H7*/H6*) is very strong and the cross signal Me2*/H5* is even stronger in case of the minor conformation than in the major conformation. This NOE pattern indicates an α-face complexation of the double bond in case of the minor conformation (see Scheme 1b). Due to the severe signal overlaps an experimental differentiation between the different conformational states is not possible, however, minimization of steric hindrance between the α-face cuprate and **1** make conformation I more probable than II or III.

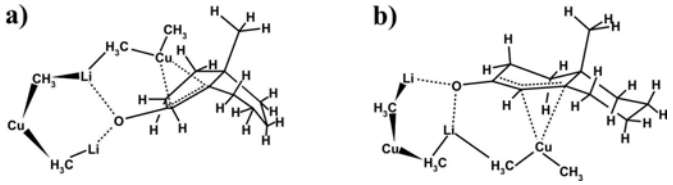

Scheme 1. Schematic representations of a) the major conformation and b) the minor conformation of the π-complexes composed of **1** and **2** or **2**•LiI in diethyl ether. For details see text.

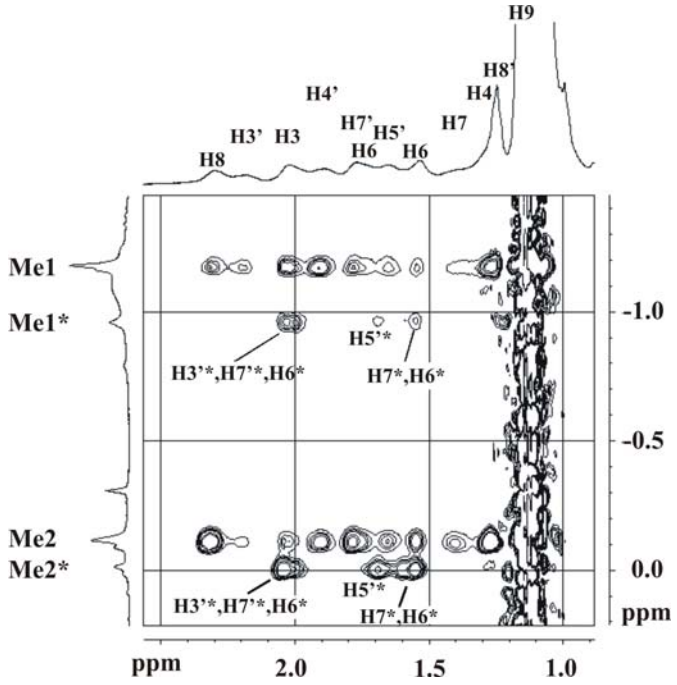

Figure 4. Section of a ^{1}H, ^{1}H NOESY spectrum of the π-complexes composed of **1** and **2**•LiI in diethyl ether at 180 K. The different pattern of the cross signals of the two π-complexes indicate considerable different structures. All signals of the minor intermediate are labeled with an asterisk, for a visualization of the numbers see Figure 1a and 3b.

The presented NOE data allow a first insight into the structural arrangement of π-complexes composed of cuprates and sterically demanding enones (see Scheme 1): a) In case of **1,** β-face as well as α-face π-complexes can be observed as intermediates with the β-face complex being the major species; b) in both intermediates the structural arrangement of the cuprate unit relative to the double bond is very similar as indicated by identical scalar coupling pattern across copper; c) upon π-complexation the conformational preference of **1** in the major conformation changes in favour of structure II for the enone part and III for the cyclohexyl part. These results rationalize the observed stereochemistry of 1,4 methylations of methyloctalones by copper species for the first time experimentally, which exclusively yields β-methyloctalones.[36,38,40] The exclusive formation of β-methyloctalones in combination with the β-face π-intermediate as major species leads to the conclusion that in case of **1**, the more stable intermediate is also related to the energetically lower transition states which was often doubted in cuprate reaction pathways. In addition, the energetic differences of the remaining reaction pathway including several transition states around the Cu(III) intermediate are sufficiently pronounced to suppress the conversion of the less populated α-face π-intermediate completely. Furthermore, the presented structure of the major β-face π-complex

explains the previously reported effects of different substitution patterns of **1** on the yield of 1,4-methylation of **1**:[37-40] e.g. substitution in position 7 reduces the yield of product considerably, however, with substituents in position 7' no 1,4 methylation product is obtained.

4.3.2. Influence of salt on π-complexes of 1

In the first NMR observation of π-complexes of **1**, Bertz and coworkers reported that with one equivalent of **2**·LiI the formation of π-complexes was not observed in diethyl ether at –50 °C, but two isomeric enolates were detected whose precise nature remained to be established.[22] Also in later studies using rapid-injection NMR and 2-cyclohexenone, a ratio of two equivalents of cuprate to one equivalent of enone is reported for the formation of the observed π-complexes in THF.[27,46] This is in striking contrast to the heterodimeric structure as decisive reactive core for 1,4-addition reactions which was many times proposed in theoretical studies and also in NMR spectroscopic investigations in THF.[27,46] For heterodimers it was also stated that the $LiXLi^+$ moiety (X = I, CN) has better carbonyl complexing properties than $Li\text{-}MeCuMe\text{-}Li^+$. In consequence, it should be possible to detect appropriate π-intermediates at 1:1 ratios of enone to **2**·LiX (X = I, CN), with MeCuMe as π-complexing unit and LiXLi as carbonyl complexing unit. However, in accordance to the experimental results reported from Bertz and Ogle in diethyl ether and THF,[22,27,46] only small traces of cuprate enone π-complex were detected using **1** and one equivalent of **2**·LiX (X = I, CN) in diethylether. With the enones **3a**, **3b**, and **4** (see below) even no π-complex formation at all was observed with one equivalent of **2**·LiX (X = I, CN).

In case two equivalents of **2**·LiX (X = I, CN) react with **1**, π-complexes are observed which show signal pattern of the π-complexing cuprate units in their ^1H, ^{13}C HMQC spectra which are extremely similar to this of saltfree **2** (see Figure 5). The direct comparison of the three HMQC spectra show that the positioning of the four cross signals assigned to the major and minor conformations of the π-complexes, are nearly identical in all spectra. In addition, the relative intensities of the four cross peaks remain stable upon varying the cuprate from **2** over **2**·LiI to **2**·LiCN. Both observations indicate that in case of two equivalents of **2** per enone neither the presence of two additional equivalents of salt nor the type of salt affect the structures of the π-complexing units of both conformations. Furthermore, the ratio between the two conformations is not affected.

In contrast to the stability of the chemical shifts, the presence and the type of salt severely influence the line widths of the signals. In general, broad line widths indicate either different aggregation levels in the three samples or different amounts of deviating conformations in fast exchange on the NMR time scale. But the previously reported different aggregation levels of cuprate reagents in diethyl ether[17,20,47,48] and the diffusion measurements on the π-complexes with **3a**, **3b**, and **4** (see below) makes the interpretation of the line widths in terms of aggregation levels highly probable. Since the short transversal relaxation times of the proton signals in the salt containing sample do not allow the measurement of reliable diffusion coefficients by NMR experiments, only a qualitative estimation of the aggregation of these π-intermediates with **1** in diethyl ether is possible. A comparison of the line widths in the three HMQC spectra suggests that the aggregation level of the intermediate with LiI is the lowest. The salt free intermediate shows an increased aggregation level and the intermediate with LiCN exhibits by far the broadest line widths hinting at the highest aggregation level within the three samples. Interestingly, these observations fit exactly to the aggregation behaviour of the sterically hindered cuprate $(Me_3SiCH_2)_2CuLi$ in diethyl ether.[20] Furthermore, the disaggregation of the supramoleculare structures or the composition of these higher aggregates could be connected to the reactivity in 1,4-addition reactions to enones.[17]

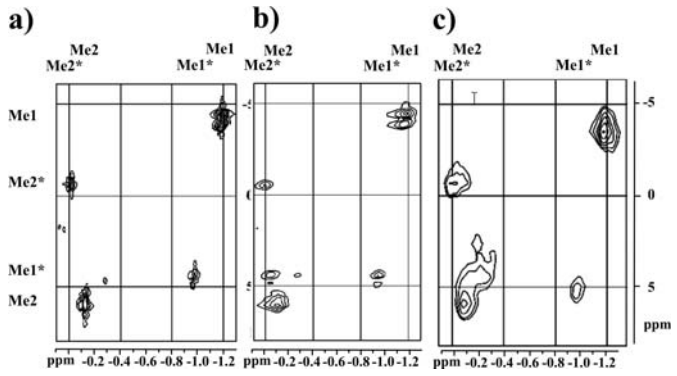

Figure 5. Sections of a ^{1}H, ^{13}C HMQC spectra of the π-complexes composed of **1** and two equivalents of a) **2**•LiI, b) **2**, and c) **2**•LiCN in diethyl ether at 180 K. The similarity of the chemical shift patterns indicate similar π-complexing cuprate units in all three cases. The increasing line widths (a<b<c) hint at different aggregation levels in solution.

In THF which supports the formation of solvent separated ion pairs, considerably reduced aggregation levels are reasonable and in case of the free cuprate reagents it was shown that the contact ion pairs exist only in very low concentrations.[16,18] Thus, it is not in contrast to the results reported here that recently in THF smaller aggregates were proposed as the main

species for π-complexes of **2**·LiX (X = I, CN, MeCuMe) and cyclohexenone.[46] Interestingly, in this study in THF no evidence for homodimeric π-complexes was found despite the necessary 2:1 ratio of cuprate to enone and therefore a heterodimeric π-complex is explicitely stated with a Li-I-Li^+ or a Li-CN-Li^+ moiety as carbonyl complexing unit. An investigation of this open question for the π-intermediates in diethyl ether was not possible with the π-complexes composed of **1** and **2** or **2**·LiX (X = I, CN), due to overlapping signals in the region of the cuprate reagents, the existence of the two π-complex conformers, and the broad line widths. Therefore, it was inevitable to simplify the intermediate spectra in order to investigate the carbonyl complexing unit and to determine the aggregation tendencies of the salt containing π-intermediates in diethyl ether.

4.3.3. Spectrum simplification by enantiomeric intermediates

As outlined above, the complexation of the enone from β-face and α-face creates two diastereomeric cuprate enone π-complexes which appear in the NMR spectra as two sets of signals and complicate the interpretation of the spectra. An elegant solution to this problem is the use of achiral enones. The β- and α-face complexation of achiral enones results in enantiomeric π-complexes, not distinguishable by NMR spectroscopy in achiral solvents. This results in a simple but effective reduction of the intermediate signals as shown in the HMQC spectra on the cuprate section of the π-complexes with chiral **1** and achiral **4** in Figure 6.

Also the ^{13}C spectra of the π-complexes reveal in the fingerprint region of the enone that the number of π-complexes is reduced to one NMR detectable type in case of achiral enones (see Figure 7d compared to Figure 2a). By using structurally simple achiral enones and conventional low temperature NMR it is essential for the observation of π-intermediates in diethyl ether to reduce the reaction rate by substituent effects. Therefore, the sterically hindered and achiral enones **3a**, **3b**, and **4** (see Scheme 2) were chosen to investigate the structure of the carbonyl complexing unit and the aggregation level of π-intermediates in 1,4-addition reactions.

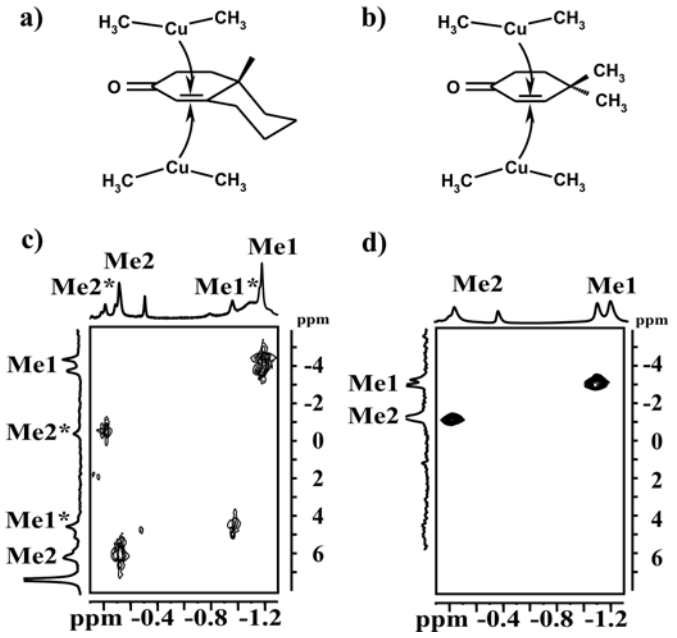

Figure 6. Schematic representations of the β- and α-face complexation of chiral (a) and achiral enones (b) and cuprate sections of the corresponding ^{1}H, ^{13}C HMQC spectra of the π-complexes composed of **1** and two equivalents of **2** (c), and **4** and two equivalents of **2**•LiI (d) in diethyl ether at 180 K. With achiral enones (shown exemplarily on **4**) enantiomeric π-complexes are formed, which produce only one set of signals in the NMR spectra.

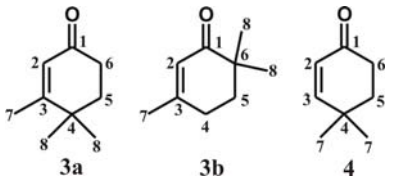

Scheme 2. Selected sterically hindered, achiral enones, which build NMR observable, enantiomeric cuprate enone π-complexes in diethyl ether at 173 K.

The π-complexes of **3a**, **3b**, and **4** with **2**·LiX (X = I, CN) were found to be stable for days even in diethyl ether by applying conventional low temperature NMR spectroscopy at 170 K. In contrast, the sterically less hindered enones 3-methylcyclohexenone and cyclohexenone reacted too fast to allow extensive two-dimensional NMR investigations. These results show that not only substituents in position 3 and 4,[22,28,30,35] but also in position 6 support the stability of π-complexes. Furthermore, multiple substitution allows the use of the small methyl groups as substituents and enones as substrates even in diethyl ether as solvent which show high reactions rates in 1,4-additions by supporting the formation of the reactive cuprate contact ion pairs and aggregates. In THF, providing slower reaction rates for 1,4-additions

due to the preference of solvent separated ion pairs,[16,19] π-complexes of **2**·LiX (X = I, CN) even with unsubstituted cyclohexenone were observed with the aid of rapid injection NMR.[27,46]

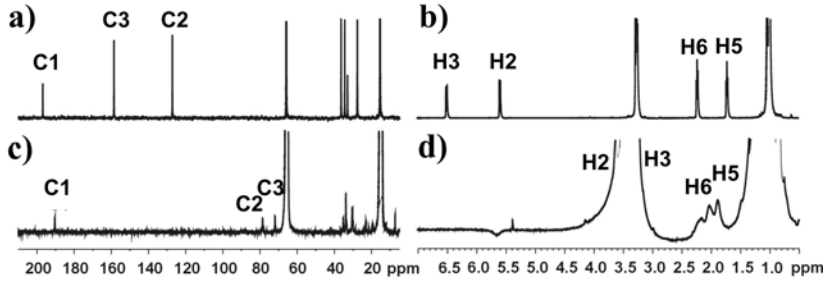

Figure 7. Typical change of ^{13}C-spectra (a, c) and ^{1}H-spectra (b, d) of free enones (a, b) upon π-complexation with two equivalents of **2**·LiX (X = I, CN) (c, d), exemplarily shown on **4** and **2**•LiI in diethyl ether at 170 K.

In a small screening using the achiral enones **3a**, **3b**, and **4** and the salt containing cuprates **2**·LiX (X = I, CN), for each combination only one set of π-complex signals were detected as exemplarily shown in Figure 7. In order to detect also minor conformations or long range NOE contacts very high concentrations of **2**·LiX (0.7 M) were used initially. Due to the high aggregation tendency of **2**·LiCN in diethyl ether,[20] this concentration produced a gel-like texture of the π-complexes at 170 K unsuitable for NMR investigations. Therefore, following the procedure previously reported by us for the free reagent **2**·LiCN,[17] six equivalents of THF were added, which disaggregate the π-intermediates of **2**·LiCN. The resulting π-complexes were found to be appropriate for NMR studies and showed an aggregation level alike those of **2**·LiI. In all six combinations the formation of the resulting π-complexes can be easily seen on the basis of the characteristic changes of the chemical shift patterns in the ^{1}H- and ^{13}C spectra of the enones (see Figure 7). For all π-complexes composed of **3a**, **3b**, and **4** and **2**·LiI or **2**·LiCN upfield shifts $\Delta\delta^{13}$C of about - 12 ppm, - 44 ppm, and - 85 ppm for the carbon signals of C1, C2, and C3 were observed. The corresponding changes $\Delta\delta^{1}$H are about 2.1 ppm for H2 and H3 (for the exact ^{1}H and ^{13}C chemical shifts of all six π-complexes see Tables S4-S7 in Supporting Information). Furthermore, there is no difference in the chemical shifts of any of the three enones depending on the cuprate **2**·LiI or **2**·LiCN. But the intermediate is built only in a ratio 2:1 (cuprate:enone) without any additional species like pure carbonyl complexes.

Also the cuprate signals of the six π-complexes reveal some characteristic features. The cuprate chemical shift sections of the ^{1}H- and the ^{13}C spectrum in Figure 8 show exemplarily

that in every complex the typical methyl group signals of the π-complexing cuprate unit (Me1, Me2) are observed. Furthermore, a signal labelled Cuprate is detected in each sample, its intensity depending strongly on the exact 2:1 ratio between cuprate and enone. The chemical shifts of these Cuprate signals are in principle similar to the chemical shifts of the free reagents **2**·LiX (X = I, CN), respectively, but show deviations depending on the kind of enone (see section carbonyl complexing moiety). Furthermore, in every intermediate spectrum signals of substitution side reactions are observed which are caused by traces of methyl halides in the commercial MeLi solutions used for the synthesis of **2**·LiX (X = I, CN).[12] Thus, ethane is detected in each spectrum and a transient symmetrical species (**5**), whose unusual ^{1}H, ^{13}C chemical shift combination of ~ -0.3 ppm and ~14 ppm, respectively, fits to the tetraalkyl Cu(III) species reported recently.[10-12]

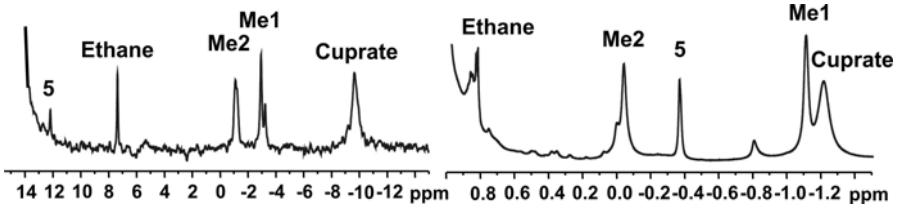

Figure 8. Characteristic signals patterns of the cuprates in π-intermediates as exemplarily shown on the ^{13}C-spectrum (left) and ^{1}H-spectrum (right) of **4** and two equivalents of **2**·LiI in diethylether at 170 K.

4.3.4. Aggregation level of π-intermediates

Recently, a direct correlation between the reactivity of cuprates in 1,4 addition reactions to enones and the aggregation level (for **2**•LiCN) or the aggregate structure (for **2**•LiI) of the free cuprate reagents was revealed.[17] Therefore the question, whether the trend of LiCN containing cuprates to form larger oligomers[20] is also valid for the π-intermediates or whether the addition of enones leads to a disaggregation, is very interesting in terms of structure-reactivity correlations.

The already mentioned gel-like texture of π-complexes with **2**•LiCN shows impressively the distinct tendency of LiCN containing π-complexes to form higher aggregates. Regrettably, with the gel like texture it was not possible to quantify the degree of aggregation. However, in accordance with our previous results for the free reagents a disaggregation of these larger aggregates is possible upon addition of THF. By using six equivalents of THF the aggregate

sizes of the π-intermediates with **2**•LiCN were reduced coincidentally to those of π-complexes with **2**•LiI. These experimental results confirm the previous observation that the salt is involved in the connection of the different aggregate units.

In order to analyze which of the compounds observed in the intermediate spectra really participate in the π-complex aggregate, ^{1}H-diffusion measurements of the different intermediates were performed. Despite the improved sample preparation the broad line widths and sometimes overlapping signals still hampered a detailed interpretation of the data. While clearly different and reproducible diffusion coefficients were found for the individual compounds, any trends reflecting the kind of salt or the type of enone were within the error range. Therefore for each compound the average diffusion coefficient of all intermediates is given in Table 1.

Table 1. Average diffusion coefficients D [10^{-9} m²/s] of the compounds observed in the spectra of the π-complexes composed of **2**•LiI or **2**•LiCN and **3a**, **3b** or **4** in diethyl ether at 170 K.

Cuprate	**Me1**	**Me2**	**Enone**	**ethane**
0.12	0.15	0.15	0.29	0.6
(±0.08)	(±0.03)	(±0.04)	(±0.09)	(±0.2)

The very similar diffusion coefficients of 0.12, 0.15 and 0.15*10^{-9} m²/s for Cuprate, Me1, and Me2 in Table 1 clearly show that in diethyl ether all cuprate moieties in the intermediate samples participate in a large π-complex aggregate. A comparative diffusion experiment on pure **2**·LiCN under otherwise identical experimental conditions, particularly the addition of six equivalents of THF, yielded a considerably larger diffusion coefficient of 0.22 ±0.01*10^{-9} m²/s. This indicates that the addition of enone does not disaggregate the oligomeric structures of the cuprate reagents, but increases even the size of the whole aggregate species.

In comparison to the cuprate signals those of the enones show a larger average D value of 0.29 10^{-9} m²/s with an error range of ± 0.09*10^{-9} m²/s. At first glance this is surprising since scalar couplings indicate a covalent bonding between Me1/Me2 and the enone (see below). However, baseline separated proton signals representing exclusively enones bound in the π-complex are not available. Therefore, contributions of free enone or product falsify this D value which explains also the large error range. Furthermore, the significantly larger diffusion constants of 0.6*10^{-9} m²/s of ethane is appropriate to its size and confirms that ethane exists

as individual species separated from the large π-complex aggregate which is in agreement with the missing cross peaks in the NOESY spectra.

4.3.5. π-complexing moiety

In the π-complexes of **1** the mixture of conformations necessitates a ^{13}C labeling of the cuprates and the measurement of INEPT-INADEQUATE spectra to detect ^{13}C, ^{13}C scalar couplings between Me1/C3 and Me1*/C3*, respectively, which was already a progress compared to the previous twofold labeling of cuprate and enone.[23,33] The simplification of the spectra by using achiral enones and in case of **2**·LiCN disaggregation by THF, improved the quality of the spectra so far that even without any isotope labeling ^{1}H, ^{13}C scalar couplings between the π-complexing cuprate moieties and the enones could be observed in ^{1}H, ^{13}C HMBC spectra (see Figure 9a). The bent arrangement of the π-complexing cuprate unit in each sample was approved by cross signals between Me1 and C3, the orientation of the two methyl groups was confirmed by ^{1}H, ^{1}H NOESY spectra (see Figure S1 in Supporting Information). This proves the bent geometry of the π-complexing cuprate unit to be a general structural feature of these complexes unaffected by the presence or kind of salt and the type of enone. Furthermore, for the π-complex composed of **4** and **2**•LiCN for the first time additional cross peaks of reduced intensities were detected between Me2 and C3 and between Me1 and C2 indicating additional but smaller scalar couplings across copper (see Figure 9).

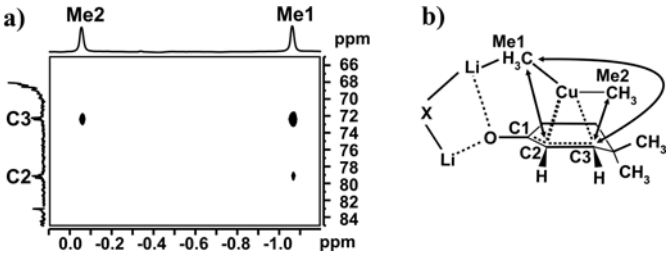

Figure 9. Section of a ^{1}H, ^{13}C HMBC spectrum of **4** and **2**•LiCN both at natural abundance in diethyl ether at 170 K. The cross signals indicate ^{1}H, ^{13}C scalar couplings across copper as indicated by the arrows in b).

Previous investigations of ^{13}C–labeled π-complexes with ynoates in THF reported only one observed $J_{C,C}$ = 12 Hz between Me1 and C3, the other coupling constants were found to be below the spectral resolution.[23,33] Since the relative signal intensities in HMBC spectra are proportional to the coupling constant, the improved sample preparation enables even without ^{13}C labeling the detection of additional structural parameters within the π-complexes. This

allows to refine the structure of these π-complexes by theoretical calculations as shown for Cu(III) intermediates.[49]

4.3.6. Carbonyl complexing moiety

Considering the requirement of two equivalents of MeCuMeLi per enone as prerequisite for the detection of π-complexes, beside the π-complexing cuprate unit (Me1, Me2) an additional equivalent of MeCuMeLi is present in solution. The respective signals of these second cuprate units are labeled Cuprate and in principle their chemical shifts are similar to those observed for the free cuprate reagents in diethyl ether. Despite this similarity, the diffusion coefficients obtained for these species indicate unambiguously the participation of this moiety in the π-complex aggregate (see above). Now the question arises, whether the species labeled Cuprate is really the carbonyl complexing moiety or somehow otherwise included into the π-complex aggregate.

In case the Cuprate species is spatially close to the carbonyl group, the chemical shifts of the Cuprate species should be affected by the type of enone and especially sterical hindrance around the carbonyl should lead to chemical shift deviations. The respective chemical shift differences observed for the six π-intermediates are given in Table 2 and they correspond very well to the steric demand of **3a**, **3b**, and **4**. The largest chemical shift disturbations by far are observed for **3b** with the two methyl substituents next to the carbonyl group (see Scheme 2). In contrast, the two methyl groups of **4** which are oriented in the opposite direction of the carbonyl unit, cause nearly no deviations and **3a** leads to medium chemical shift changes.

Table 2. ^{1}H and ^{13}C (in brackets) chemical shift differences Δδ [ppm] of the species Cuprate compared to the free cuprate reagents at 170 K in diethyl ether. Δδ [ppm] = δ(free reagents **2**·LiX (X = I, CN)) - δ(Cuprate in π-intermediates).

	3a	**3b**	**4**
2·LiI	0.09 (-0.1)	-0.19 (+0.1)	-0.01 (-0.1)
2·LiCN	0.03 (+0.3)	-0.12 (+1.0)	-0.01 (0.0)

Surprisingly, neither NOE cross peaks nor exchange cross peaks between Me1/Me2 and Cuprate have been detected in any of the six intermediates. In many samples this can be

explained by the low intensity and the large line widths of the two signals in combination with the small chemical shift differences leading to potential cross peaks very close to the diagonale. But also in samples with chemical shift differences of 0.29 ppm no cross signals were detected. Furthermore, no NOE interactions between the Cuprate moiety and an enone were detected in any of the intermediates. This might be explained by the large distances between Cuprate protons and those of the enones. For instances, even in π-complexes with **3b**, which show the highest chemical shift differences and has a methylation pattern pointing roughly in the direction of the carbonyl group, the through space distance between the methyl protons of **3b** and those of Cuprate is still around 4.4 Å according to model structures. This distance is quite large in terms of observable NOE contacts in the presence of quadrupole nuclei such as copper and lithium. Even in small peptides without additional leakage terms for cross relaxation pathways, structural evidence from missing NOE contacts is taken into account only for distances lower than 3.5 Å.[50] Due to this discrepancy and the fact that in previous experimental NMR investigations of π-complexes composed of **2**·LiX (X = I, CN) and cyclohexenone in THF no evidence of a homodimeric π-complex was found[27,46] we investigated the principal carbonyl complexation properties of **2**, **2**·LiI, and **2**·LiCN on cyclohexanone.

4.3.7. Carbonyl complexes of cyclohexanone

A 1:1 ratio of **2** to cyclohexanone was chosen to generate competitive conditions for the salt and the cuprate units in terms of carbonyl complexation, which are comparable to the situation in the π-complexes. Beside this fact otherwise identical experimental conditions were used such as addition of six equivalents of THF in case of **2**·LiCN. In all three resulting complexes a downfield shift of about 6 ppm to 219.0 ppm is observed for the carbon signal of the carbonyl group which is in agreement with previous investigations of the influence of carbonyl complexation on ^{13}C chemical shifts.[22,51,52] The ^{1}H and ^{13}C chemical shifts of the cuprate moieties in these complexes with cyclohexanone and as free reagents are given in Table 3. The comparison of the chemical shifts in Table 3 provides additional information. Upon carbonyl complexation significant chemical shift changes are observed for all three types of cuprates with the largest chemical shift differences detected for **2**·LiCN. In case the salt units in **2**·LiI and **2**·LiCN complex the carbonyl groups of cyclohexanone exclusively, this would result in chemical shifts of the cuprate moiety of **2**·LiI and **2**·LiCN similar to those of the free reagent **2**. The other extreme would be that the salt does not contribute at all to the

aggregate around the carbonyl. Then, the chemical shifts of **2**·LiI and **2**·LiCN would be expected to be similar to those of the complex with **2**. The chemical shifts experimentally detected for the complexes with **2**·LiI and **2**·LiCN indicate a mixture of both extreme scenarios and suggest mixed aggregates composed of cuprate and salt units.

Table 3. ^{1}H, and ^{13}C chemical shifts δ [ppm]of **2**, **2**· LiI and **2**· LiCN as free reagents and as complexes with cyclohexanone in diethyl ether (plus six equivalents of THF in case of **2**· LiCN) at 170 K.

	2		**2·LiI**		**2·LiCN**	
	δ (^{1}H)	**δ (^{13}C)**	**δ (^{1}H)**	**δ (^{13}C)**	**δ (^{1}H)**	**δ (^{13}C)**
complex	-1.13	-9.3	-1.17	-9.1	-1.06	-9.3
free reagent	-1.14	-9.6	-1.20	-9.5	-1.27	-9.9

Furthermore, the aggregate sizes of the three complexes with cyclohexanone were investigated with the aid of diffusion experiments. Again, the diffusion coefficients obtained for the three complexes varied only within the error range. The averaged diffusion coefficient for the cuprate units is $0.15 \pm 0.02*10^{-9}$ m²/s and that of the cyclohexanone $0.13 \pm 0.06*10^{-9}$ m²/s. Interestingly, in these complexes which are not able to perform 1,4-addition reactions and show only a small amount of 1,2-addition products in their spectra, the two diffusion coefficients of the cuprate and the enone are very similar. This corroborates that in case of enone complexes the deviating diffusion coefficients of the enones are caused by free enone and/or product of the 1,4 addition reaction (see above).

The diffusion coefficients of the cyclohexanone complexes are very similar to those obtained for the cuprate species in the π-complexes. This result indicates that the absence of the double bond does not affect the aggregation level of the complexes significantly and that carbonyl complexing aggregates are responsible for the formation of higher aggregates in diethyl ether. In this context the identical chemical shift of 219.0 ppm for all three cuprate cyclohexanone complexes indicate two points: First, the saltfree cuprate **2** is able to complex the carbonyl group properly, and second, the strength of the carbonyl complexation is not affected by the presence or absence of salt in diethyl ether in case the size of the aggregates is similar. These experimental observations are in excellent agreement with our previously proposed correlation between aggregate size and composition and reactivity of the cuprates.[17]

Thus, the combined results of diffusion coefficients, chemical shift data and NOE investigations clearly show the potential of cuprate units to complex carbonyl groups. Furthermore, the cuprate moieties are shown to participate in the carbonyl complexing aggregate which is responsible for the formation of higher aggregates in diethylether. However, an exclusive carbonyl complexation by simple homodimeric units as shown in theoretically calculated structures is not supported by the experimental data. The sum of the presented experimental data rather indicate more complicated mixed aggregates composed of salt and cuprate moieties.

4.4 Conclusion

In order to rationalize the high diastereoselectivities of organocuprates in conjugate addition reactions to sterically demanding enones, the structural features of π-intermediates composed of Me_2CuLi or Me_2CuLi LiX (X = I, CN) and 10-methyl-$\Delta^{1,9}$-2-octalone in diethyl ether were investigated in detail. The formation of two intermediate cuprate enone π-complexes on both sides of the double bond is observed for the first time, with the β-face π-complex as major species. In this major π-complex conformation the sterical hindrance between the cuprate moieties and the enone is minimized by a change of the preferred conformation of 10-methyl-$\Delta^{1,9}$-2-octalone supporting the formation of the β-face π-complex. Furthermore, neither the structures nor the relative population of the two π-complexes are affected by the presence or the type of salt in the cuprate reagents and the more stable intermediate is related to the stereochemistry of the product observed. These results rationalize for the first time experimentally the exclusive formation of β-methyloctalones.

In the second part a small NMR screening of intermediate π-complexes with $Me_2CuLi{\cdot}LiX$ (X = I, CN) and three different enones is presented to investigate the aggregate structure and the aggregation level of cuprate enone π-complexes as well as the influence of the type of salt on these intermediates. For this study achiral enones are chosen, since the resulting enantiotopic π-complexes appear as single species in the NMR spectra and simplify the spectra so far that for the first time NMR diffusion experiments on cuprate intermediates are possible. The observed diffusion coefficients show that in diethyl ether all cuprate moieties in the intermediate samples participate in a large π-complex aggregate. Compared to pure cuprate reagents the addition of enone even increases the size of the whole aggregate species. Similar aggregation trends of the free cuprate reagents and the π-complex species corroborate

the previously proposed importance of the supramolecular structure for the reactivity of organocuprates. Comparative studies on all six cuprate enone intermediates and on carbonyl complexes with cyclohexanone and saltfree as well as salt containing cuprates were performed to investigate the structure and the role of the π- and the carbonyl complexing moieties. The refined π-complex preparation allowed the detection of additional scalar couplings across copper even in intermediates without any isotope labeling. The resulting screening shows that the bent geometry of the π-complexing cuprate unit is a general structural feature of these complexes unaffected by the presence or kind of salt and the type of enone. Furthermore, diffusion experiments on cyclohexanone complexes show that the carbonyl complexing aggregates are responsible for the formation of higher aggregates in diethyl ether. In principle, saltfree dimethylcuprate is able to complex the carbonyl group properly and the participation of cuprate moieties in the carbonyl complexing aggregate part is shown. However, the experimental data do not support a simple cuprate moiety for the carbonyl complexation but rather more complex mixed aggregates composed of salt and cuprate moieties. These results allow for the first time an insight into the supramolecular structures of π-intermediates which are decisive for the reactivities of organocuprates in conjugate addition reactions.

4.5 Experimental Section

Synthesis and sample preparation of the π-complexes: The samples are prepared using Schlenck technique with Argon as inert gas. The respective cuprate (0.4 mmol) is synthesized following the known procedure[53,54] and a trace (2-3 drops) of benzene (C_6H_6) is added as viscosity reference.[17] The apparatus is then cooled down to -110°C and the enone (0.2 mmol in 0.4 ml Et_2O-d_{10}) is added very slowly while stirring. The colorless cuprate solution turns orange and is poured into the NMR tube. In the case of the cyanocuprate samples six equivalents of THF are added prior to the transfer. At -110°C the samples of the π-complexes are stable for 1-2 days; for longer storage they should be frozen in liquid nitrogen. It is essential to constantly keep to temperatures below -100°C while handling the NMR tubes. All enones 1, 3a, 3b, and 4 build π-complexes which can clearly be recognized in the change of the color from colorless to orange.

4.5.1. NMR Data Collection and Processing

The NMR spectra were recorded on a Bruker DRX500 and DMX500 spectrometer equipped with a 5 mm broadband triple-resonance Z-gradient probe (maximum gradient strength 53.6 G/cm). All diffusion measurements were performed with a convection-suppressing pulse sequence[55] in pseudo 2D mode and processed with the Bruker software package t1/t2. For each experiment, 16 dummy scans and 32 actual scans were used with a relaxation delay of 2 s and a diffusion delay of 60 ms. The shape of the gradients was sinusoidal, with a length of 2 ms, and the strength was varied in 10 increments (5-95%) of the gradient ramp created by Bruker software DOSY. The INEPT-INADEQUATE was assembled using an INEPT-transfer and an INADEQUATE-sequence. The spectra were carried out with 256 dummy scans and 128 actual scans, TD(F2) = 2k, TD(F1) = 300, and 1.5 s of relaxation delay for acquisition. The data were processed with SI(F2) = 2k and SI(F1) = 512. The ^{1}H,^{1}H NOESY measurements were carried out using 16 scans , TD(F2) = 4k, TD(F1) = 300, 8 s of relaxation delay for acquisition, and a mixing time of 1 s. The data were processed with SI(F2) = 4k and SI(F1) = 512. The ^{1}H,^{13}C HMQC spectra were recorded with 4 scans, TD(F2) = 4k, TD(F1) = 256, and a relaxation delay of 8 s. The data were processed with SI(F2) = 4k and SI(F1) = 512. The ^{1}H,^{13}C HMBC spectra were measured using 32 scans with TD(F2) = 16k and TD(F1) = 400 and a relaxation delay of 6 s. Data were processed with SI(F2) = 2k and SI(F1) = 512. The temperatures for all measurements were calibrated with methanol as internal temperature standard and were controlled by a Bruker BVT 3000 temperature unit.

4.6 References

(1) Krause, N. *Modern Organocopper Chemistry*; Wiley-VCH: Weinheim, 2002.

(2) Lipshutz, B. H. In *Organometallics in Synthesis*; Schlosser, M., Ed.; Wiley: Chichester, U.K., 1994.

(3) *Organocopper Reagents: A practical approach*; Taylor, R. J. K., Ed.; Oxford University Press: Oxford, U.K., 1994.

(4) Krause, N. In *Metallorganische Chemie*; Spectrum Akademischer Verlag: Heidelberg, Germany, 1996, pp 175-191.

(5) Krause, N. *Angew. Chem. Int. Ed.* **1999**, *38*, 79-81.

(6) Gschwind, R. M. *Chem. Rev.* **2008**, submitted.

(7) Krause, N.; Gerold, A. *Angew. Chem. Int. Ed.* **1997**, *36*, 186-204.

(8) Woodward, S. *Chem. Soc. Rev.* **2000**, *29*, 393-401.

(9) Bertz, S. H.; Cope, S.; Murphy, M.; Ogle, C. A.; Taylor, B. J. *J. Am. Chem. Soc.* **2007**, *129*, 7208-9.

(10) Bertz, S. H.; Cope, S.; Dorton, D.; Murphy, M.; Ogle, C. A. *Angew. Chem. Int. Ed. Engl.* **2007**, *46*, 7082-5.

(11) Bartholomew, E. R.; Bertz, S. H.; Cope, S.; Dorton, D. C.; Murphy, M.; Ogle, C. A. *Chem. Comm.* **2008**, 1176-1177.

(12) Gaertner, T.; Henze, W.; Gschwind, R. M. *J. Am. Chem. Soc.* **2007**, *129*, 11362-11363.

(13) Nakamura, E.; Mori, S. *Angew. Chem. Int. Ed.* **2000**, *39*, 3750-3771.

(14) Mori, S.; Nakamura, E. In *Modern Organocopper Chemistry*; Krause, N., Ed.; Wiley-VCH: Weinheim, 2002.

(15) Nakamura, E.; Yoshikai, N. *Bull. Chem. Soc. Jpn.* **2004**, *77*, 1-12.

(16) John, M.; Auel, C.; Behrens, C.; Marsch, M.; Harms, K.; Bosold, F.; Gschwind, R. M.; Rajamohanan, P. R.; Boche, G. *Chem. Eur. J.* **2000**, *6*, 3060-3068.

(17) Henze, W.; Vyater, A.; Krause, N.; Gschwind, R. M. *J. Am. Chem. Soc.* **2005**, *127*, 17335-17342.

(18) Gschwind, R. M.; Rajamohanan, P. R.; John, M.; Boche, G. *Organometallics* **2000**, *19*, 2868-2873.

(19) Bertz, S. H.; Chopra, A.; Eriksson, M.; Ogle, C. A.; Seagle, P. *Chem. Eur. J.* **1999**, *5*, 2680-2691.

(20) Xie, X.; Auel, C.; Henze, W.; Gschwind, R. M. *J. Am. Chem. Soc.* **2003**, *125*, 1595-1601.

(21) Gschwind, R. M.; Xie, X.; Rajamohanan, P. R.; Auel, C.; Boche, G. *J. Am. Chem. Soc.* **2001**, *123*, 7299-7304.

(22) Bertz, S. H.; Smith, R. A. *J. Am. Chem. Soc.* **1989**, *111*, 8276-8277.

(23) Canisius, J.; Mobley, T. A.; Berger, S.; Krause, N. *Chem. Eur. J.* **2001**, *7*, 2671-2675.

(24) Christenson, B.; Olsson, T.; Ullenius, C. *Tetrahedron* **1989**, *45*, 523-34.

(25) Hallnemo, G.; Olsson, T.; Ullenius, C. *J. Organomet. Chem* **1985**, *282*, 133-144.

(26) Lindstedt, E. L.; Nilsson, M.; Olsson, T. *J. Organomet. Chem* **1987**, *334*, 255-261.

(27) Murphy, M. D.; Ogle, C. A.; Bertz, S. H. *Chem. Commun.* **2005**, 854-856.

(28) Nilsson, K.; Ullenius, C.; Krause, N. *J. Am. Chem. Soc.* **1996**, *118*, 4194-4195.

(29) Sharma, S.; Oehlschlager, A. C. *Tetrahedron* **1989**, *45*, 557-68.

(30) Ullenius, C.; Christenson, B. *Pure Appl. Chem.* **1988**, *60*, 57-64.

(31) Vellekoop, A. S.; Smith, R. A. J. *J. Am. Chem. Soc.* **1994**, *116(*2902-13.

(32) Krause, N. *J. Org. Chem* **1992**, *57*, 3509-3512.

(33) Krause, N.; Wagner, R.; Gerold, A. *J. Am. Chem. Soc.* **1994**, *116*, 381-382.

(34) Eriksson, J.; Davidsson, O. *Organometallics* **2001**, *20*, 4763-4765.

(35) Nilsson, K.; Andersson, T.; Ullenius, C.; Gerold, A.; Krause, N. *Chem. Eur. J.* **1998**, *4*, 2051-2058.

(36) Breit, B.; Demel, P. In *Modern Organocopper Chemistry*; Krause, N., Ed.; Wiley-VCH: Weinheim, 2002.

(37) Bertz, S. H.; Smith, R. A. J. *Tetrahedron* **1990**, *46*, 4091-4100.

(38) Marshall, J. A.; Fanta, W. I.; Roebke, H. *J. Org. Chem.* **1965**, *31*, 1016-1020.

(39) Marshall, J. A.; Roebke, H. *J. Org. Chem.* **1967**, *33*, 840-843.

(40) Kabbara, J.; Flemming, S.; Nickisch, K.; Neh, H.; Westermann, J. *Liebigs Ann.* **1995**, 401-406.

(41) Aamouche, A.; Devlin, F. J.; Stephens, P. J. *J. Am. Chem. Soc.* **2000**, *122*, 7358-7367.

(42) Hikichi, S.; Hareau, G.; Sato, F. *Tetrahedron Lett.* **1997**, *38*, 8299-8302.

(43) Hareau-Vittini, G.; Hikichi, S.; Sato, F. *Angew. Chem. Int. Ed.* **1998**, *37*, 2099-2101.

(44) Weigelt, J.; Otting, G. *Journal of Magnetic Resonance, Series A* **1995**, *113*, 128-130.

(45) Reif, B.; Kock, M.; Kerssebaum, R.; Kang, H.; Fenical, W.; Griesinger, C. *Journal of Magnetic Resonance, Series A* **1996**, *118*, 282-285.

(46) Bertz, S. H.; Carlin, C. M.; Deadwyler, D. A.; Murphy, M. D.; Ogle, C. A.; Seagle, P. *J. Am. Chem. Soc.* **2002**, *124*, 13650-13651.

(47) Lipshutz, B. H.; Keith, J.; Buzard, D. J. *Organometallics* **1999**, *18*, 1571-1574.

(48) Bertz, S. H.; Nilsson, K.; Davidsson, Ö.; Snyder, J. P. *Angew. Chem. Int. Ed.* **1998**, *37*, 314-317.

(49) Hu, H.; Snyder, J. P. *J. Am. Chem. Soc.* **2007**, *129*, 7210-7211. (50) De Pol, S.; Zorn, C.; Klein, C. D.; Zerbe, O.; Reiser, O. *Angew. Chem. Int. Ed.* **2004**, *43*, 511-514.

(51) House, H. O.; Wilkins, J. M. *J. Org. Chem.* **1976**, *41*, 4031-4033.

(52) House, H. O.; Chu, C.-Y. *J. Org. Chem.* **1976**, *41*, 3083-3091.

(53) Behrens, C., diploma thesis, Philipps-Universität Marburg, 2000.

(54) John, M., diploma thesis, Philipps-Universität Marburg, 1999.

(55) Jerschow, A.; Mueller, N. *J. Magn. Reson.* **1997**, *125*, 372-375.

4.7 Supporting Information

Table S1. ^{1}H, and ^{13}C chemical shifts [ppm]of **1** in the major conformation of the π-complexes with 2 equivalents of **2**·LiX (X = I, CN) in diethyl ether at 170 K. The chemical shifts of **1** are not affected by the type of cuprate used.

Atom	δ(^{1}H)	δ(^{13}C)	Atom	δ(^{1}H)	δ(^{13}C)
1	3.59	82.6	6 6	1.54 1.76	22.8
2	–	191.4	7’ 7	1.79 1.39	29.9
3’ 3	2.19 2.03	32.8	8’ 8	1.26 2.31	32.9
4 4’	1.28 1.89	36.2	8a	–	80.5
4a	–	37.3	9	1.06	23.7
5’	1.65	39.5			

Table S2. ^{1}H, and ^{13}C chemical shifts [ppm] of **1** in the minor conformation of the π-complexes with 2 equivalents of **2**·LiX (X = I, CN) in diethyl ether at 170 K. The chemical shifts of **1** are not affected by the type of cuprate used.

Atom	δ(^{1}H)	δ(^{13}C)	Atom	δ(^{1}H)	δ(^{13}C)
1*	3.50	84.2	6* 6*	2.04 1.54	24.1
2*	–	186.0	7* 7’*	2.03 1.55	31.3
3’* 3*	2.20 2.03	33.6	8’*	2.27 1.20	33.75
4* 4’*	1.98 1.22	35.9	8a*	–	79.6
4a*	–	37.3	9*	1.06	23.7
5’*	1.65	39.5			

Table S3. ^{1}H, and ^{13}C chemical shifts [ppm] of **2**·LiI in the major conformation (Me1, Me2) and in the minor conformation (Me1*, Me2*) of the π-complexes with **1** in diethyl ether at 170 K.

	δ(^{1}H)	**δ(^{13}C)**
Me2	-0.12	5.76
Me1	-1.18	-4.0 (d)
Me2*	-0.02	-0.77
Me1*	-0.96	4.56

Table S4. ^{1}H, and ^{13}C chemical shifts [ppm] of the enones **3a**, **3b**, and **4** in the π-complexes with **2**·LiX (X = I, CN) in diethyl ether at 170 K. The chemical shifts of **3a**, **3b**, and **4** are not affected by the kind of cuprate used.

Atom	**3a δ (^{1}H)**	**3a δ (^{13}C)**	**3b δ (^{1}H)**	**3b δ (^{13}C)**	**4 δ (^{1}H)**	**4 δ (^{13}C)**
1	~	187.0	~	**198.1**	–	189.5
2	3.57	85.1	**3.47**	**78.9**	3.66	78.7
3	~	77.5	~	**75.1**	3.26	71.8
4	~	32.9	**2.26**	**38.9**	–	31.9
5	2.13	35.7	**1.78**	**36.3**	1.82	35.2
6	2.01 2.15	33.5	~	**40.3**	2.41	33.8
7	1.32	19.3	**1.58**	**30.0**	1.05	30.3 31.3
8	1.00	26.5 26.7	**2.35**	**28.3**	–	189.5

Table S5. ^{1}H, and ^{13}C chemical shifts [ppm] of the cuprate species in the π-complexes with **3** in diethyl ether at 170 K.

	2·LiI/**3a**		**2**·LiCN/**3a**	
	δ (^{1}H)	**δ (^{13}C)**	**δ (^{1}H)**	**δ (^{13}C)**
Cuprate	**-1.11**	**-9.6**	-1.24	-9.6
Me1	**-1.08**	**-3.0**	-1.09	-2.9
Me2	**-0.12**	**4.9**	-0.14	4.9

Table S6. ^{1}H, and ^{13}C chemical shifts [ppm] of the cuprate species in the π-complexes with **3a** in diethyl ether at 170 K.

	2·LiI/**3b**		**2**·LiCN/**3b**	
	δ (^{1}H)	**δ (^{13}C)**	**δ (^{1}H)**	**δ (^{13}C)**
Cuprate	**-1.39**	**-9.4**	-1.39	-8.9
Me1	**-1.10**	**-5.7**	-1.20	-5.7
Me2	**-0.56**	**2.6**	-0.47	2.0

Table S7. ^{1}H, and ^{13}C chemical shifts [ppm] of the cuprate species in the π-complexes with **4** in diethyl ether at 170 K.

	2·LiI/**4**		**2**·LiCN/**4**	
	δ (^{1}H)	**δ (^{13}C)**	**δ (^{1}H)**	**δ (^{13}C)**
Cuprate	**-1.21**	**-9.6**	-1.28	-9.9
Me1	**-1.09**	**-3.0**	-1.06	-0.97
Me2	**-0.02**	**-1.04**	-0.06	-4.53

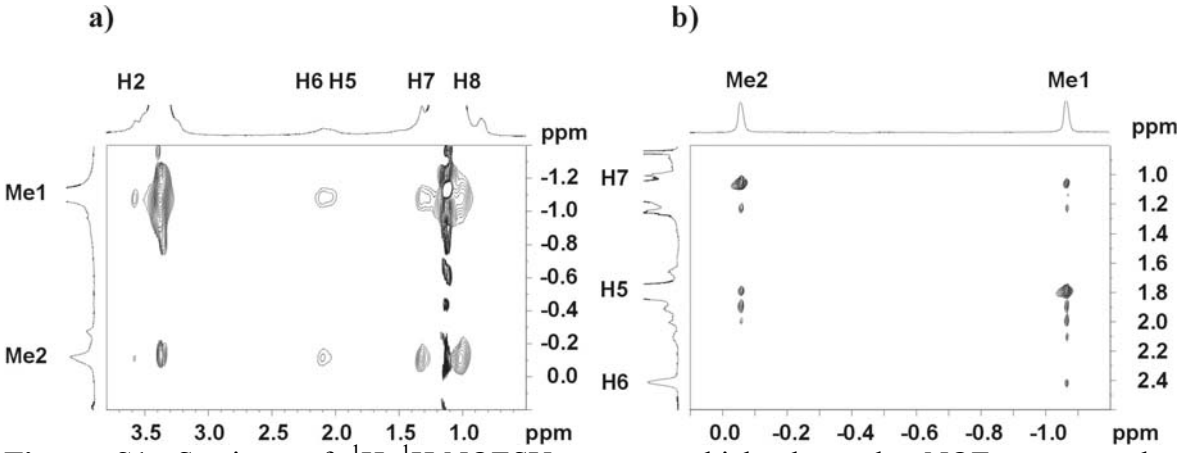

Figure S1. Sections of ^{1}H, ^{1}H-NOESY-spectra, which show the NOE cross peaks to differentiate **Me1** and **Me2** in the intermediates of **2**· LiI and enone **3a** (a) as well as **2**· LiCN and enone **4** (b) in diethylether at 170 K.

The sections of ^{1}H, ^{1}H-NOESY-spectra in Figure S1 show exemplarily the NOE contacts between the π-complexing cuprate unit and the enone in case of the complexes **2**·LiI/**3a** and **2**·LiCN/**4**. In both intermediates **Me1** is oriented towards the carbonyl group as indicated by stronger cross peaks between **Me1** and **H2** as well as between **Me1** and to the CH_2 groups **H5** and **H6**. Furthermore, in the complex **2**·LiCN/**4** (Figure S1b) stronger contacts between **Me2** and the methyl group (**H7**) confirm the orientation of **Me1** and **Me2**.

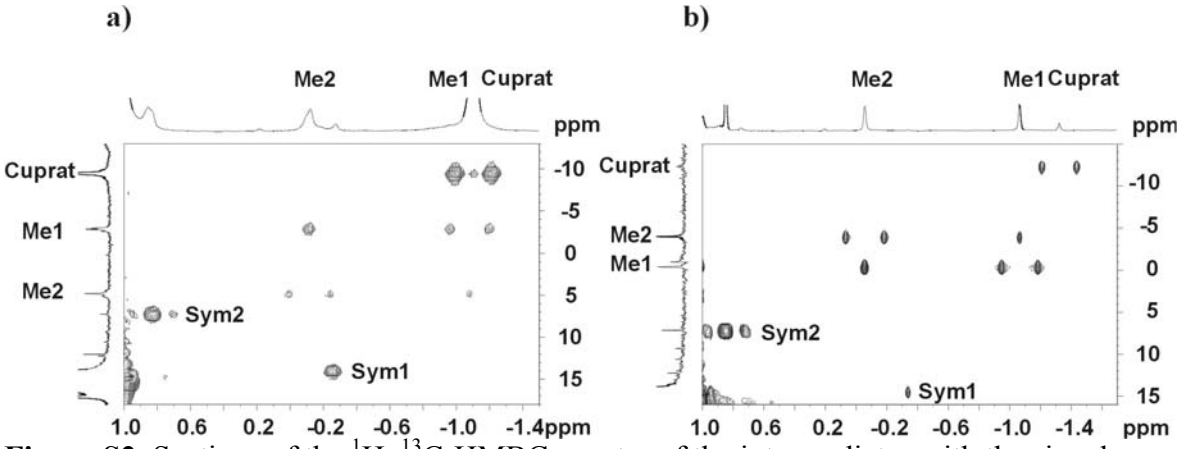

Figure S2. Sections of the ^{1}H, ^{13}C-HMBC-spectra of the intermediates with the signals between **Me1** and **Me2** of **2**· LiI and **3a** (a) and **2**· LiCN and **4** (b) in diethyl ether at 170 K.

Figure S2 shows clearly the connection between Me1 and Me2. For Cuprate no isolated cross signal is detected, which might be explained by the quick exchange of lithium in cuprate species, which leads generally to non observable scalar couplings across lithium.

5. NMR-Detection of Cu(III) Intermediates in Substitution Reactions of Alkyl Halides with Gilman Cuprates*

Tobias Gärtner, Wolfram Henze, Ruth M. Gschwind

Starting from unidentified species, detected by Wolfram Henze, the remaining work described in this communication, e.g. stabilisation and identification of the Cu(III) intermediate, was performed during my PhD thesis.

---

*Tobias Gärtner, Wolfram Henze, Ruth M. Gschwind
J. Am. Chem. Soc. **2007**, 129, 11362-11363

5.1 Abstract

The first NMR observation of the long-proposed Cu(III) intermediate in a substitution reaction of methylhalides with organocuprates is presented. One-dimensional ^{1}H and HMBC spectra give for the first time direct experimental evidence for a square planar coordination of the Cu(III) intermediate in solution. The presence of 4,4-dimethylcyclohexenone increases the detectable amount of the trimethylcyano Cu(III) species significantly, whereas in pure substitution reactions the proposed tetraalkyl Cu(III) species seems to be more stable in diethyl ether.

5.2 Discussion

For some decades organocopper(I) reagents have provided a uniquely important synthetic methodology for highly selective C-C-bond formation.[1a] Typical reactivity patterns of organocuprates include, e.g., conjugate addition reactions to α,ß unsaturated enones or S_N2-like substitution reactions of alkyl halides.[1] The formation of the key carbon–carbon bond in these reactions has long been proposed to be mediated by a Cu(III) intermediate.[1-5]

In a very recent publication Bertz and Ogle described the first experimental observation of a Cu(III) intermediate in a conjugate addition reaction of Gilman cuprates to 2-cyclohexenone by rapid injection NMR using THF as solvent.[6] We have now been able to stabilize the first Cu(III) intermediate of a substitution reaction of Gilman cuprates with alkyl halides in diethyl ether. Moreover, we have developed a method of preparing NMR samples and found conditions under which it is possible to stabilize these Cu(III) intermediates for several days, thus allowing for extensive two-dimensional NMR investigations with conventional low temperature NMR.

Interestingly, our study started in a similar way to that of Bertz and Ogle, with the stabilization of intermediate species in the conjugate addition reactions of Gilman cuprates to enones. However, the different solvents employed in these two independent studies produce significant differences. In THF mainly solvent separated ion pairs exist[7] inducing slow reaction rates in conjugate addition reactions.[8,9] In contrast, in diethyl ether the dimeric or even oligomeric contact ion pairs react rapidly.[8] Therefore, the reaction rate has to be slowed down by alkyl substitution of the enones[10] to enable the detection of intermediate cuprate enone π-complexes.[9] For in-depth investigations of the supramolecular structure of such

intermediate π-complexes, as well as the position of the cyano groups therein, we prepared the cyano-Gilman cuprates **1**[11] with isotopically labeled $Cu^{13}CN$, and added 4,4-dimethylcyclohexenone **2** at 180 K (see Scheme 1 Route 1).

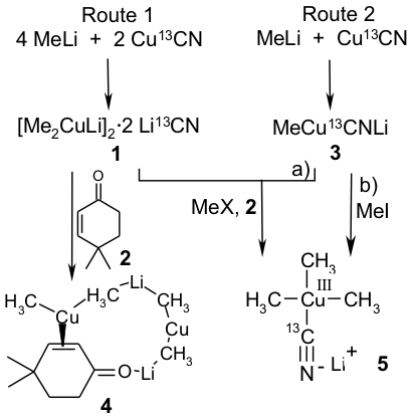

Scheme 1. Two routes to obtain **5** in diethyl ether. Addition of enone **2** to a solution of **1** yields π-complex **4** as the main product. MeX represents traces of methyl halides in commercial MeLi solutions (see text).

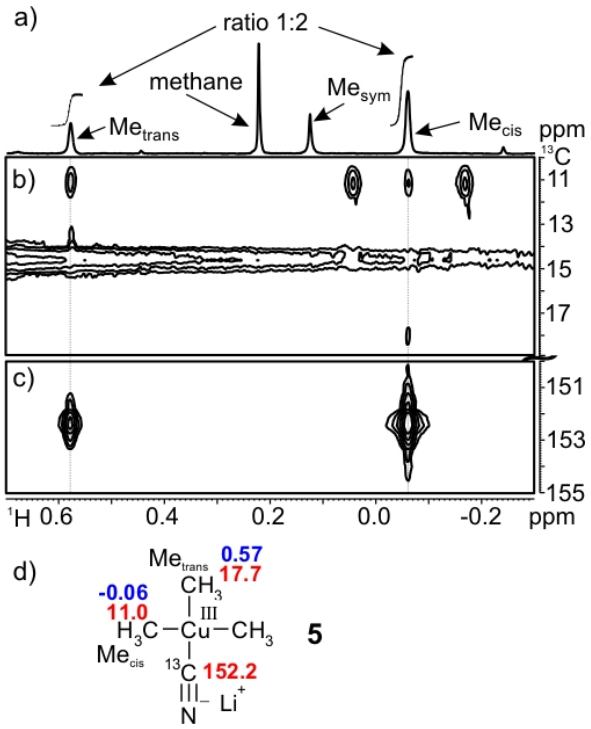

Figure 1. Selected high field sections of a 1D ^{1}H spectrum (a) and a $^{1}H,^{13}C$ HMBC spectrum (b,d) of the products obtained by Route 2a at 180 K in diethyl ether. The proton spectrum (a) shows for **5** a 1:2 ratio of Me_{trans} and Me_{cis} as well as signals of methane and a species Me_{sym}; b) the methyl section (b) and the cyanide section (c) of the HMBC spectrum show that two chemically equivalent methyl groups together with a third methyl group and a cyanide group are attached to copper. This indicates a square planar copper (III) intermediate **5** shown in (d) in its form as monomeric contact ion pair with ^{13}C (red) and ^{1}H (blue) chemical shifts.

Surprisingly, in addition to the expected π-complex **4** we observed very small traces of **5** in a $^{1}H,^{13}C$ HMBC spectrum. The amount of **5** under these experimental conditions was so small that in the one-dimensional ^{1}H spectrum no signal of **5** was detected due to limitations in the dynamic range of the receiver. Only the tremendous signal enhancement of the methyl groups, connected *via* $^{3}J_{H,C}$ scalar coupling to the ^{13}C labeled cyanide group, allowed for the observation of **5** in the HMBC spectrum. By using the heteroleptic cuprate **3** and increasing the ratio of the enone relative to **3** (Scheme 1 Route 2a) we were able to suppress the appearance of the π-complex completely and to increase the amount of **5** considerably. This allowed the in-depth investigation of **5** with two-dimensional NMR experiments.

The high field sections of the ^{1}H spectrum and the $^{1}H,^{13}C$ HMBC spectrum with the signals and cross peaks of **5** are shown in Figure 1. From the HMBC section in Figure 1c it is directly evident that one cyanide group shows cross peaks to two kinds of methyl group. In the corresponding proton spectrum (Figure 1a) the integrals of these methyl groups show a 1:2 ratio indicating that two out of the three methyl groups attached to copper are chemically equivalent. Also, the methyl section of the HMBC spectrum (Figure 1b) confirms the structure of **5** to be a square planar coordinated Cu(III) species with three methyl groups and one cyano group attached, showing cross peaks between Me_{trans} and Me_{cis} as well as cross peaks from both $^{3}J_{H,C}$ and $^{1}J_{H,C}$ scalar couplings for Me_{cis}.

The relative values of the proton and carbon chemical shifts of **5** (Figure 1d) are in good agreement with the chemical shifts reported for the conjugate addition Cu(III) intermediate by Bertz[6] and Snyder.[12] There, Bertz, Ogle and Snyder claim that the copper coordination sphere is square planar based on precedent[13-15] and on high level theoretical calculations.[12] In our experimental setup using exclusively methyl groups as alkyl substituents the square planar coordination of **5** is directly evident from the proton spectrum and the HMBC spectrum discussed above. In addition our results are in perfect agreement with crystal field theory. Square planar d^8 Cu(III) complexes are expected to be diamagnetic with quite sharp NMR signals and chemical shifts close to those of organic compounds as shown in Figure 1. In contrast, tetrahedral d^8 Cu(III) complexes would be paramagnetic, with 2 unpaired electrons among the three t_2 orbitals. This would lead to very broad signals and extreme low field shifts of the protons close to the paramagnetic center.

In the beginning of our study the mechanistic origin of the detected Cu(III) intermediate was less evident. Experiments with entirely ^{13}C-labeled MeLi showed that all three methyl groups in **5** originate from the MeLi solution and neither the NOESY nor the HMBC spectra

of both isotopically labeled and unlabeled **5** showed any cross peaks to the enone indicating no detectable interaction between **5** and enone **2** (data not shown). However, in the HMBC spectra of the ^{13}C labeled compounds, small amounts of $^{13}CH_3I$ were observed originating from the synthesis of MeLi (see 2.3.1 Experimental Section). The commercially available solution of MeLi used in the previous experiments also contains traces of halides.

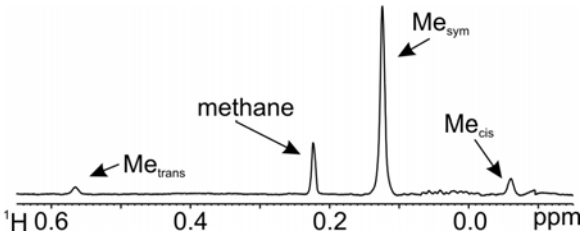

Figure 2. High field sections of a 1D ^1H spectrum of the products obtained by Route 2b at 180 K in diethyl ether. The signal intensities of **5** and methane are significantly reduced compared to Route 2a, the signal of Me_{sym} is significantly larger.

Considering the well known substitution reactions of alkyl halides with Gilman cuprates[1c,16] it was highly probable that we stabilized the first Cu(III) intermediate of a substitution reaction with Gilman cuprates. To prove this hypothesis we prepared **5** according to Scheme 1 Route 2b. The corresponding proton spectrum is shown in Figure 2.

The two methyl signals of **5** are clearly visible and the HMBC spectrum of this substitution reaction also shows an identical pattern to that discussed above for **5** (see 2.3.2 Additional NMR Data). Compared to the first approach the signal intensity of **5** is significantly reduced, indicating a beneficial influence of the enone in the generation or stabilization of **5**. The substitution reaction also produces, besides **5**, the proton signals of ethane (data not shown), methane, and a quite large amount of a third species (hereafter named Me_{sym}) compared to Figure 1a. The corresponding HMBC pattern (see 2.3.2 Additional NMR Data) indicates a symmetrical species with a proton carbon chemical shift combination very similar to those methyl groups in the two square planar coordinated Cu(III) intermediates known so far which are located trans to alkyl groups (Figure 1d and ref.[6]). Additionally, based on theoretical calculations Snyder predicted that tetra alkyl square planar Cu(III) complexes are more stable than **5** by approx. 20 kcal/mol.[12] Therefore, we speculate that the ^1H and ^{13}C signals of Me_{sym} might belong to a tetramethyl Cu(III) species.

In summary, we present the first experimental observation of the long proposed Cu(III) intermediate in a substitution reaction with organocuprates. The one dimensional proton and the HMBC spectrum for the first time provide direct experimental evidence for a square planar coordination of the Cu(III) intermediate in solution. The presence of 4,4-

dimethylcyclohexenone increases the detectable amount of the trimethylcyano Cu(III) species significantly, whereas in pure substitution reactions the proposed tetraalkyl Cu(III) species seems to be more stable in diethyl ether.

5.3 References

(1) (a) Krause, N. *Modern Organocopper Chemistry*; Wiley-VCH: Weinheim, 2002. (b) Nakamura, E.; Mori, S. *Angew. Chem. Int. Ed.* **2000**, *39*, 3750-3771. (c)Whitesides, G. M.; Fischer, W. F.; SanFilippo, J.; Bashe, R. W.; House, H. O. *J. Am. Chem. Soc.* **1969**, *91*, 4871-4882.

(2) House, H. O. *Acc. Chem. Res.* **1976**, *9*, 59-67.

(3) Murphy, M. D.; Ogle, C. A.; Bertz, S. H. *Chem. Commun.* **2005**, 854-856.

(4) Bertz, S. H.; Human, J.; Ogle, C. A.; Seagle, P. *Org. Biomol. Chem.* **2005**, *3*, 392-394.

(5) Nakamura, E.; Mori, S.; Morokuma, K. *J. Am. Chem. Soc.* **2000**, *122*, 7294-7307.

(6) Bertz, S. H.; Cope, S.; Murphy, M.; Ogle, C.; Taylor, B. J. *J. Am. Chem. Soc.* **2007**, *129*, 7208-7209.

(7) Gschwind, R. M.; Rajamohanan, P. R.; John, M.; Boche, G. *Organometallics* **2000**, *19*, 2868-2873.

(8) (a) John, M.; Auel, C.; Behrens, C.; Marsch, M.; Harms, K.; Bosold, F.; Gschwind, R. M.; Rajamohanan, P. R.; Boche, G. *Chem. Eur. J.* **2000**, *6*, 3060-3068. (b) Henze, W.; Vyater, A.; Krause, N.; Gschwind, R. M. *J. Am. Chem. Soc.* **2005**, *127*, 17335-17342.

(9) Bertz, S. H.; Carlin, C. M.; Deadwyler, D. A.; Murphy, M. D.; Ogle, C. A.; Seagle P. H. *J. Am. Chem. Soc.* **2002**, *124*, 13650-13651.

(10) Nilsson, K.; Andersson, T.; Ullenius, C.; Gerold, A.; Krause, N. *Chem. Eur. J.* **1998**, *4*, 2051-2058.

(11) For the position of CN^- in Gilman cuprates see: (a) Kronenburg, C. M. P.; Jastrzebski, J. T. B. H.; Spek, A. L.; van Koten, G; *J. Am. Chem. Soc.* **1998**, *120*, 9688-9689. (b) Gschwind, R. M.; Xie, X.; Rajamohanan, P. R.; Auel, C.; Boche, G. *J. Am. Chem. Soc.* **2001**, *123*, 7299-7304. (c) Xie, X.; Auel, C.; Henze, W.; Gschwind, R. M. *J. Am. Chem. Soc.* **2003**, *125*, 1595-1601. (d) Boche, G.; Bosold, F.; Marsch, M.; Harms, K. *Angew. Chem. Int. Ed.* **1998**, *37*, 1684-1686.

(12) Hu, H.; Snyder, J. P. *J. Am. Chem. Soc.* **2007**, *129*, 7210-7211.

(13) Willert-Porada, M. A.; Burton, D. J.; Baenziger, N. C. *J. Chem. Soc., Chem. Comm* **1998**, 1633-1634.

(14) Naumann, D.; Roy, T.; Tebbe, K.-F.; Crump, W. *Angew. Chem. Int. Ed.* **1993**, *32*, 1482-1483.

(15) Melník, M.; Kabesová, M. *J. Coord. Chem* **2000**, *50*, 323-338.

(16) Corey, E. J.; Posner, G. H. *J. Am. Chem. Soc.* **1968**, *90*, 5615-5616.

(17) John, M.; Auel, C.; Behrens, C.; Marsch, M.; Harms, K.; Bosold, F.; Gschwind, R. M.; Rajamohanan, P. R.; Boche, G. *Chem. Eur. J.* **2000**, *6*, 3060-3068.

5.4 Supporting Information

5.4.1. Experimental Section

All cuprate samples were prepared by a method described by John et al.[17] Having the cuprate in hand it was cooled down to 170K and a solution of 4,4-dimethylcyclohexenone or MeI in DEE-d_{10} was added depending on the synthesis. The amount of MeI as well as the amount of 4,4-dimethylcyclohexenone was adjusted to the synthesis of the cuprate solution. The ratio of DEE and DEE-d_{10} varied due to different amounts of remaining DEE during the cuprate synthesis.

^{13}C labelled MeLi was synthesised via a halide metal exchange.

The solvent of an 18 ml n-BuLi solution (40 mmol, 2.25 mol/l) in pentane was evaporated and replaced by 20 ml diethylether. After that 5 g (31.3 mmol) $^{13}CH_3I$ was added at a temperature of -78°C. Storing the solution at this temperature 15 hours a colourless precipitate was observed. The solvent then was removed with a syringe and distilled diethylether was added. After heating up the mixture to room temperature the MeLi was recrystalized at -78°C. Washing the MeLi this way 3 times, 15 ml ^{13}C labelled MeLi solution (0.74 mol/l) were obtained.

NMR-data in DEE-d_{10} at 180 K:

	$\delta(^1H)$	**$\delta(^{13}C)$**	**$\delta(^7Li)$**
$^{13}CH_3Li$	-1.85 (d, $J_{C,H}$ = 97 Hz)	-12.48 (s)	2.5 (s)

5.4.2. Additional NMR Data

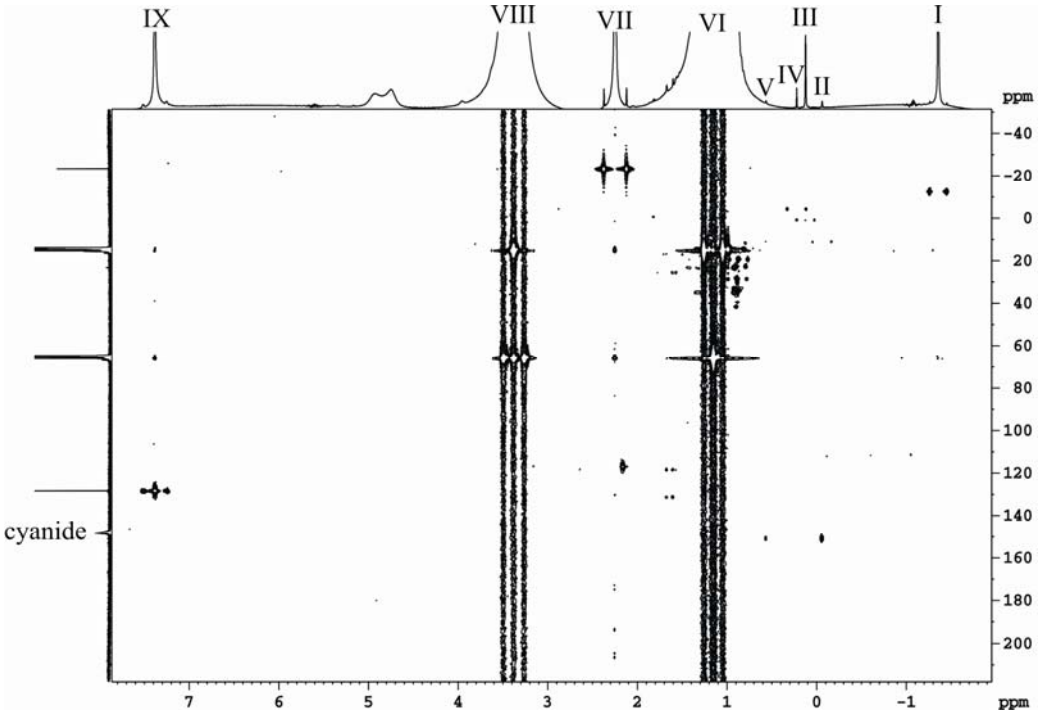

peak number	^{1}H chemical shift [ppm]	^{13}C chemical shift [ppm]	group
I	-1.35	-12.8	compound **3**
II	-0.06	11.0	compound **5** Me_{cis}
III	0.12	0.5	Me_{sym}
IV	0.23	-2.3	methane
V	0.57	17.7	compound **5** Me_{trans}
VI	1.14	15.0	CH_3 diethylether
VII	2.25	-23.5	MeI
VIII	3.39	65.6	CH_2 diethylether
IX	7.39	128.6	benzene
		148.4	cyanide

Figure 3. Complete ^{1}H,^{13}C HMBC spectrum in the study of the substitution reaction.

5.4.3. NMR Data Collection and Processing

The NMR spectra were recorded on a Bruker Avance 600 spectrometer equipped with a 5mm broadband triple resonance Z-gradient probe.

^{1}H,^{13}C HMBC measurements were carried out with a standard Bruker pulse program using 32 number of scans, 16 dummy scans, TD(F2) = 16k and TD(F1) = 400 with a relaxation delay of 2s. The processing parameters were TD(F1) = 1k and TD(F2) = 1k. The temperatures for all measurements were controlled by a Bruker BVT E 3900 temperature unit.

6. Ligand Exchange Reactions in Cu(III) complexes: Mechanistic Insights by Combined NMR and DFT Studies

Tobias Gärtner, Eiichi Nakamura, Ruth M. Gschwind

to be published in Chem. Comm.

6.1 Abstract

NMR studies of $^{13}C/^{12}C$ isotopic pattern in Cu(III) intermediates and reaction products together with DFT calculations of possible reaction pathways indicate an intermolecular S_N2 like substitution mechanism for ligand exchange reactions in square planar Cu(III) complexes, which is slow at synthetic conditions compared to reductive elimination.

6.2 Discussion

In the past two years, high-resolution NMR studies revealed the elusive experimental evidence for Cu(III) intermediates in conjugate addition reactions[1] as well as S_N2' and S_N2-type cross coupling reactions[2-4] of organocuprates, which had been proposed for years in comprehensive theoretical studies.[5] In these NMR investigations not only the mechanistically expected Cu(III) intermediates but also tetra-alkyl Cu(III)-species ($[Me_4Cu]^-$ [4] and $[Me_3EtCu]^-$[3]) were detected, and for $[Me_3EtCu]^-$ in THF an unexpected temperature stability up to -10°C was reported.[3] Furthermore, the formation of several tri-alkyl Cu(III)-complexes with different electron donating hetero-ligands was demonstrated.[6] The existence of these additional Cu(III) complexes are signs of possible ligand exchange reactions in square planar Cu(III) complexes, which would allow for targeted chemical reactions with Cu(III) complexes. Therefore, in this contribution possible intra- and intermolecular ligand exchange processes in Cu(III) intermediates are investigated by NMR and DFT calculations.

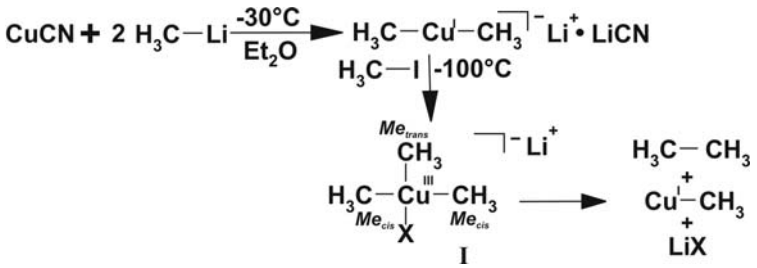

Scheme 1. Model reaction yielding the $[Me_3CuX]^-$ (X=I,CN) intermediate **I** and the the products ethane, MeCu and LiX.

As a model, the S_N2 reaction of dimethyl cuprate (derived from CuCN and MeLi) with methyliodide in diethyl ether was selected (see Scheme 1), in which we have previously detected $[Me_3CuCN]^-$ (**I**).[4] In order to make ligand exchange processes in **I** detectable, 100 % ^{13}C-labelling was used for the methyl groups in the cuprate and ^{13}C at natural

abundance for MeI. According to the reaction mechanism previously proposed for this S_N2-type cross coupling reaction,[3,7] the incorporation of the unlabelled methyl group of MeI should be trans selective to the heteroligand X, which would result exclusively in the isotopomer **Ia** (see Fig. 1). The $^1H,^{13}C$ HMBC pattern of **Ia** should show no central peak (^1H-^{12}C) for Me_{cis}, and no doublet splitting (^1H-^{13}C) in the cross peak between Me_{trans} and Me_{cis}, which are indicative for the existence of isotopomer **Ib**. However, in the experimental spectrum (see Fig. 1) the patterns of both isotopomers are detected in considerable amounts.

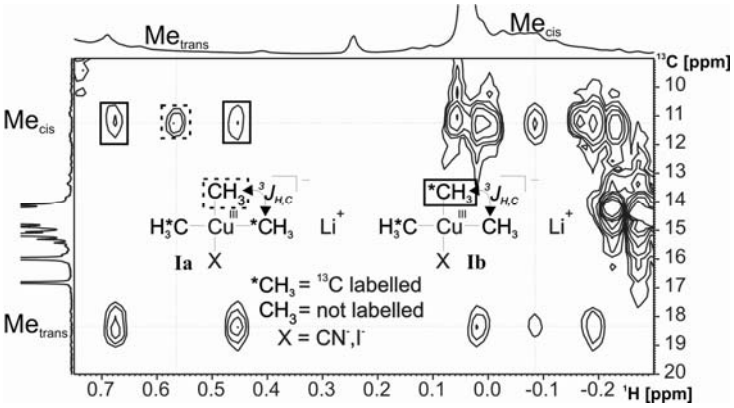

Figure 1. Section of an $^1H,^{13}C$ HMBC at -100 °C in diethyl ether which shows the cross peak patterns of both isotopomers **Ia** and **Ib** as highlighted on the cross peak between Me_{trans} and Me_{cis}.

The mixture of **Ia** and **Ib** indicates ligand exchange processes in **I** or an reaction mechanism differing from the proposed trans-addition.[3] To distinguish between these two possibilities, the isotopic pattern of the reaction product ethane was investigated, which is formed at temperatures above – 90°C (see Figure 2). Surprisingly, a comparison with simulated spectra showed the exclusive formation of $H_3{}^{12}C$-$^{13}CH_3$, contributions of $H_3{}^{13}C$-$^{13}CH_3$ were not detected (see Fig.2). This isotope pattern of the product ethane is in agreement with the postulated syn-elimination from the "direct" Cu(III) intermediate **Ia** and hints at ligand exchange processes being slow compared to elimination at usual synthetic temperatures.

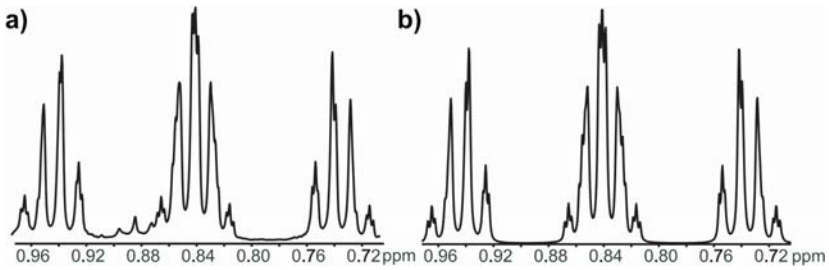

Figure 2. a) experimental and b) simulated isotopic pattern of $H_3{}^{12}C$-$^{13}CH_3$.

Therefore, intermolecular exchange processes were considered as possible reaction pathway for **I**. The model reaction (Scheme 1) was applied using an excess amount of ^{13}C-labelled MeLi, and MeI at natural abundance. The resulting ^{1}H spectrum reveals a considerably increased amount of a symmetrical species, which shows with 0.04 ppm (^{1}H) and 4.7 ppm (^{13}C) a typical chemical shift combination of Cu(III)-complexes.[1-4] In addition, the presence of both $^{13}CH_3$ and $^{12}CH_3$ groups and an unusual temperature stability is observed up to 300 K is observed (data not shown). These results suggest that Li containing species, e.g. MeLi, may be involved in intermolecular ligand exchange processes in square planar Cu(III)-complexes. However, an unambiguous identification of this symmetrical species has not yet been possible so far.

Therefore, DFT-functional calculations (B3LYP) were performed to gain further insight into the mechanism of the ligand exchange reactions in Cu(III) complexes,. First, the relative stabilities of differently substituted trimethyl Cu(III) complexes **1**-**5** relative to trimethyl cuprate **0** were calculated (see Scheme 2). In agreement with previously reported results about the special stability of tetraalkyl Cu(III) complexes,[3] **2** was found to be ~25-50 kcal/mol more stable than **1** or **3**-**5**. Considering the high energy differences between **0** and **1**-**5** ligand exchange processes via **0** are improbable. Calculations of **1**-**5** with additional Li^+ coordination result in substantially lower energies for all complexes (~143-136 kcal/mol see SI) while the relative stabilities remain similar.

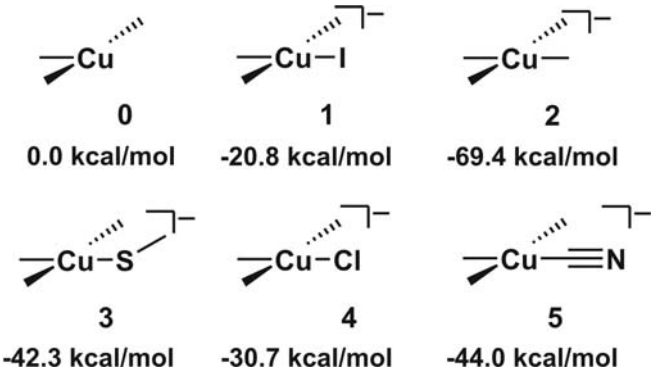

Scheme 2. DFT calculated relative energies of trimethylcuprate **0** and several $Me_3Cu(III)X^-$ complexes **1** - **5** with different ligands.

The square planar geometry and the d^8 electron configuration of the Cu(III) complexes resemble to the well known Pt(II) and Au(III) complexes, for which both pseudorotation and S_N2 substitution are accepted models for isomerisation processes.[8-10] Therefore, various complex geometries as possible intermediates were calculated on the basis of the

pseudorotational processes reported for Pt(II) and Au(III) complexes. However, up to now no evidence for an intermediate with three not distinguishable Me groups around Cu has been found (data not shown).

Next, an intermolecular S_N2-like substitution mechanism was calculated with **4** and MeLi as reaction partners (see Scheme 3). Despite the fact that the Li^+ coordinated Cu(III) complexes show lower energies, the non coordinated anionic complexes **4** and **2** were calculated as starting material and product, because they represent the anions of the solvent separated ion pairs expected in Li^+ coordinating solvents.[11] As first step in the pathway, the Li^+ of MeLi coordinates to chlorine resulting in a stabilisation of -34.1 kcal/mol compared to **4**, which corroborates the stabilization potential of Li^+ in gas phase calculations already shown above for **1**-**5**. The following substitution transition state **$TS_{4\text{-}2}$** has a surprisingly small activation energy of only 10.5 kcal/mol compared to the reductive elimination from the Cu(III) intermediate, for which an activation energy of ~18 kcal/mol was calculated for **4**.[7] The next LiCl coordinated product complex shows the lowest energy of -55.7 kcal/mol. This directly reflects the driving force of the reaction. As final product **2** is calculated. This again has a higher energy due to the gas phase condition of the calculation. This reaction pathway reveals that intermolecular ligand exchanges in Cu(III) complexes should be possible, in case MeLi or other appropriate reaction partners are present in solution.

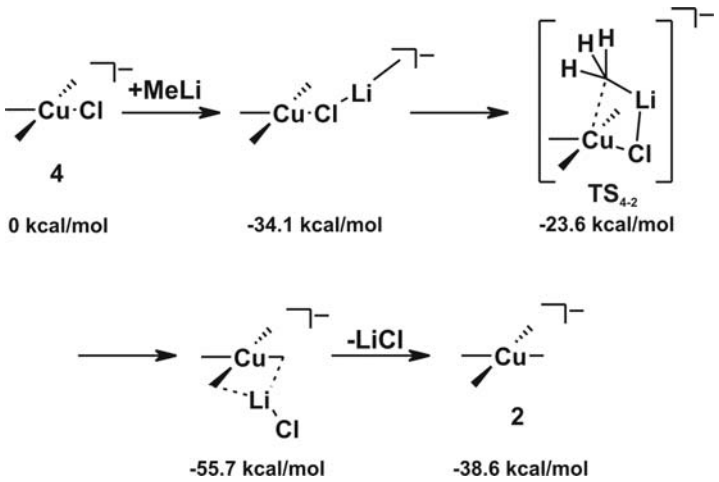

Scheme 3 Theoretical calculated reaction mechanism between **4** and excess MeLi for the formation of tetra-alkyl Cu(III)-complexes.

In this combined NMR and DFT study for the first time mechanistic insights into ligand exchange processes on square planar Cu(III) complexes are presented. Specific ^{13}C labelling and the interpretation of the resulting isotopomeric patterns reveal that ligand

exchange processes occur in Cu(III) complexes, but are slow compared to elimination under usual synthetic cross coupling conditions. Related theoretical calculations reveal an intermolecular S_N2 substitution mechanism for these transformations and the low energy of the transition state suggests that also other ligand exchange reactions should be possible on Cu(III) intermediates.

6.3 References

(1) Bertz, S. H.; Cope, S.; Murphy, M.; Ogle, C. A.; Taylor, B. J. *J. Am. Chem. Soc.* **2007**, *129*, 7208-9.

(2) Bartholomew, E. R.; Bertz, S. H.; Cope, S.; Murphy, M.; Ogle, C. A. *J. Am. Chem. Soc.* **2008**, *130*, 11244-11245.

(3) Bertz, S. H.; Cope, S.; Dorton, D.; Murphy, M.; Ogle, C. A. *Angew. Chem. Int. Ed. Engl.* **2007**, *46*, 7082-5.

(4) Gaertner, T.; Henze, W.; Gschwind, R. M. *J. Am. Chem. Soc.* **2007**, *129*, 11362-11363.

(5) Nakamura, E.; Mori, S. *Angew. Chem. Int. Ed.* **2000**, *39*, 3750-3771.

(6) Bartholomew, E. R.; Bertz, S. H.; Cope, S.; Dorton, D. C.; Murphy, M.; Ogle, C. A. *Chem. Commun.* **2008**, 1176-1177.

(7) Nakamura, E.; Mori, S.; Morokuma, K. *J. Am. Chem. Soc.* **2000**, *122*, 7294-7307.

(8) Chval, Z.; Sip, M.; Burda, J. V. *Journal of Computational Chemistry* **2008**, *29*, 2370-2381.

(9) Cooper, J.; Ziegler, T. *Inorg. Chem.* **2002**, *41*, 6614-6622.

(10) Louw, W. J. *Inorg. Chem.* **2002**, *16*, 2147-2160.

(11) John, M.; Auel, C.; Behrens, C.; Marsch, M.; Harms, K.; Bosold, F.; Gschwind, R. M.; Rajamohanan, P. R.; Boche, G. *Chem. Eur. J.* **2000**, *6*, 3060-3068.

6.4 Supporting Information

6.4.1. Experimental section

All cuprate samples were prepared by a method described by John et al.[1] The synthesis of the cuprate was directly done in Et_2O-d_{10} to exclude protonated Et_2O. The protonated Et_2O form the ^{13}C-labelled MeLi solution was removed as much as possible before the addition to the

Cu-salt suspension. Having the cuprate in hand it was cooled down to 170K and a solution MeI in DEE-d_{10} was added depending on the synthesis. The amount of MeI was adjusted to the synthesis of the cuprate solution.

(1) John, M.; Auel, C.; Behrens, C.; Marsch, M.; Harms, K.; Bosold, F.; Gschwind, R. M.; Rajamohanan, P. R.; Boche, G. *Chem. Eur. J.* **2000**, *6*, 3060-3068.

6.4.2. NMR Data Collection and Processing

The NMR spectra were recorded on a Bruker Avance 600 spectrometer equipped with a 5mm broadband triple resonance Z-gradient probe.

$^{1}H,^{13}C$ HMBC measurements were carried out with a standard Bruker pulse program using 32 number of scans, 16 dummy scans, TD(F2) = 16k and TD(F1) = 400 with a relaxation delay of 2s. The processing parameters were TD(F1) = 1k and TD(F2) = 1k. The temperatures for all measurements were controlled by a Bruker BVTE 3900 temperature unit.

6.4.3. DFT functional Calculations

All calculations were done using the GAUSSIAN 03 package.[2] All geometry optimisations were performed with the DFT-method and the B3LYP hybrid functional, using SDD for copper, iodine and gold and 6-31+G(d) for all other atoms. Local minima have zero and transition states (TS) have one and only one imaginary frequency. The intrinsic reaction coordinate (IRC) analysis[3-5] was carried out to confirm that stationary points are smoothly connected to each other. All energies used throughout are zero-point corrected and calculated for the gas-phase.

(2) Gaussian 03, R. C.; Frisch, M. J.; Trucks, G. W.; Schlegel, H. B.; Scuseria, G. E.; Robb, M. A.; Cheeseman, J. R.; Montgomery, J. A.; Jr., T. V.; Kudin, K. N.; Burant, J. C.; Millam, J. M.; Iyengar, S. S.; Tomasi, J.; Barone, V.; Mennucci, B.; Cossi, M.; Scalmani, G.; Rega, N.; Petersson, G. A.; Nakatsuji, H.; Hada, M.; Ehara, M.; Toyota, K.; Fukuda, R.; Hasegawa, J.; Ishida, M.; Nakajima, T.; Honda, Y.; Kitao, O.; Nakai, H.; Klene, M.; Li, X.; Knox, J. E.; Hratchian, H. P.; Cross, J. B.; Adamo, C.; Jaramillo, J.; Gomperts, R.; Stratmann, R. E.; Yazyev, O.; Austin, A. J.; Cammi, R.; Pomelli, C.; Ochterski, J. W.; Ayala, P. Y.; Morokuma, K.; Voth, G. A.; Salvador, P.; Dannenberg, J. J.; Zakrzewski, V. G.; Dapprich, S.; Daniels, A. D.; Strain, M. C.; Farkas, O.; Malick, D. K.; Rabuck, A. D.; Raghavachari, K.; Foresman, J. B.; Ortiz, J. V.; Cui, Q.; Baboul, A. G.; Clifford, S.; Cioslowski, J.; Stefanov, B. B.; Liu, G.;

Liashenko, A.; Piskorz, P.; Komaromi, I.; Martin, R. L.; Fox, D. J.; Keith, T.; Al-Laham, M. A.; Peng, C. Y.; Nanayakkara, A.; Challacombe, M.; Gill, P. M. W.; Johnson, B.; Chen, W.; Wong, M. W.; Gonzalez, C.; Pople, a. J. A.; Gaussian, I., Wallingford CT, 2004.

(3) Fukui, K. *Acc. Chem. Res.* **1981**, *14*, 363-368.

(4) Gonzalez, C.; Schlegel, H. B. J. *Chem. Phys.* **1989**, *90*, 2154-2161.

(5) Gonzalez, C.; Schlegel, H. B. J. *Phys. Chem.* **1990**, *94*, 5523-5527.

6.4.4. DFT calculated relative energies of Li coordinated complexes

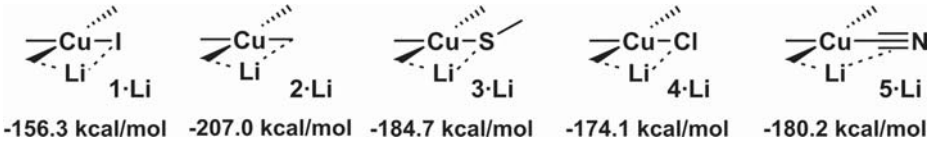

Figure S1. Relative energy of **1·Li**, **2·Li**, **3·Li**, **4·Li**, and **5·Li** compared to trimethylcuprate **0**.

6.4.5. Energies and Cartesians Coordinates of Stationary Points

0:
SCF Done: E(RB+HF-LYP) = -317.020249468

Center Number	Atomic Number	Atomic Type	Coordinates (Angstroms) X	Y	Z
1	29	0	-0.008292	-0.272814	-0.012622
2	6	0	-1.951413	-0.384792	0.014465
3	6	0	0.059662	1.659128	-0.000026
4	6	0	1.925083	-0.442156	0.014348
5	1	0	-2.413613	-0.041631	-0.919232
6	1	0	-2.164023	-1.463192	0.132623
7	1	0	-2.408591	0.150714	0.854833
8	1	0	1.045107	1.981606	-0.326506
9	1	0	-0.743778	1.977590	-0.661707
10	1	0	-0.140777	1.900005	1.044788
11	1	0	2.403851	-0.095962	-0.908638
12	1	0	2.396987	0.045213	0.874652
13	1	0	2.065307	-1.535803	0.102516

1:
SCF Done: E(RB+HF-LYP) = -328.574201787

Center Number	Atomic Number	Atomic Type	Coordinates (Angstroms) X	Y	Z
1	29	0	1.132747	0.002327	-0.035048
2	6	0	1.214050	-1.998898	-0.069319
3	6	0	3.082381	-0.014931	0.137819
4	6	0	1.238165	2.001274	-0.067717

5	53	0	-1.580615	0.001482	0.016969
6	1	0	1.151283	-2.343440	0.973186
7	1	0	2.148147	-2.369406	-0.512717
8	1	0	0.355104	-2.391550	-0.623348
9	1	0	3.466237	-0.124337	-0.883012
10	1	0	3.384870	-0.872162	0.745529
11	1	0	3.434026	0.922164	0.577311
12	1	0	1.355724	2.344199	0.970659
13	1	0	0.316716	2.422089	-0.481881
14	1	0	2.103242	2.341745	-0.653391

2:

SCF Done: E(RB+HF-LYP) = -356.978702898

Center Number	Atomic Number	Atomic Type	Coordinates (Angstroms) X	Y	Z
1	29	0	-0.001021	0.000186	-0.000798
2	6	0	-1.915501	-0.567960	0.023174
3	6	0	0.568262	-1.914221	-0.022325
4	6	0	-0.565625	1.916093	-0.022261
5	6	0	1.915088	0.565803	0.023050
6	1	0	-2.045849	-1.542805	0.515101
7	1	0	-2.233761	-0.665304	-1.027825
8	1	0	-2.559816	0.177430	0.511534
9	1	0	0.670145	-2.227242	1.029836
10	1	0	-0.179642	-2.560066	-0.504820
11	1	0	1.540940	-2.047334	-0.517682
12	1	0	-1.548046	2.051566	-0.497329
13	1	0	0.174571	2.555350	-0.525175
14	1	0	-0.641765	2.237104	1.029661
15	1	0	2.237170	0.652458	-1.027613
16	1	0	2.554250	-0.178622	0.519798
17	1	0	2.048076	1.543784	0.507837

3:

SCF Done: E(RB+HF-LYP) = -755.221020566

Center Number	Atomic Number	Atomic Type	Coordinates (Angstroms) X	Y	Z
1	29	0	-0.573067	0.036559	-0.000023
2	6	0	-2.440588	0.667823	0.000077
3	6	0	-1.274099	-1.840411	0.000057
4	6	0	0.011289	1.949503	-0.000074
5	16	0	1.543747	-0.847671	-0.000098
6	6	0	2.827799	0.471306	0.000163
7	1	0	-3.163616	-0.155138	-0.000158
8	1	0	-2.580986	1.291095	-0.892207
9	1	0	-2.581022	1.290617	0.892690
10	1	0	-1.900113	-1.981500	0.892629
11	1	0	-1.900192	-1.981634	-0.892440
12	1	0	-0.465188	-2.582008	0.000081
13	1	0	-0.832141	2.651945	0.000096
14	1	0	0.627649	2.134735	-0.891294
15	1	0	0.628069	2.134778	0.890838
16	1	0	3.812073	-0.014994	-0.000276
17	1	0	2.763806	1.113042	-0.886670
18	1	0	2.764232	1.112244	0.887612

4:
SCF Done: E(RB+HF-LYP) = -777.346099947

Center Number	Atomic Number	Atomic Type	Coordinates (Angstroms) X	Y	Z
1	6	0	0.313918	-2.000057	-0.059091
2	29	0	0.264708	0.001545	-0.011426
3	6	0	2.210525	-0.031441	0.081233
4	17	0	-2.049832	0.016770	0.035448
5	6	0	0.376091	2.000413	-0.057548
6	1	0	0.217546	-2.347670	0.980156
7	1	0	1.238642	-2.406605	-0.490927
8	1	0	-0.557371	-2.339217	-0.629985
9	1	0	2.559337	-0.173199	-0.949044
10	1	0	2.535814	-0.875804	0.696950
11	1	0	2.599874	0.909753	0.480648
12	1	0	0.566037	2.351105	0.967848
13	1	0	-0.584636	2.392071	-0.407054
14	1	0	1.192174	2.346185	-0.707439

5:
SCF Done: E(RB+HF-LYP) = -409.959979428

Center Number	Atomic Number	Atomic Type	Coordinates (Angstroms) X	Y	Z
1	29	0	-0.190975	0.001609	-0.004652
2	6	0	-2.149757	-0.007237	0.009118
3	6	0	-0.270909	2.008635	-0.001284
4	6	0	1.748728	0.001464	0.000506
5	6	0	-0.261672	-2.006133	-0.002396
6	7	0	2.921935	0.001466	0.003153
7	1	0	-2.557113	0.915907	0.437205
8	1	0	-2.460923	-0.082493	-1.042460
9	1	0	-2.535930	-0.876116	0.555093
10	1	0	-1.041750	2.351820	-0.704142
11	1	0	0.695155	2.456505	-0.254051
12	1	0	-0.559295	2.312751	1.015286
13	1	0	-1.094084	-2.363331	-0.622644
14	1	0	-0.440163	-2.308391	1.039902
15	1	0	0.680493	-2.443954	-0.347012

$TS_{4\text{-}2}$:
SCF Done: E(RB+HF-LYP) = -824.789509229

Center Number	Atomic Number	Atomic Type	Coordinates (Angstroms) X	Y	Z
1	29	0	-0.488749	-0.131857	0.000040
2	6	0	-0.534215	-0.130547	-1.984758
3	6	0	-2.368160	-0.663857	-0.000300
4	6	0	-0.534756	-0.130418	1.984784
5	6	0	0.483846	2.691432	-0.000011
6	17	0	2.166183	-0.966192	0.000174
7	3	0	1.837593	1.169985	-0.000461
8	1	0	-1.404736	0.418404	-2.367326
9	1	0	-0.570518	-1.169616	-2.339015

10	1	0	0.385318	0.341220	-2.353602
11	1	0	-2.583244	-1.237890	0.903378
12	1	0	-2.582446	-1.239060	-0.903428
13	1	0	-2.919615	0.281534	-0.001174
14	1	0	-0.571763	-1.169413	2.339180
15	1	0	-1.405058	0.419098	2.367035
16	1	0	0.384976	0.340869	2.353740
17	1	0	0.714621	3.305151	0.892356
18	1	0	-0.606323	2.543804	0.000109
19	1	0	0.714324	3.305391	-0.892289

7. NMR Spectroscopy on Zintl Anions in Liquid Ammonia

For these studies, I did the NMR spectroscopic investigations, while the synthesis of the solids and sample preparation was done by Stefanie Joseph.

Tobias Gärtner, Stefanie Joseph, Nikolaus Korber, Ruth M. Gschwind

to be published as soon as possible

7.1 Introduction

Since the first observation of group 14 polyanions[1,2] and their structural characterisation,[3] the Pb-, Sn- and Ge-polyanions have been the basis for successful synthetic approaches.[4] Here, very impressive examples are the determination of a new elemental modification of germanium[5-7] or the formation of endohedral Pb-, Sn- or Ge-clusters with transition metals embedded in the polyanion cage.[8-17] In contrast to that and despite the great importance of Si-compounds nowadays, an analogous solution chemistry of polysilicides has not been established for a long time. In 2004 it was shown for liquid ammonia and pyridine as solvent that Si_9^{3-}, Si_9^{2-} (schematic structure Figure 1c) and Si_5^{2-} anions (schematic structure Figure 1b) are observable in crystals after the extraction of binary solids,[18,19] in which the existence of Si_9^{4-} and Si_4^{4-} (schematic structure Figure 1a and 1c) was proven.[20,21] Recently, it was even possible to obtain the prototypical structure of Si_9^{4-} in ammonia solvate crystals after the extraction of a solid with the nominal composition $K_6Rb_6Si_{17}$.[22]

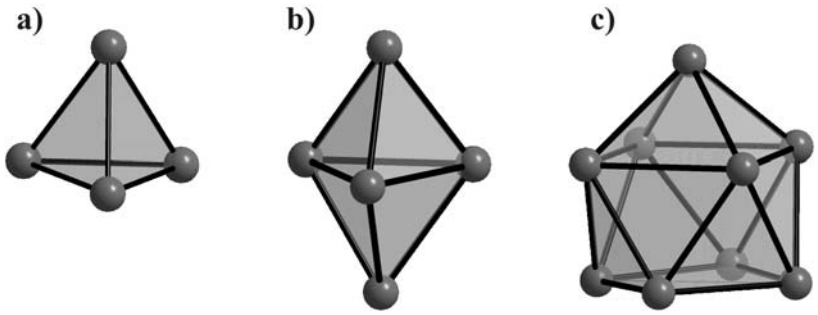

Figure 1. Schematic structures of a) Si_4-, b) Si_5- and c) Si_9-polyanions.

Although the solvate crystal structures and solid structures have been characterised very well by now, for synthetic transformations of polysilicide anions only the reaction with diphenylzinc[23] to get $[Si_9ZnPh]^{3-}$ and the formation of $[\{Ni(CO)_2\}_2(\mu\text{-}Si_9)_2]^{8-}$ with $Ni(CO)_2(PPh_3)_2$ in liquid ammonia are reported.[24]

The small number of examples of transition metal complexes of polysilicides and the fact that in the solid Si_9^{4-} and Si_4^{4-} are observed, whereas the solvate crystals comprise Si_9^{4-}, Si_9^{3-}, Si_9^{2-} and Si_5^{2-}, suggest chemical transformations or electron transfers to occur in solution. Up to now, the interpretation of the behaviour of silicides in solution has only been derived from

these discrepancies in solid and crystal structures described above, because first attempts to use high resolution NMR techniques failed, which was explained by long relaxation times.[19] New NMR methods dealing with long relaxation times, however, encouraged us in collaboration with the group of Korber *et al.* to start measurements on these highly air and temperature sensitive samples.

For these polysilicide anions up to now no chemical shift values are reported. In Figure 2 the two comparable compounds $[(Si_4)(SiMe^tBu_2)_4]$ with a Si_4-square (Figure 2a) and $[(Si_4)(Si^tBu_3)_4]$ with a Si_4-tetrahedron (Figure 2b) are shown.[25-28] For the cyclobutadiene analogue (Figure 2a) ^{29}Si chemical shifts for the Si-atoms of 10 ppm and 17 ppm were presented,[27] whereas the same compound, used as ligand for an Fe-complex, showed chemical shifts of -15.8 ppm and 24.6 ppm.[28] Amazingly, for the tetrahedral compound given in Figure 2b a ^{29}Si chemical shift of -244 ppm was reported for the Si_4 tetrahedron, which is so far the most highfield shifted value for ^{29}Si.[25,26] In a complex similar to that of Figure 2b with a Si_4 tetrahedron, three $SiMeDis_2$ substituents (Dis = $CH(SiMe_3)_2$) and one negative charge, the ^{29}Si chemical shifts were -153 ppm, -1 ppm, -0.3 ppm, and 13.6 ppm.[29] The most highfield shifted signal was assigned to the Si_4 core and the moving of the substituents was considered to be the reason for the equivalence within the Si_4 tetrahedron.[29] The remaining three chemical shifts were assigned to the three Si-atoms in the substituents. All these mentioned chemical shifts are referenced to TMS. Interestingly, for these compounds long T_1 relaxation times have never been mentioned.

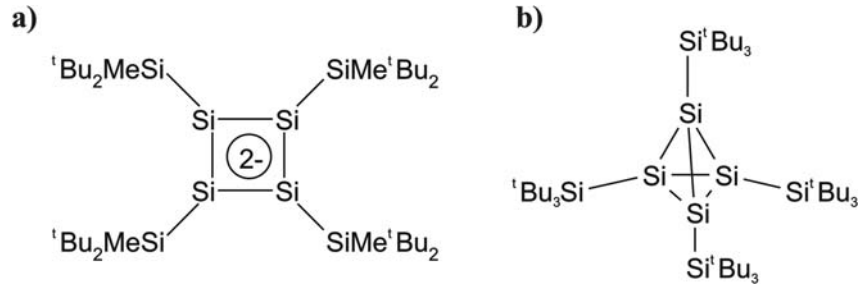

Figure 2. Two examples with a square shape[27] and a tetrahedral shape[26] showing a huge difference of ^{29}Si chemical shifts.

7.2 Discussion

7.2.1. NMR Methods

Originally, the Driven Equilibrium Fourier Transform (DEFT) sequence (Figure 3a) was designed to shorten measurement times for ^{13}C-spectra, in which especially quaternary carbon atoms have long T_1 relaxation times.[30] In this sequence the signal is detected during the acquisition time τ after the first 90° pulse and the magnetisation is refocused with the 180° pulse during the second time interval τ. The second 90° pulse then stores the magnetisation again along the +z-axis, which is the starting point for the second cycle without a relaxation delay.

It was reported that the originally DEFT method was used for ^{29}Si measurements in large volume coils.[31] Therefore, the DEFT sequence was applied to the ^{29}Si-isotope for a sample containing Tetramethylsilane (TMS), Hexamethyldisilacide (HMDS) and Octamethylcyclotetrasiloxane (OMS) in $CDCl_3$. It could be proven for the test sample that the lower signal-to-noise ratio in the DEFT spectrum, compared to the single pulse experiment, can be compensated by a higher number of scans, resulting in a still 15 times shorter measurement time due to shorter relaxation times. Nevertheless, the concentration has to be very high due to the unfavourable nuclear properties, i.e. a low natural abundance of 4.67% and a gyromagnetic ratio of $\gamma = -5.3190 \cdot 10^7$ rad $s^{-1}T^{-1}$.

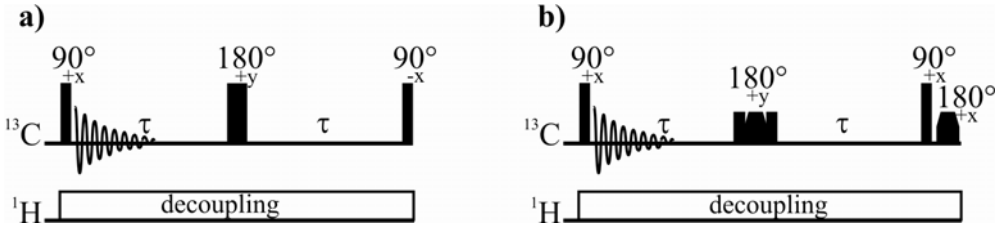

Figure 3. a) Original Driven Equilibrium Fourier Transform (DEFT) sequence written by Becker *et al.*[30] and b) modified Uniform Driven Equilibrium Fourier Transform (UDEFT) with adiabatic 180° refocusing pulses.[32]

A big disadvantage of the DEFT method is the dependency on pulse miscalibrations, magnetic field inhomogeneity, convection and frequency offsets. Cumulating these effects during acquisition leads to an overall bad signal-to-noise ratio.[32] To circumvent these disadvantages, the UDEFT sequence (Figure 3b) was chosen for the investigations on the polysilicide samples. In UDEFT measurements adiabatic pulses are used for the improvement

of the signal-to-noise ratio and these adiabatic pulses are less sensitive to pulse imperfections, frequency offsets and field inhomogeneities.[32] In the sequence, the adiabatic pulses are used for refocusing instead of the 180° pulse and in the end to restore the magnetisation along +z (Figure 3b). Nevertheless, a proper setup of pulse length and magnetic field is still inevitable.

As mentioned before, differently shaped polysilicide anions are proposed to be in solution and ^{29}Si chemical shift values for these compounds are missing completely. Therefore, the ^{29}Si DOSY measurement is considered to be a method to assign signals with different chemical shifts to the same molecule.

Despite the low natural abundance and in agreement with literature,[33] it could be shown that with high concentrations in the test sample even ^{29}Si DOSY (Diffusion Ordered Spectroscopy) measurements are accessible, in which a relative differentiation of different molecule sizes is possible. However, for absolute diffusion values the signal-to-noise ratio and the DOSY parameters (little delta = δ, big delta = Δ, and eddy current delays) have to be considered for a minimisation of the experimental error. The optimisation for these parameters has not been done yet, because the concentration of the polysilicide samples and therefore the signal-to-noise ratio was too low for a DOSY measurement.

7.2.2. NMR Measurements of Polysilicides in Liquid Ammonia

As the past investigations of polysilicides had been done in the group of Korber by using liquid ammonia, the measurement conditions were optimised for this solvent at low temperatures. Therefore, proper shim values have been created and the sample preparation has been optimised.

In the 1950´s it was reported that in pure liquid NH_3, which is completely free of water and has no amide impurities, it is possible to obtain a triplet, resulting from the $^{1}J(^{1}H,^{14}N)$ coupling.[34-37] With the optimised experimental conditions, indeed this could be reproduced for a real silicide containing sample. Moreover, in our case the $^{1}J(^{1}H,^{15}N)$ was visible, too (Figure 4a). But already smallest traces of impurities of water or amide, enhancing chemical exchange in solution, led to a signal in which the triplet and doublet splitting is lost. This effect can be used as a sensor for the quality of the sample and as an indicator for a possible contribution of the solvent in degrading processes. Indeed, a loss of the coupling was observed when during the sample preparation moisture could not be excluded (Figure 4b).

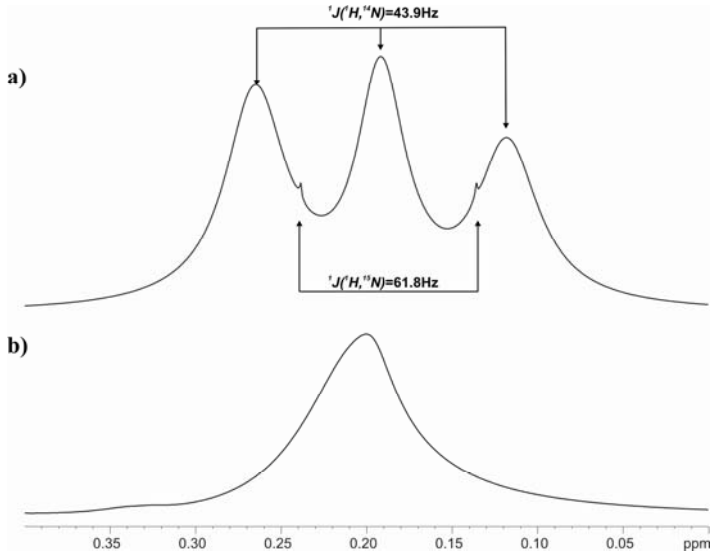

Figure 4. a) ^{1}H spectra of pure liquid ammonia showing the $^{1}J(^{1}H,^{14}N)$ and $^{1}J(^{1}H,^{15}N)$ couplings and b) the ^{1}H spectrum of liquid ammonia with impurities, leading to the loss of the ^{1}J splitting of the signal.

Using the ^{1}H signal of liquid NH_3 as spy for the sample quality, the first measurements were performed and an overall sweep of 190 kHz around the central frequency was covered, because unpublished theoretical calculated chemical shifts proposed values upfield shifted as well as downfield shifted for the different silicides. After a few measurements at -40°C, which is the temperature for the formation of the solvate crystal structures, it was not possible to detect any signal at all. Neither for the silicide nor for a degraded substance could a signal be observed, which indicates low concentrations although the samples showed a considerable colour. Regarding the proposed long T_1 relaxation times, the UDEFT sequence as well as the single pulse experiment, with pulse angles between 5° and 90° and long relaxation delays, was applied. However, in none of these measurements any signals were observed. Therefore, the temperature dependence of the sample was investigated. In a measurement at 300 K, which should enhance the concentration, the NH_3 spy indicated degradation of the silicides. For that reason, the sample was cooled down to -80°C already during preparation and stored at this temperature for the whole measurement. Again no signal was observed, but the NH_3 splitting still was detectable, indicating a very good quality of the sample. In addition, an intensive deep orange colour indicated dissolved compounds, but at concentrations which are not detectable by NMR. To increase the concentration the temperature was raised rapidly first to -45°C and then, as no signals were detected, further to -25°C. The measurements were started immediately after the target temperatures had been reached.

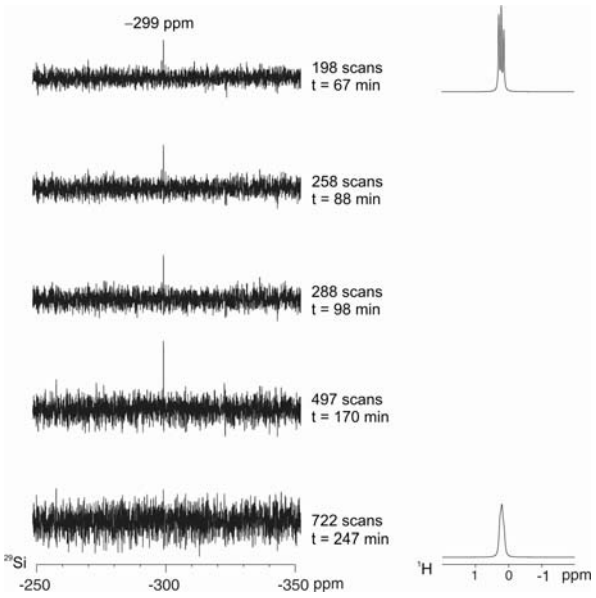

Figure 5. Measured ^{29}Si-spectra after different number of scans and the corresponding ^{1}H spectra before and after the ^{29}Si-measurement, demonstrating the instability of the sample.

At -25°C for the first time we were able to detect a ^{29}Si-signal for a polysilicide sample, which was derived from the direct extraction of a mixed $K_6Rb_6(Si,Sn)_{17}$ solid (containing 20% enriched ^{29}Si) in the NMR tube. In the beginning, the signal intensity rose, as it is expected, but after a time interval of ~ 4 hours no signal could be detected anymore. Furthermore, the T_1 relaxation times seem to be smaller than expected, because in these single pulse measurements a pulse angle of 30° and a relaxation delay of 20 s were sufficient to obtain the detected spectra. Additionally, the measurements revealed that the compound is not stable for a long time, because the corresponding ^{1}H spectrum showed the triplet at the beginning of the measurement, but the coupling was lost after the ^{29}Si measurement was aborted because of the signal loss. This directly indicates the instability of the polysilicide sample and correlates the appearance and disappearance of the ^{29}Si-signal with the loss of the coupling in the ^{1}H-spectrum of the NH_3 (Figure 5). The same behaviour could be reproduced with a sample containing $K_6Rb_6Si_{17}$ (containing 20% enriched ^{29}Si) and $Rb_{12}Sn_{17}$ in mixture.

The chemical shift of this Si signal in solution at -299 ppm is speculated to be the Si_4^{4-} anion, because the corresponding solid-state NMR of the solid $K_6Rb_6Si_{17}$ (containing 20% enriched ^{29}Si), from which also the solution sample was prepared, showed a singlet at -310 ppm (Figure 6). This singlet was attributed to the Si_4^{4-}, as comparable NMR data exist for A_4Si_4 compounds (A = Na-Cs; -280 ppm to -310 ppm).[38]

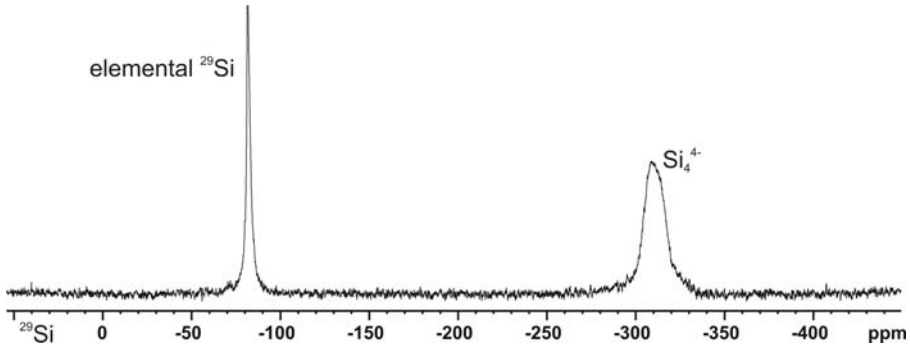

Figure 6. ^{29}Si solid-state NMR spectrum of the $K_6Rb_6Si_{17}$ solid showing residual elemental silicon and Si_4^{4-}.

Additionally, the fact that Si_4^{4-} has never been observed in solvate crystal structures before might now be explained by a degradation of the polysilicide, but this suggestion needs to be confirmed. Nevertheless, Si_9^{4-} is still a compound bearing a lot of questions, because the compound is found in crystals at -40°C, but can be observed neither in solid-state NMR nor in solution NMR.

7.3 Conclusion

Since the beginning of ^{29}Si measurements in liquid ammonia, it has been possible to demonstrate that with test samples the expected quite long T_1 relaxation times can be treated by UDEFT spectroscopy. Furthermore, it was possible to show that in principle DOSY is also applicable to ^{29}Si. A restriction for both methods, however, is that the concentration has to be very high. This condition is up to now not fulfilled for the silicide samples.

Upon variation of the temperature during the measurement, the concentration of the dissolved silicide in the sample could be increased for a short time interval so that the very first ^{29}Si signal of a silicide compound in solution could be detected. Additionally, a surprising disappearance of the ^{29}Si signal was detected at longer measurement times, which can be followed by the ^{1}H NMR spectrum of NH_3. The ammonia signal loses its multiplett structure, which can be explained by a degradation of the compound.

7.4 References

(1) Joannis, A. *C. R. Hebd. Sceances Acad. Sci.* **1891**, *113*, 795.

(2) Joannis, A. *C. R. Hebd. Sceances Acad. Sci.* **1892**, *114*, 585.

(3) Fässler, T. F. *Coord. Chem. Rev.* **2001**, *215*, 347-377.

(4) Sevov, S. C.; Goicoechea, J. M. *Organometallics* **2006**, *25*, 5678-5692.

(5) Fässler, T. F. *Angew. Chem.* **2007**, *119*, 2624-2628.

(6) Fässler, T. F. *Angew. Chem. Int. Ed.* **2007**, *46*, 2572-2575.

(7) Guloy, A. M.; Ramlau, R.; Tang, Z.; Schnelle, W.; Baitinger, M.; Grin, Y. *Nature* **2006**, *443*, 320-323.

(8) Esenturk, E. N.; Fettinger, J.; Eichhorn, B. *Chem. Commun.* **2005**, 247 - 249.

(9) Esenturk, E. N.; Fettinger, J.; Eichhorn, B. *J. Am. Chem. Soc.* **2006**, *128*, 9178-9186.

(10) Esenturk, E. N.; Fettinger, J.; Lam, Y. F.; Eichhorn, B. *Angew. Chem.* **2004**, *116*, 2184-2186.

(11) Esenturk, E. N.; Fettinger, J.; Lam, Y. F.; Eichhorn, B. *Angew. Chem. Int. Ed.* **2004**, *43*, 2132-2134.

(12) Goicoechea, J. M.; Sevov, S. C. *J. Am. Chem. Soc.* **2005**, *127*, 7676-7677.

(13) Kesanli, B.; Halsig, J. E.; Zavalij, P.; Fettinger, J. C.; Lam, Y.-F.; Eichhorn, B. W. *J. Am. Chem. Soc.* **2007**, *129*, 4567-4574.

(14) Scharfe, S.; Fässler, T. F.; Stegmaier, S.; Hoffmann, S. D.; Ruhland, K. *Chem. Eur. J.* **2008**, *14*, 4479-4483.

(15) Wang, J. Q.; Stegmaier, S.; Fässler, T. F. *Angew. Chem.* **2009**, *121*, 2032-2036.

(16) Wang, J. Q.; Stegmaier, S.; Fässler, T. F. *Angew. Chem. Int. Ed.* **2009**, *48*, 1998-2002.

(17) Zhou, B.; Denning, M. S.; Kays, D. L.; Goicoechea, J. M. *J. Am. Chem. Soc.* **2009**, *131*, 2802-2803.

(18) Goicoechea, J. M.; Sevov, S. C. *J. Am. Chem. Soc.* **2004**, *126*, 6860-6861.

(19) Goicoechea, J. M.; Sevov, S. C. *Inorg. Chem.* **2005**, *44*, 2654-2658.

(20) Hoch, C.; Wendorff, M.; Röhr, C. *J. Alloys Compd.* **2003**, *361*, 206-221.

(21) Queneau, V.; Todorov, E.; Sevov, S. C. *J. Am. Chem. Soc.* **1998**, *120*, 3263-3264.

(22) Joseph, S.; Suchentrunk, C.; Kraus, F.; Korber, N. *Eur. J. Inorg. Chem.* **2009**, *2009*, 4641-4647.

(23) Goicoechea, J. M.; Sevov, S. C. *Organometallics* **2006**, *25*, 4530-4536.

(24) Joseph, S.; Hamberger, M.; Mutzbauer, F.; Härtl, O.; Meier, M.; Korber, N. *Angew. Chem.* **2009**, *121*, 8926-8929.

(25) Meyer-Wegner, F.; Scholz, S.; Sänger, I.; Schödel, F.; Bolte, M.; Wagner, M.; Lerner, H.-W. *Organometallics* **2009**.

(26) Wiberg, N.; Finger, C. M. M.; Auer, H.; Polborn, K. *J. Organomet. Chem.* **1996**, *521*, 377-386.

(27) Lee, V. Y.; Takanashi, K.; Matsuno, T.; Ichinohe, M.; Sekiguchi, A. *J. Am. Chem. Soc.* **2004**, *126*, 4758-4759.

(28) Takanashi, K.; Lee, V. Y.; Ichinohe, M.; Sekiguchi, A. *Angew. Chem. Int. Ed.* **2006**, *45*, 3269-3272.

(29) Ichinohe, M.; Toyoshima, M.; Kinjo, R.; Sekiguchi, A. *J. Am. Chem. Soc.* **2003**, *125*, 13328-13329.

(30) Becker, E. D.; Feretti, J. A.; Farrar, T. C. *J. Am. Chem. Soc.* **2002**, *91*, 7784-7785.

(31) Mann, M. D.; Chmelka, B. F. *Anal. Chem.* **2000**, *72*, 5131-5135.

(32) Piotto, M.; Bourdonneau, M.; Elbayed, K.; Wieruszeski, J. M.; Lippens, G. *Magn. Reson. Chem.* **2006**, *44*, 943-947.

(33) Harris, R. K.; Kinnear, K. A.; Morris, G. A.; Stchedroff, M. J.; Samadi-Maybodi, A.; Azizi, N. *Chem. Commun.* **2001**, 2422 - 2423.

(34) Ogg, R. A. *J. Chem. Phys.* **1954**, *22*, 560-561.

(35) Ogg, R. A. *Discuss. Faraday Soc.* **1954**, *17*, 215 - 220.

(36) Ogg, R. A.; Ray, J. D. *J. Chem. Phys.* **1957**, *26*, 1515-1516.

(37) Roberts, J. D. *J. Am. Chem. Soc.* **2002**, *78*, 4495-4496.

(38) Stearns, L. A.; Gryko, J.; Diefenbacher, J.; Ramachandran, G. K.; McMillan, P. F. *J. of Solid State Chem.* **2003**, *173*, 251-258.

8. Summary

Despite organocuprates have early been recognised to be effective reagents for C-C-couplings in 1,4-addition reactions to enones or in S_N2 and S_N2' couplings, the structures of the free reagent, the reaction intermediates and ,furthermore, experimental evidences for the reaction mechanisms had not been known for decades. Complex dynamic equilibria and supramolecular structures in solutions of organocuprates longed for elaborate DOSY, HOE, and NOE NMR spectroscopic methods. Combinations of step by step structural approaches as well as optimised NMR experiments for structural details of organocopper compounds allowed for the determination of the free organocuprate monomers and their tendency to form supramolecular assemblies in non-polar solvents. It was observed that the linear cuprate monomers form homodimeric assemblies, which are bridged via weak ionic interacting Li^+ ions. These homodimers then even tend to aggregate in a chain like supramolecular assembly. Furthermore, the observed different reactivities for organocuprates in reactions with Micheal-acceptors were directly correlated with these supramolecular aggregates in solution. Moreover, detailed investigations on the stabilised intermediates of addition and substitution reactions finally answered the question about the reaction mechanisms of organocuprates in 1,4-addition reactions to enones and in S_N2 or S_N2' cross couplings. These real amazing results observed during decades could be summarised in the review, which has been published in the Patais´s series.

The review already comprises our experimental investigations on organocuprate π-complexes as initial intermediates for the 1,4-additions. Here, the diastereoselectivity and reactivity was rationalised on the basis of structural details. It was possible for the first time to get insight into the π-complexes with chiral enones and to describe even the conformation of the enone in the intermediate. Additionally, with DOSY measurements on π-complexes of $Me_2CuLi{\cdot}LiX$ (X = CN, I) with three different achiral enones, the aggregation behaviour in these intermediates could be demonstrated. Amazingly, in $^1H,^{13}C$ HMBC measurements scalar couplings across copper were detected in π-complexes of $Me_2CuLi{\cdot}LiX$ (X = CN, I) with an achiral enone for the first time without ^{13}C labelled compounds. For the residual salt, which is known to influence the reactivity, it could be shown that it only participates in the complexation of the carbonyl group of the enone.

The suppression of the formation of π-intermediates in turn directly led to the first NMR detection of the elusive and for a long time proposed Cu(III)-intermediate of the S_N2-like

substitution reactions of organocuprates with primary alkyl halides. From the observed ^{1}H and $^{1}H,^{13}C$ HMBC spectra it was evident that the substitution reaction intermediate with a square planar coordination had been stabilised and NMR spectroscopically observed. The intermediate, which was obtained after the reaction of $Me_2CuLi \cdot LiCN$ with MeI, showed two chemically different Me-substituents and one cyanide attached to the same Cu-center. In contrast to the π-intermediates, which allowed for a transfer of magnetisation across copper, the square planar Cu(III)-intermediates first were only detectable due to the tremendous signal enhancement, caused by the $^{3}J_{H,C}$ coupling to the ^{13}C-labelled cyanide.

In further experiments, the ^{13}C-labelling was extended to the methyl groups of the cuprate to distinguish between the groups of the cuprate and of the MeI, which was used in ^{13}C natural abundance. This experiment should reveal possible dynamic processes in the Cu(III)-complex, because investigations by the group of Ogle hinted at ligand exchanges. And indeed, in a HMBC measurement two different isotopomers could be assigned due to different coupling patterns, according to the position of the methyl group in natural abundance. Considering the product ethane of the model reaction, the ligand exchange in the transient Cu(III)-intermediate turned out to be slow compared to the reductive elimination at normal reaction conditions. Nevertheless, knowing about the mechanism could be the entrance to a new part of organocopper chemistry. Therefore, DFT functional calculations were performed to gain insight into possible ligand exchange mechanisms. It could be calculated that Li^+ has a great stabilising influence on the Cu(III)-complexes and theoretical hints were found for a S_N2 substitution in square planar complexes, as it is known for other d^8 configured complexes of isoelectronic Pt(II) or Au(III) complexes.

Besides NMR spectroscopic investigations on organocopper compounds, this thesis also comprises NMR investigations on the main group element silicon in polysilicide Zintl anions dissolved in liquid ammonia. First, the DEFT and DOSY methods were implemented for the ^{29}Si isotope, using a test sample, to support the challenging task of investigations of polysilicides in solution. Additionally, the coupling between ^{1}H and ^{14}N, which indicates pure ammonia with no impurities, could be used as a spy to prove the quality of the sample. With that sensor and an unusual temperature series, in which the sample was warmed up in two steps sizes between -80°C and -25°C in a very short period of time, finally the concentration could be increased to such an amount that the first detection of a silicide compound in solution was possible, even without special NMR methods. A direct correlation with the ammonia spy revealed the soluble silicides to be very labile.

Finally, during this thesis predominantly transient air, moisture, and temperature sensitive compounds had been detected for the first time and a contribution to the elucidation of reaction mechanisms could be done.

As the conditions for the stablilisation of Cu(III)-complexes have been optimised, it should be possible to enter a new part of organocopper chemistry. Here, NMR spectroscopy is the method of choice, as NMR can monitor the transformation processes in solution.

Moreover, as the basis for NMR spectroscopic measurements on polysilicid Zintl anions was made with the first detection of a ^{29}Si signal of polysilicides, further chemical attempts to increase the concentration and the stability in solution should reveal even more detailed NMR spectroscopic results about Polysilicide Zintl anions in liquid ammonia.

9. Zusammenfassung

Trotz der frühen Erkenntnis, dass Organocuprate effektive Reagenzien für C-C-Kupplungen in 1,4-Additionsreaktionen oder in S_N2 und S_N2' Substitutionen sind, waren die experimentellen Nachweise für die Strukturen des freien Reagens, die Reaktionsintermediate und darüberhinaus die Reaktionsmechanismen über Jahrzehnte hinweg unbekannt. Die komplizierten dynamischen Gleichgewichte und die supramolekularen Strukturen in Organocupratlösungen verlangten nach speziell ausgearbeiteten DOSY, HOE, und NOE NMR spektroskopischen Methoden. Eine schrittweise Annäherung an veschiedene Struktureinheiten in Kombination mit optimierten NMR Experimenten für strukturelle Details von Organokupferverbindungen erlaubte die Ermittlung des Organocupratmonomers und dessen Tendenz in unpolaren Lösungsmitteln supramolekulare Aggregate zu bilden. Es wurde beobachtet, dass die linearen Cupratmonomere homodimere Aggregate bilden, die über schwach ionisch wechselwirkende Li^+ Ionen miteinander verbrückt sind. Diese Homodimere wiederum neigen dazu in kettenartigen Strukturen zu aggregieren. Ausserdem war es möglich die beobachteten Unterschiede in den Reaktivitäten von Organocupraten gegenüber Michael-Akzeptoren direkt mit der supramolekularen Aggregation in Lösung zu korrelieren. Zudem konnten schließlich detailierte Untersuchungen an den stabilisierten Intermediaten von Additions- und Substitutionsreaktionen die Frage nach dem Reaktionsmechanismus in 1,4-Additionsreaktionen von Cupraten an Enone, S_N2 und S_N2' Kreuzkupplungen beantworten. Diese wirklich erstaunlichen Ergebnisse, die über Jahrzehnte hinweg beobachtet wurden, konnten in einem Übersichtsartikel zusammengefasst werden, der im Rahmen der Buchreihe „Patai´s series“ veröffentlicht wurde.

Dieser Übersichtsartikel beinhaltet bereits unsere experimentellen Untersuchungen an den Organocuprat π-Intermediaten, die das Eingangsintermediat der 1,4-Additionreaktion bilden. Hierbei wurde aufgrund struktureller Details die Diastereoselektivität und die Reaktivität erklärt. Es war erstmals möglich Einblicke in die Struktur der π-Komplexe chiraler Enone zu erlangen und sogar die Konformation des Enons im Intermediat zu bescheiben. Zudem konnte das Aggregationsverhalten in diesen Intermediaten mit DOSY-Messungen an π-Komplexen von $Me_2CuLi{\cdot}LiX$ (X = CN, I) und drei verschiedenen achiralen Enonen aufgezeigt werden. Erstaunlicherweise war es in $^1H,^{13}C$ HMBC-Messungen erstmals sogar möglich im π-Komplex von $Me_2CuLi{\cdot}LiX$ (X = CN, I) mit einem achiralen Enon skalare Kopplungen über das Cu-Atom hinweg zu detektieren, ohne dass ^{13}C-markierte Verbindungen verwendet

wurden. Für die restliche Salzeinheit, die bekannterweise die Reaktivität beeinflusst, konnte gezeigt werden, dass sie nur die Carbonylfunktion des Enons komplexiert.

Die Unterdrückung der Bildung des π-Intermediates führte dazu, dass das schwer erfassbare und lange Zeit vorhergesagte Cu(III)-Intermediat der S_N2-ähnlichen Substitutionsreaktionen von Organocupraten mit primären Alkylhalogeniden detektiert werden konnte. Die ^1H und $^1H,^{13}C$ HMBC Spektren zeigen auf, dass das Substitutionsintermediat, das eine quadratisch planare Koordination aufweist, stabilisiert und NMR spektroskopisch detektiert wurde. Das Intermediat der Reaktion von $Me_2CuLi{\cdot}LiCN$ mit MeI wies zwei chemisch unterschiedliche Methylsubstituenten und ein Cyanid Anion auf, die alle am selben Cu-Atom gebunden waren. Im Gegensatz zu den π-Intermediaten, die es ohne ^{13}C Markierung erlaubten Magnetisierung über das Cu-Atom hinweg zu übertragen, waren die quadratisch planaren Cu(III)-Intermediate anfangs nur wegen der enormen Signalverstärkung durch die $^3J_{H,C}$ Kopplung zu ^{13}C markiertem Cyanid detektierbar.

In weiteren Experimenten wurden zusätzlich zum Cyanid die Methylgruppen des Cuprats ^{13}C markiert, um zwischen Gruppen des Cuprats und des Methyliodids, welches in ^{13}C natürlicher Häufigkeit eingesetzt wurde, zu unterscheiden. Dieses Experiment sollte Aufschluss über mögliche dynamische Prozesse im Cu(III)-Komplex liefern, da bereits Untersuchungen der Gruppe von Ogle auf Ligandenaustauschreaktionen hinwiesen. Im $^1H,^{13}C$ HMBC konnten in der Tat aufgrund unterschiedlicher Kopplungsmuster zwei verschiedene Isotopomere, je nachdem, in welcher Position sich die unmarkierte Methylgruppe befindet, zugeordnet werden. Unter Berücksichtigung des Produktes Ethan der Modellreaktion, stellte sich heraus, dass im Vergleich zur reduktiven Eliminierung unter Normalbedingungen der Ligandenaustausch im Cu(III)-Intermediat langsam ist. Trotzdem könnte das Wissen über den Mechanismus der Zugang zu einer neuen Organokupferchemie sein. Deshalb wurden DFT Rechnungen durchgeführt, um Einblicke in mögliche Ligandenaustauschmechanismen zu erhalten. Anhand der Rechnungen konnte gezeigt werden, dass Li^+ einen großen stabilisierenden Einfluss auf die Cu(III)-Komplexe hat und es wurden Hinweise gefunden, die auf eine S_N2-Substitution im quadratisch-planaren Komplex hindeuten, wie es für andere d^8 konfigurierte, isoelektronische Pt(II)- und Au(III)-Komplexe bekannt ist.

Neben den NMR spektroskopischen Untersuchungen an Organokupferverbindungen beinhaltet diese Arbeit auch NMR Untersuchungen am Hauptgruppenelement Silicium in Polysilicid-Zintl-Anionen, welche in flüssigem Ammoniak gelöst sind. Zuerst wurden anhand

einer Testprobe DEFT und DOSY Methoden implementiert um die Untersuchungen an Polysiliziden in Lösung zu unterstützen. Zusätzlich konnte die Kopplung zwischen ^{1}H und $^{14}N/^{15}N$, wie sie in reinem Ammoniak ohne Verunreinigungen auftritt, herangezogen werden um die Probenqualität zu überprüfen. Mit diesem Sensor und einer unüblichen Temperaturreihe, bei der die Probe in zwei großen Schritten von -80°C auf -25°C aufgewärmt wurde, konnte die Konzentration schließlich so erhöht werden, dass das erste Signal einer Silicidverbindung in Lösung detektiert werden konnte, ohne dass spezielle NMR Methoden notwendig waren. Der direkte Vergleich mit der NH_3-Sonde zeigte zudem, dass das gelöste Silicid sehr unbeständig ist.

Zusammenfassend konnten in dieser Arbeit hauptsächlich kurzlebige luft-, feuchtigkeits- und temperaturempfindliche Verbindungen erstmalig NMR spektroskopisch detektiert werden. Auch zur Aufklärung von Reaktionsmechanismen konnte beigetragen werden.

Da die Bedingungen für die Stabilisierung von Cu(III)-Komplexen optimiert werden konnten, ist der Zugang zu einem neuen Teil der Organokupferchemie geöffnet. NMR ist hierbei die Methode der Wahl, um diese Chemie in Lösung weiter zu verfolgen.

Nachdem der Grundstein für NMR spektroskopische Messungen an Polysilicid Anionen mit der ersten Detektion eines ^{29}Si signals gelegt ist, sollten überdies weitere Versuche die Konzentrationsverhältnisse zu verbessern und die Stabilität zu erhöhen dazu führen, noch detailiertere Struktureigenschaften von Polysilicid-Zintl-Anionen in flüssigem Ammoniak herauszufinden.

10. Appendix

10.5 Publications

T. Gärtner, E. Nakamura, R. M. Gschwind
"Ligand Exchange Reactions in Cu(III) complexes: Mechanistic Insights by Combined NMR and DFT Studies" *Chem. Comm.* **2009**, in preparation.

T.Gärtner, S. Joseph, N. Korber, R. M. Gschwind
"NMR Spectroscopy on Zintl Anions in Liquid Ammonia"
to be published as soon as possible **2009**, in preparation.

T.Gärtner, S. Joseph, R. M. Gschwind
"Supramolecular Aggregation – An Additional Note"
Z. Naturforsch. **2009**, in preparation.

W. Henze, T. Gärtner, R. M. Gschwind
"Organocuprate Conjugate Addition: The Structural Features of Diastereomeric and Supramolecular π-Intermediates" *J. Am. Chem. Soc.* **2008**, 130, 13718-13726

T. Gärtner, W. Henze, R. M. Gschwind
"NMR-Detection of Cu(III) Intermediates in Substitution Reactions of Alkyl Halides with Gilman Cuprates" *J. Am. Chem. Soc.* **2007**, 129, 11362-11363.

T. Gärtner, R. M. Gschwind
"NMR of Organocopper Compounds" in The Chemistry of Organocopper Compunds Rappoport, Zvi / Marek, Ilan (Eds.), Wiley-VCH, 1st edition - November 2009.

10.6 Posters and Oral Presentations

T. Gärtner, W. Henze, R. M. Gschwind
Poster: „*"Higher Order" Cuprates – NMR-Iinvestigations on Intermediates of Gilman-Cuprates in Addition-Reactions to Enones"*
1st European Chemistry Congress **2006**, Budapest, Hungary.

T. Gärtner, R. M. Gschwind
Poster: „*Organocuprates – Intermediate Studies in 1,4-Addition Reactions"*
8th International Symposium on Carbanion Chemistry **2007**, Madison, USA.

T. Gärtner

Oral Presentation: „*NMR Detection of Cu(III)-Intermediates*“

Christmas Colloquium of the Department of Organic Chemistry, University of Regensburg, **2007**

T. Gärtner, R. M. Gschwind

Poster: „*NMR Detection of Cu(III) Intermediates in S_N-Reactions of Organocuprates*“

23rd International Conference on Organometallic Chemistry **2008**, Rennes, France.

T. Gärtner, R. M. Gschwind

Poster: „*NMR Detection of Cu(III) Intermediates in S_N-Reactions of Organocuprates*“

GDCh Discussion Group meeting NMR **2008**, Regensburg, Germany.

10.7 Curriculum Vitae

Tobias Gärtner

*19.11.1980, Neumarkt i. d. Opf.

Education

10/2006-12/2009	Dissertation: “NMR Spectroscopic Studies on Organocopper Compounds and Silicon Zintl anions” University of Regensburg
01/2006-09/2006	Diploma Thesis “NMR Investigations on Cuprates“ University of Regensburg
10/2001-12/2005	Studies of Chemisrty, University of Regensburg
07/2000-09/2001	Military Service and Elderly Care
09/1991-06/2000	A-level (Abitur) at the Willibald-Gluck-Gymnasium Neumarkt i. d. Opf.

Fellowships

07/2009-08-2009	FY2009 JSPS (Japan Society for the Promotion of Science) Research Fellowship

Research Experience

10/2006-12/2009	PhD student, Institute of Organic Chemistry, University of Regensburg, supervisor: Prof. Dr. Ruth M. Gschwind
07/2009-08/2009	Research collaboration with Prof. Eiichi Nakamura, Department of Chemistry, The University of Tokyo

Teaching Experience

10/2006-current	Teaching assistant in laboratory courses for chemists, biologists, biochemists and teachers; supervisor for diploma students